OLFACTORY LEARNING IN *DROSOPHILA*

Learning from Models

JOHANNES NEHRKORN

Dissertation der
Graduate School of Systemic Neurosciences der
Ludwig-Maximilians-Universität München

Submitted 31th of August, 2015

Graduate School of
Systemic Neurosciences
LMU Munich

Dissertation at the

Graduate School of Systemic Neurosciences
Ludwig-Maximilians-Universität München
Munich, Germany

OLFACTORY LEARNING IN *DROSOPHILA*

Learning from Models

Submitted by
JOHANNES NEHRKORN
Munich, 31th of August, 2015

SUPERVISOR AND FIRST REVIEWER
Prof. Dr. Andreas V. M. Herz

SECOND REVIEWER
Prof. Dr. Alexander Borst

DATE OF SUBMISSION
31th of August, 2015

DATE OF ORAL DEFENSE
3rd of February, 2016

Für Thea.

ABSTRACT

Animals are able to form associative memories and benefit from past experience. In classical conditioning an animal is trained to associate an initially neutral stimulus by pairing it with a stimulus that triggers an innate response. The neutral stimulus is commonly referred to as conditioned stimulus (CS) and the reinforcing stimulus as unconditioned stimulus (US). The underlying neuronal mechanisms and structures are an intensely investigated topic.

The fruit fly *Drosophila melanogaster* is a prime model animal to investigate the mechanisms of learning. In this thesis we propose fundamental circuit motifs that explain aspects of aversive olfactory learning as it is observed in the fruit fly. Changing parameters of the learning paradigm affects the behavioral outcome in different ways.

The relative timing between CS and US affects the hedonic value of the CS. Reversing the order changes the behavioral response from conditioned avoidance to conditioned approach. We propose a timing-dependent biochemical reaction cascade, which can account for this phenomenon.

In addition to form odor-specific memories, flies are able to associate a specific odor intensity. In aversive olfactory conditioning they show less avoidance to lower and higher intensities of the same odor. However the layout of the first two olfactory processing layers does not support this kind of learning due to a nested representation of odor intensity. We propose a basic circuit motif that transforms the nested monotonic intensity representation to a non-monotonic representation that supports intensity specific learning.

Flies are able to bridge a stimulus free interval between CS and US to form an association. It is unclear so far where the stimulus trace of the CS is represented in the fly's nervous system. We analyze recordings from the first three layers of olfactory processing with an advanced machine learning approach. We argue that third order neurons are likely to harbor the stimulus trace.

CONTENTS

1

INTRODUCTION

1.1 LEARNING AND MEMORY

Learning is the ability of an organism to change its behavior based on experience. Therefore an external input has to lead to the change of an internal state. By storing this new state in a memory, the organism is able to behave differently to a subsequent exposure to the same stimulus.

In the work of this thesis we work on the topic of associative learning. Here the organism learns to link initially independent stimuli or behaviors together by training. There is a common separation between two sub-types of associative learning, called operant conditioning and classical conditioning. In operant conditioning an innate behavior is strengthened or weakened by an external stimulus. Classical conditioning links an innate behavioral response to a previously neutral stimulus. We focus on classical conditioning in this thesis and continue therefore with a detailed introduction to the topic.

1.1.1 *Classical Conditioning*

Classical conditioning is the process of linking an innate behavioral stimulus response with an initially neutral stimulus. This requires first an unconditioned stimulus (US) that produces an innate unconditioned response (UR). For example, upon touching a hot surface one naturally pulls back the hand. And secondly it requires an initially neutral stimulus, the conditioned stimulus (CS), which elicits no behavioral response. This could

be the sound of a bell. In the training phase of classical conditioning the CS is temporally paired with the US by presenting them together. If the training was successful, that means if an association between both stimuli is formed, a subsequent presentation of the CS alone triggers a conditioned response (CR). It is worth making a distinction between UR and CR, as they are not necessarily identical.

Classical condition became famous by Ivan Pavlov's seminal work around the turn of the 20^{th} century ([1], therefore known as Pavlovian conditioning). In his experiments Pavlov trained dogs to associate the presentation of food with the sound of an electric bell. In this setup the presentation of food acts as US. A dog's natural (unconditioned) response to food is an increased saliva secretion rate. The sound of the bell acts as CS and elicits no behavioral response before training. In the training trial Pavlov presented first the sound followed by the presentation of food. After repeated training trails the sound alone triggered an increased salivation, indicating that the dogs indeed formed and association between US and CS.

A comprehensive overview about classical conditioning can be found in Murphy and Lupfer [2]. In the next section I will focus on the relevant aspects of classical conditioning for this thesis and describe the corresponding experimental paradigm used for acquiring the data that underlies the proposed models in this thesis.

1.1.2 *Olfactory Learning*

Drosophila melanogaster has been used successfully as model animal to investigate learning and memory on both a behavioral and functional level. A well-established paradigm of associative learning is an aversive olfactory learning paradigm introduced by Quinn et al. [3] and refined by Tully and Quinn [4]. As described above associative learning consists of linking an unconditioned stimulus (US) with unconditioned response (UR) with a conditioned stimulus (CS) to reveal a conditioned response

(CR). Olfactory learning uses an odor stimulus as CS and electric shock serves as aversive CS. The electric shock triggers a reflexive avoidance response.

In the experiment, flies are typically trained *en masse* in groups of about 50 flies. The flies are put into a training tube that is lined with an electric wire to deliver the shock. The tube's diameter is small such that flies cannot fly and are in contact with the electric wire. During the whole experiment, air is sucked through the tube at a constant rate. Odor is diluted in liquid and placed in an odor cup. The cup is designed such that it can be mounted onto the tube and allows air to flow through it. Odor evaporates in the air and is delivered to the flies in the tube.

During the training phase first a control odor is delivered to the flies. Then, after a temporal gap on the order of minutes the training odor is placed at the end of the tube and an electric shock is delivered by applying a voltage difference to the electric wire.

After training, flies are transferred into the middle of a "T-maze". The maze consists of two tubes extending in opposite directions, again with odor cups at the end and air flowing through both cups and tubes towards the middle of the maze where the air is sucked out. One cup contains the trained odor, the other the control odor. Flies can now move into either arm.

To evaluate the flies learning ability, flies in both tubes are counted and a preference index (PI) is calculated as the difference between the number of flies on both sides normalized by the total number of flies: $\mathrm{PI} = (\#_{\text{trained odor}} - \#_{\text{control odor}})/\#_{\text{total}}$. The PI ranges from -1 to 1, where 1 means all flies moved to the side of the trained odor, 0 equal number of flies in both arms and -1 that all flies went on the side of the control odor.

The choice of the flies in the maze will be influenced by their innate response to the odor. To avoid a misinterpretation of the PI a reciprocal control group is trained. For this group training and control odor are switched and $\mathrm{PI}_{\text{control}}$ is calculated. Then

a learning index (LI) is calculated as the mean PI of trained and reciprocal group as $LI = (PI + PI_{\text{control}})/2$. Assuming that innate odor preference and trained odor preference sum linearly the LI gives the net associative effect of training. It ranges from -1 to 1, where 0 means no associative training could be observed. A positive LI corresponds to a conditioned approach towards the trained odor in the test, a negative LI to a conditioned avoidance.

1.1.3 *Relative Timing of US and CS*

An experimental parameter that influences the net associative effect of training, i.e., the LI, is the temporal relationship between CS and US. The inter stimulus interval (ISI) expresses the relative timing between CS and US. It is the time between onset of the electric shock[1] and onset of the odor stimulus (see Fig. 1, upper left part for an illustration). Plotting the LI vs. the corresponding ISI results in a behavioral response curve sketched in the lower part of Fig. 1 (for the corresponding experiment, see Tanimoto et al. [5]).

For large ISIs on the order of tens of seconds, both positive and negative, the LI is not different from zero, which indicates that flies are not able to associate odor and shock.

For negative ISIs the odor precedes electric shock. We refer to cases with a stimulus-free interval between both stimuli as *trace conditioning*. The flies need to bridge this stimulus-free interval to form an association until the presentation of the electric shock. We call this neural stimulus correlate of the odor the olfactory stimulus trace. As indicated in the lower left part of Fig. 1, flies are indeed able to bridge this gap and show a conditioned avoidance response in the test situation (see also Galili et al. [6]). In this case the flies learn that the odor predicts the electric shock.

1 The electric shock is usually not delivered as continuous current through the wire but as pulse of electric shocks over a certain amount of time. We refer to this as one reinforcement stimulus.

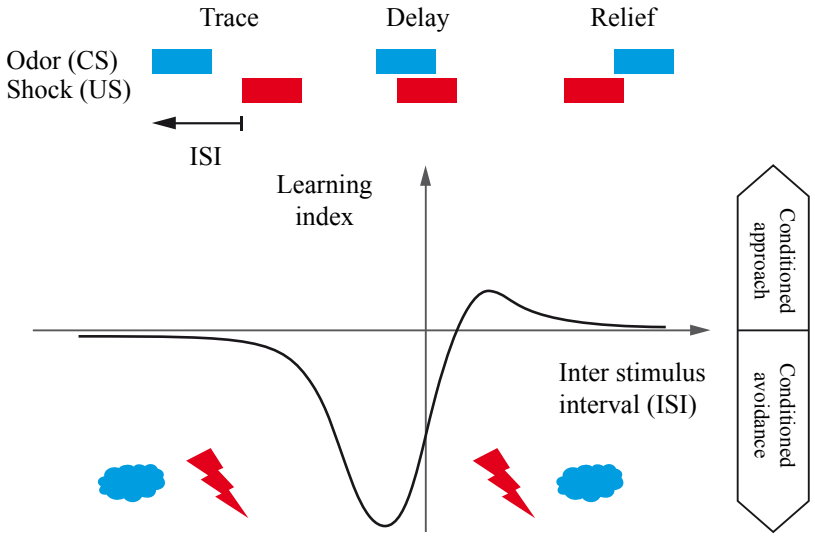

Figure 1: Timing-dependent behavioral response curve for aversive classical conditioning. In training, an unconditioned stimulus (US), e.g., electric shock, is paired with a conditioned stimulus (CS), e.g., an odor. Presenting the conditioned stimulus alone tests the associative strength. The timing between the two is characterized by the inter stimulus interval (ISI), which we define from onset of the shock to onset of the odor. The upper part shows different timing relations: When the odor (blue) precedes the electric shock and there is a stimulus free interval between the two, we refer to it as *trace conditioning*. *Delay conditioning* refers to the situation when odor precedes shock, but both stimuli overlap in time. For the reversed order, shock before odor, we use the term *relief learning*. The lower part depicts the learning index (LI) of a behavioral learning experiment with odor and shock as CS and US. The LI measures the associative effect between CS and US in an experiment, which leads to either a conditioned approach (positive LI) or conditioned avoidance (negative LI, see main text for a detailed explanation of the learning paradigm and how the LI is calculated). When the odor precedes the shock (negative ISIs), the trained odor is avoided in the test; whereas the trained odor is approached, if shock precedes the odor (positive ISIs). We interpret this bimodality of the behavioral response curve as a change in the hedonic value of the CS that depends on the relative timing of CS and US.

For shorter negative ISIs odor and shock stimulus overlap in time. We call this *delay conditioning*. Similar to trace conditioning, the odor signals the onset of electric shock and triggers a conditioned avoidance response after training. Compared to trace conditioning the LI is larger for a single training trial. Flies form a stronger association for shorter ISIs.

Interestingly the reversal of the order of both stimuli changes not only the sign of the ISI but also the sign of the resulting LI (see the right side of the lower part of Fig. 1). Flies show a conditioned approach towards the trained odor in the test. We interpret this as a change of the hedonic value of the US. The associative strength is less strong than for delay conditioning and the ISI range for learning is smaller.

The opponent process theory proposed by Solomon and Corbit [7] and Solomon [8] provides a basis to understand the change from a conditioned avoidance to conditioned approach. In this theory an unconditioned stimulus changes an organism's state from neutral to an evoked state A. After offset of the stimulus, the state variable does not simply decay back to the neutral state but rebounds into an opposite state B. From the opposite state it decays back to the neutral state. Applying this concept to electric shock as US the evoked state A corresponds to a state of pain; whereas the opposing state is a relief from pain. For positive ISIs the presentation of the odor falls into the time window where the fly is in a state of relief. Consequently the odor is positively associated and the flies show a conditioned approach in the test. We therefore refer to this type of learning as *relief learning*.

Tanimoto et al. [5] only used single training trials for all ISIs which led to the behavioral response curve depicted in Fig. 1. It is interesting to note however that repeated training trials lead to the same asymptotic LIs for trace and delay conditioning [6]. Galili et al. [6] could also show the effect of changing the ISI monotonically for repeated training trials. Increasing the ISI from trial to trial leads to a better behavioral performance than decreasing the ISIs. Past experience enables the fly to bridge longer time intervals between both stimuli.

1.1.4 *Stimulus Intensity*

Stimulus intensity affects the LI in a behavioral experiment. For electric shock as US, larger number of electric shocks increases the behavioral performance [4]. Increasing the voltage of the electric shock also increases the LI [4, 9].

At first increasing odor intensity also increases learning performance. For higher intensities learning performance however decreases again [10].

Yarali et al. [10] investigated the effect of a mismatch of odor intensity during training and test. In a first step three odor intensities are defined (low, medium and high). These are chosen such that learning performance increases with increasing intensity. Then groups of flies are trained at the medium intensity and tested either at low, medium or high intensity. Testing at the same medium intensity results in a baseline LI. When tested against a lower intensity the resulting LI is smaller than the baseline LI, as one would expect from the way the three intensities were chosen. But also when tested against a higher intensity the learning index is smaller than the baseline LI. We conclude that flies are able to form intensity specific associations of an odor.

1.2 THE FRUIT FLY *drosophila melanogaster*

For more than 100 years the fruit fly *Drosophila melanogaster* has been a widely used model organism in various fields of biology, including genetics, behavior, learning and memory and development. Despite the relatively small number of about 300 000 neurons in their brain it shows a remarkable behavioral diversity. For a review of the history of research with *Drosophila melanogastsr* see Bellen et al. [11].

1.2.1 *Neuronal Organization of the Olfactory System*

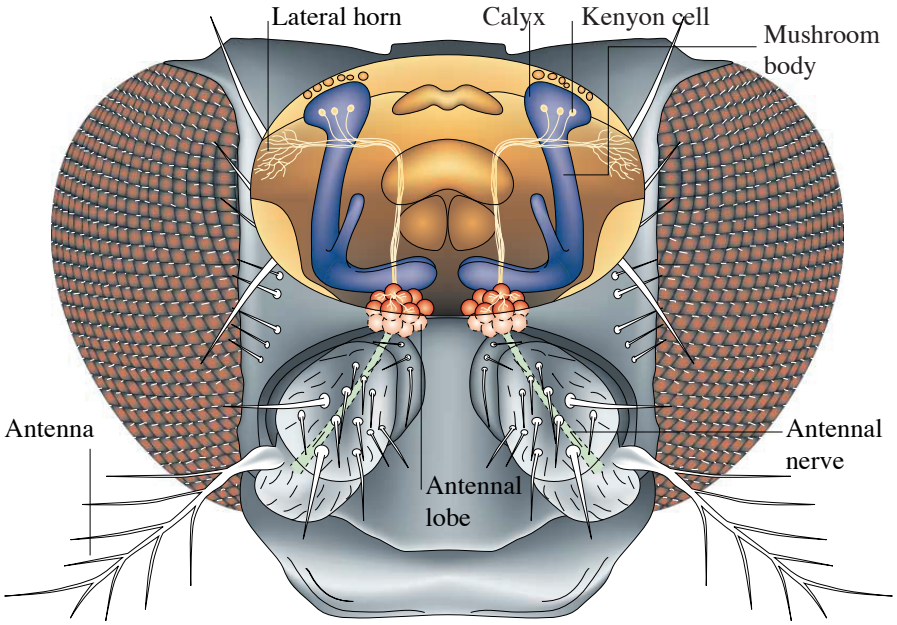

Figure 2: Sketch of *Drosophila* head with olfactory pathway. Odor molecules bind to olfactory receptor neurons that express receptors in the antennae. Olfactory receptor neurons project via the antennal nerve (green) to the antennal lobes where they form synapses with projection neurons in anatomical clusters called glomeruli (red sphere-like structures). Projection neurons (yellow fibers) carry odor information to the lateral horn and the mushroom body calyx (mushroom body depicted in blue). In the mushroom body calyx they form synapses with Kenyon cells. Taken from [12].

The neuronal organization of the olfactory system shares remarkable similarities between different species of invertebrates, but also between invertebrates and vertebrates. [12–16]. Here I concentrate on the olfactory system of *Drosophila melanogaster*.

The first step of odor detection happens on sensory hairs, called sensilla, on antennae and maxillary palps (see Fig. 2 for an illustration). Odor molecules enter through pores in the sensilla, which house the dendrites of first order sensory neurons, called olfactory receptor neurons (ORNs) [17]. Upon uptake of sen-

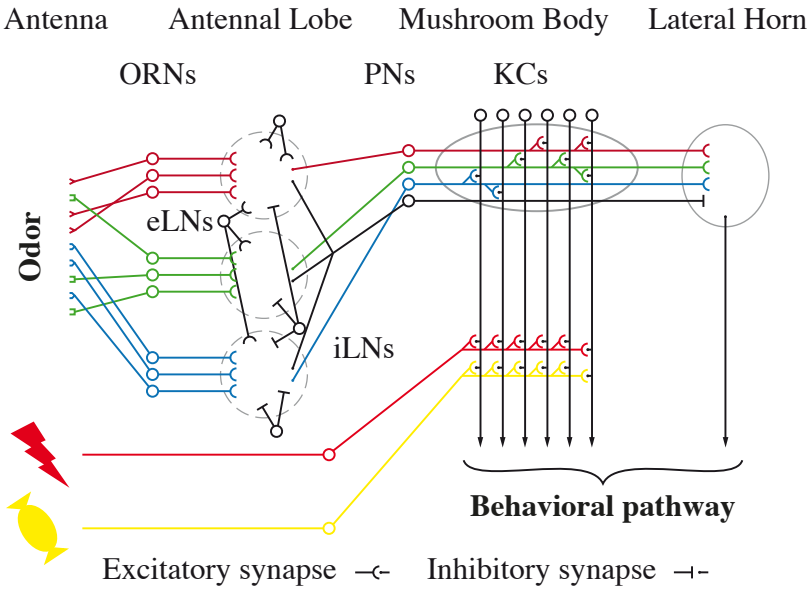

Figure 3: Schematic depiction of fruit fly olfactory system. It is organized in a hierarchical layered structure. In the antenna, olfactory receptors (ORs) expressed by OR neurons (ORNs) bind odor molecules, which leads to spiking activity of ORNs. Each ORN typically expresses only one receptor type. ORNs project to the antennal lobe (AL), the first brain structure of olfactory processing. All ORNs expressing the same receptor type converge onto the same neuronal structure, called glomerulus (depicted as gray dashed circle). The convergence ratio is high, between 10 to 100 ORNs project to the same glomerulus. In the glomeruli ORNs form excitatory synapses with projection neurons (PNs). Odor information is processed in the AL by different types of local neurons (LNs), both inhibitory and excitatory (iLNs, eLNs). LNs are both uni- and multi-glomerular, innervating only one, a few or almost all glomeruli. PNs transfer the odor information to two distinct third order regions, the mushroom body (MB) and the lateral horn (LH). In the MB PNs form synapses with $\sim$2500 Kenyon cells (KCs). Connections are quasi-random and sparse. The MB is the center of associative learning where also the appetitive and aversive reinforcement signals are transmitted. Odor representation in the LH is topographically structured. The LH provides an innate evaluation of odors. The output of both structures drives the behavioral response.

sillum lymph, odorant molecules are transported via binding proteins to the olfactory receptors expressed by the ORNs. A transduction cascade leads to spiking activity in ORNs. These early steps of olfactory transduction, including uptake of odorant molecules by olfactory receptors and the spike generation within the ORN have been studied and modeled in detail [18–21].

Each sensillum houses dendrites from two to four ORNs [22, 23]. Each individual ORN expresses only one functional receptor type [24]. Around 50 different olfactory receptor types are known, and each receptor type is expressed by 10 to 100 cells [23, 25–27]. The olfactory system includes around 1200 ORNs. ORNs send their axons to the first processing stage in the fly olfactory system, the antennal lobe (AL). The antennal lobe consists of anatomically distinct neuropils called glomeruli. All ORNs expressing the same receptor type project to the same glomerulus [24], giving a total number of around 50 glomeruli. Glomerular positions are stereotypic between types, which makes identification of individual glomeruli in different flies possible [28–30].

In the glomeruli ORNs form excitatory synapses with second order neurons, the so-called projection neurons (PNs). Just as individual ORNs only innervate a single glomerulus, excitatory PNs are monoglomerular, meaning they only receive input from one glomerulus [31]. On average there are three excitatory PNs per glomerulus, making a total number of around 150 PNs. On the other hand multiglomerular PNs are mainly inhibitory and innervate many glomeruli. In addition to ORNs and PNs a network of local neurons is present within the AL. Excitatory and inhibitory LNs can be local to one glomerulus or connect multiple glomeruli with each other [32–34].

From the AL PNs convey the olfactory information to two distinct brain regions. Uniglomerular excitatory PNs project to the mushroom body (MB) and the lateral horn (LH), whereas the majority of inhibitory multiglomerular PNs only project to the LH [35–38]. In the MB calyx, PNs form excitatory synapses with Kenyon cells (KCs). The connection pattern between AL and

MB is thought to be quasi random and sparse [39]: PNs form synapses with around 5 percent of the around 2500 KCs [12]. In contrast to the random connections from AL to MB, connections to the LH are highly stereotyped and the lateral horn contains less neurons than the MB [37, 40].

The neural organization of the later stages after MB and LH is less clear. The synaptic output of KCs converges onto only a few output neurons (∼40) [41]. The valence of a trained odor is suggested to be specific to the activity of a small subset of MB output neurons [42].

1.2.2 *Processing of Olfactory Information*

In the previous chapter I described the anatomical organization of the olfactory system. Here I will explain how odors are coded in the olfactory system and how the representation changes from one anatomical layer to the next.

The first order neurons are the ORNs. In the absence of input ORNs exhibit a level of baseline firing rate [43]. Upon binding of odors to olfactory receptors spike rates quickly peak and ORNs maintain a stable spiking activity [23, 43–47]. Instead of increasing the spike rates, ORN baseline firing rates can also be suppressed in response to an odor [43–45]. ORNs of the same type fire independently [48]. ORN response profiles are diverse: Some ORN types are broadly tuned and activated by many ligands; whereas other are narrowly tuned, responding strongly only to very few to single ligands. Most ligands activate several ORN types [43]. Increasing odor intensity leads to higher firing rates in ORNs that saturates for high intensities. The dynamic range typically covers several orders of magnitude of odor intensity. The sensitivity of different ORN types varies depending on the ligand, which means that for higher intensities also the number of activated ORN types increases [43]. The dynamics of ORN responses are to a certain degree invariant under intensity changes [49, 50]. On the level of ORNs odors are encoded

by the combination of activated ORNs with respective firing rates.

ORNs are the main excitatory drive for PNs. Depending on the receptor, around 10 to 100 ORNs express the same receptor type and converge onto the same glomerulus [23, 51]. As a consequence, PN response are more sensitive to smaller intensities and less variable from trial-to-trial compared to ORN response [52]. PN response also peak earlier than ORN responses [52, 53] and they are more sensitive to small changes in ORN firing rates than to changes at high frequencies [54].

ORNs and PNs also drive a network of excitatory and inhibitory local neurons in the AL that shape the odor representation and responses of PNs. This network has been studied in great detail [33, 34, 52, 53, 55–57]. Lateral inhibition of LNs between different glomeruli lead to a transformation that has been termed input gain control [54]. For higher intensities more ORNs are activated and activated ORNs increase their firing rate. In turn this also increases lateral inhibition between glomeruli, leading to a more balanced response of PNs with increasing odor intensity. Another effect of lateral inhibition is contrast enhancement of odor representation of different odors [54, 58].

From the AL PNs project to the LH and MB. In the MB calyx they form synapses with KCs, the MB intrinsic neurons. KCs in the MB respond sparsely and stereo-typically to different odors [59–61]. In contrast to the AL, KC responses are not conserved between different flies [62]. On the level of KCs the representation of an odor is a sparse combinatorial pattern of activated cells. The activation of LH neurons is anatomically patterned. Inhibitory neurons innervating the whole AL convey a summed inhibitory input to the LH, which leads to non-monotonic responses of at least some LH neurons [37, 40].

One aspect I disregarded in this introduction of odor processing are so-called labeled line odors. These odors most likely have a specific innate meaning to the fly, e.g., pheromones [63–67] and activate only a single ORN type. Although this labeled

line coding is very interesting from a behavioral and evolutionary point of view, in the context of learning and memory with respect to innately neutral odors, which I consider in this thesis, I will not go into more detail.

1.3 MODELING OLFACTION

After giving an overview about both anatomical and functional organization of the *Drosophila melanogaster* olfactory system, I will now introduce models of olfaction and learning that touch the topics covered in the work of this thesis.

1.3.1 *Odor Coding*

Flies are able to detect and discriminate different odors and concentration, which can be tested with the classical conditioning paradigm introduced above ([3, 4, 10], but also other insects, e.g., bees [68, 69] and mice [70]). But how are odors encoded in the fly's nervous system? Most odors activate more than one receptor type and consequently more than one glomerulus directly. As such the quality of an odor cannot be determined by extracting information from a single ORN or glomerulus but it is encoded in the combined activation pattern of all glomeruli. This is what we call a combinatorial code. A fitting auditory analogy has been suggested by Galizia and Szyszka [71]. In music a chord consists of several notes. The note itself does not reveal the chord, but changing only one note within a chord results in a very different sound.

We can describe a combinatorial code in mathematical terms by a multi-dimensional space. Each dimension in the space corresponds to the response of one unit of the code, which is in our case the response of one glomerulus. The AL activity of the $\sim$50 glomeruli can then be described by a vector of length 50, each entry indicating the activity of a given glomerulus. To consider temporal coding aspects of coding one analyzes the evo-

lution of the vector over time, which is a trajectory in the multi-dimensional space. So in each instant of time the state of the AL network corresponds to a point in the multi-dimensional space.

How can this mathematical representation then help to understand coding of odors? Fdez Galán et al. [72] performed a set of experiments in honeybees in which they recorded optically PN activity in the AL in response to a set of odors. Before odor presentation the activity is in a resting state that fluctuates around the origin. Upon odor delivery the activity quickly changes and reaches an odor specific fix point in the multi-dimensional space. The fix point is stable during the time of odor presentation and repeated presentation of the stimulus results in similar trajectories and fix points. After odor offset the activity ceases and the trajectory decays back to the origin. To visualize the evolution of the trajectories the authors performed a Principal Component Analysis (PCA)[2] [73, 74] on the multi-dimensional AL space. It turns out that more than half of the variance in the data is explained by the first three principle components.

Following the result that attractor points in the AL space represent odors this opens the possibility to separate and classify different odors within this space. A straight forward approach is the *linear discriminant analysis* (LDA, [75]). It belongs to the class of supervised machine learning models and classifies based on a geometrical distance measure between points. For KC responses of flies Turner et al. [60] employed this method to classify odors responses. First they determined a mean odor attractor for each odor from repeated measurements. Then, for each individual response, they calculate the Euclidean distance to each of the mean odor attractors. Its smallest distance to an at-

2 PCA is an orthogonal basis transformation. The new basis is chosen such that the new variables, called principle components, are linearly uncorrelated. The first principle component is along the axis of greatest variance in the original data set, the second along the second along the axis of second greatest variance and so on. PCA can be used to analyze the internal variance structure of multi dimensional data. An important measure is the variance explained by each principal component. For example, if most of the variance within a data set is explained by only the first few principle components, it might suffice to analyze the data in a lower dimensional space.

tractor classifies the response. Implicitly this introduces separating planes symmetrically between all attractors that determine the identity of each response.

A more sophisticated approach towards classifying odor response are *support vector machines* (SVMs) [76–80]. An advantage to the LDA is that also non-linear separating planes might be used for classification. SVMs work on a higher dimensional space than the original data by first projecting to this space with an appropriate kernel function. The SVM then finds a separating hyperplane that maximizes the margin between two classes. With the right kernel function also differences of only a small subgroup within the observed variables can be exploited for a classification. On the other hand SVMs require a finer tuning of parameters and an appropriate choice of kernel functions.

1.3.2 *Relative Timing of Odor and Shock*

As introduced above, changing the relative timing of CS and US changes the hedonic value of the CS: For odor - shock training, punishment is turned into reward. A question arising is whether different competing processes take place or if there is only one underlying process that explains both sides of the curve shown in Fig. 1. The latter possibility is explored in a model proposed by Drew and Abbott [81]. As basis they recognize the similarity between the time dependent experimental outcome and the effect of spike-timing-dependent plasticity (STDP).

STDP is an activity dependent synaptic modification as a result of paired firing of pre- and post-synaptic cells [82, 83]. Similar to Hebbian learning [84], the synaptic weight changes if both cells fire within a time frame of several tens of milliseconds. For Hebbian learning the change of synaptic weight is zero if both cells are active at different times and positive if both cells are active at the same time. STDP extends this mechanism with an asymmetric timing component. If the pre-synaptic cell repeatedly fires shortly before the post-synaptic cell the synaptic

weight increases, a process termed long-term potentiation. If the order of firing is reversed, i.e., the pre-synaptic spikes arrive repeatedly after the post-synaptic spike, the synaptic weight decreases, a process called long-term depression ([82], see [85] for a review). Plotting the change in synaptic efficacy against the relative timing of pre- and post-synaptic spike results in a bimodal efficacy curve. Following the first experiments this phenomenon has been described both by phenomenological and detailed mechanistic models [86–91] . More complex combinations of spikes lead to different forms of efficacy curves [92]. STDP is believed to underlie learning and information storage in neuronal circuits [93–97].

The bimodal synaptic efficacy curve qualitatively resembles the behavioral response curve of olfactory conditioning, but with time-scales different by three order of magnitude. In their model Drew and Abbott [81] propose a mechanism that bridges from the time-scale relevant for synaptic changes to the time-scale relevant for behavior. Therefore they first assume that STDP takes place in at the synapse detecting the coincidence of odor and shock. Although not directly shown for *Drosophila*, STDP could be observed in Kenyon cells of locust [98]. Second they assume prolonged firing of pre-synaptic cells at a high firing frequency. The prolonged firing mainly bridges the time between odor and shock. Appropriate timing of spikes and a number of repetitions leads to either synaptic facilitation or depression onto the conditioned avoidance circuit. In the test this will trigger the experimentally observed conditioned response.

The described mechanism elegantly applies the idea of STDP to serve as coincidence detection on a behaviorally relevant time-scale. The proposed neurons are in all likelihood Kenyon cells, that serve as coincidence detector of odor and shock in the *Drosophila* olfactory system [99]. The known properties of Kenyon cells however do not fit with the key assumptions of prolonged firing and high rates [60, 62, 100].

1.3.3 *Convergence of Odor and Shock Signal in Kenyon Cells*

Kenyon cells are necessary for flies to form olfactory memories (as recently published, also for visual memories [101]). When mushroom bodies are not intact, flies are not able to form associative memories [102–104]. Investigations with the temperature sensitive dynamin transgene *shibire*^{ts} revealed the role of KC output synapses. In this setting, synaptic transmission can be blocked by raising the temperature. Blocking output synapses from KC during training has no effect on memory acquisition. However blocking output synapses during test impairs memory retrieval, arguing for the memory to be stored upstream of KC output synapses [105–108]. As shown by several studies, KCs are also sufficient for the formation of aversive olfactory memories [109–111].

Electric shock activates a dopaminergic signal that is delivered to all KCs [112–116]. Dopamine binds to a G-protein-coupled receptor (GPCR) on KCs, which activates the G protein within the cell. An odor on the other hand only activates a small subset of KCs, which leads to an increase in intra-cellular calcium (Ca^{++}) concentration [59, 117, 118]. Both signals most likely converge on the Ca^{++}-calmodulin-sensitive rut-adenlyl cyclase [99, 119]. During training the adenlyl cyclase in odor activated KCs is synergistically activated which leads to an increased production of cAMP within these cells [99, 119]. cAMP in turn strengthens the output synapses onto the conditioned avoidance circuit [120, 121]. In the test situation the fly has to choose between the trained odor and a different odor. The trained odor activates the same cells as before, which leads to a stronger input to the conditioned avoidance circuit compared to the untrained odor. Hence the fly will move away from the trained odor, showing a conditioned avoidance response.

An adapted model by Rospars et al. [21] can describe the intracellular reaction dynamics in the KCs. A set of coupled differential equation calculates the amount of reaction components over time. In the first step a transmitter (in this case dopamine, which is activated by electric shock as described above) binds

to the G-protein-coupled receptor and forms a complex that dissociates again. When the complex is activated it acts as catalyst of the dissociation of the trimeric G protein into an activated and non-activated sub-unit. The activated sub-unit now interacts with adenylate cyclate and forms an activated complex. The activated complex dissociates again and the trimeric G protein sub-units reassemble again. The amount of activated G-protein - adenylate cyclase complex serves as output of the model.

1.3.4 *Intensity Coding*

In a sensory modality that represents increasing input intensity by monotonically increasing the neuronal response, the representation of lower intensities is nested within the representation of higher intensities. This is for example the case in olfaction on the level of ORNs and PNs, where an increase in odor intensities leads to both an increase in firing rate of active neurons and the to more neurons responding to a specific odors at higher concentrations (for *Drosophila*, see e.g., [43]). Strikingly however flies are able to form intensity specific memories [10], which argues that they need a neuronal representation of odor intensity that is not nested, arguing for non-monotonically responding neurons.

In a model by Luo et al. [58] non-monotonically responding neurons arise on the third level of olfactory processing that is in KCs. The main focus of their model is response properties of both third order neurons, KCs and LH neurons. Measured ORN responses serve a input to model. They are described by spike rates taken from the extensive data set of Hallem and Carlson [43]. It consists of responses of 24 different receptor types to a panel of 110 odors at at the same odor intensity. Responses to a subset of ten odors were also recorded at three additional intensities. In the next step the resulting PN responses are calculated by transforming the ORN responses by a non-linear functions suggested by Olsen et al. [54]. This nonlinearity leads on the one hand to a response normalization of

PN response magnitude for different odors. On the other hand it decreases the correlation between responses patterns of different odors, thus increasing the selectivity of odor response patterns. Additionally random noise is added to the calculated PN responses.

Serving as input to third order neurons the calculated PN responses are multiplied by a synaptic weight and then compared to a pre-determined threshold. If the activation is above the threshold, the third order neuron responds to the odor, otherwise it remains silent. For an analysis of response strength of third order neurons the authors calculated a response probability of each third order neuron based on repeated trials with the same odor. Following the suggested role of LH neurons in the literature of being responsible for innate odor specific responses, weights to the lateral horn are tuned such that each neuron responds almost exclusively and reliably to a single odor, independent of odor intensity. This seems to be in contrast to more recent studies suggesting non-monotonic responses of LH neurons for increasing odor intensities [37, 40].

Odor intensity specific responses arise on the level of modeled KCs. Again the authors follow experimental results and build their model accordingly. The twenty modeled PNs deliver direct excitatory input to 2500 KCs with a quasi-random connection pattern as suggested by Murthy et al. [62] (for a more recent study, see also [39]). The connections are sparse, each PN makes functional connections to only five percent of KCs and each KCs only receives input from about five percent of PNs. As a consequence model KCs respond sparsely to an odor as observed in experiments [60]. Inhibitory input is provided by one global inhibitory neuron that sums the activity of all excitatory PNs and projects to all KCs. The analysis of KC responses to different odor intensities reveals both monotonic and non-monotonic responding KCs that have their maximum of activation probability at an intermediate odor intensity. The layout and the synapses of the inhibitory neuron are the reason for non-monotonic responding KCs. When a KC receives input from a PN that is tuned to higher intensities with a strong synapse and at the same time input from a PN tuned to low in-

tensities with a smaller synaptic weight, the PN tuned to higher intensities will drive the inhibitory neuron stronger at intensities, which leads to a decrease in response probability. The large number of KCs and the random allocation of synaptic weights suggest that there will always be a subset of KCs that receive input with this specific configuration of weights and PNs. If this is however enough to explain intensity specific coding remains an open question and awaits a detailed investigation.

2

EVENT TIMING IN ASSOCIATIVE LEARNING: FROM BIOCHEMICAL REACTION DYNAMICS TO BEHAVIOURAL OBSERVATIONS

2.1 SUMMARY

Flies are able to form associative memories. For aversive olfactory conditioning the relative timing between odor and shock determines the hedonic value of the conditioned stimulus. Presenting the odor before the shock leads to conditioned avoidance (delay and trace conditioning). When shock precedes the odor flies will subsequently show conditioned approach towards the trained odor.

We present a model that explains this peculiar behavior as the effect of the same biochemical reaction cascade. We combine results from different studies and species to model the cAMP reaction cascade in Kenyon cells. The odor is represented as Ca^{++} influx into the cell and increases both the activation and deactivation rate of an activated G-protein adenylate cyclase complex in the same way. We interpret the amount of activated complex as proxy for the strengthening of the synaptic output of the Kenyon cells onto the conditioned avoidance circuit.

By design, the Ca^{++} induced increase of the reaction constant serves both as coincidence detector of odor and shock and has a bi-modal influence on the reaction product based on relative timing. When the Ca^{++} influx happens during the activation of the complex this leads to more activated complex. In contrast Ca^{++} influx during deactivation of activated complex leads to an overall smaller amount of activated complex.

Our model explains the bi-modal behavioral response curve observed in the experiment.

2.2 REFERENCE

This work was performed together with A. Yarali, R. Tanimoto and Andreas V. M. Herz. I presented a poster of the final work at CoSyne 2012.

Ayse Yarali, Johannes Nehrkorn, Hiromu Tanimoto, Andreas VM Herz (2012). Event timing in associative learning: From biochemical reaction dynamics to behavioral observations. Cosyne Abstracts 2012, Salt Lake City USA.

The paper has been published in Plos One under the reference

Yarali A, Nehrkorn J, Tanimoto H, Herz AVM (2012) Event Timing in Associative Learning: From Biochemical Reaction Dynamics to Behavioural Observations. PLoS ONE 7(3): e32885. doi:10.1371/journal.pone.0032885

OPEN ACCESS Freely available online

PLoS one

Event Timing in Associative Learning: From Biochemical Reaction Dynamics to Behavioural Observations

Ayse Yarali[1]*, Johannes Nehrkorn[1,2,3], Hiromu Tanimoto[1], Andreas V. M. Herz[2,3]

1 Max Planck Institute of Neurobiology, Martinsried, Germany, **2** Ludwig-Maximilians-Universität München, Department Biology II, Division of Neurobiology, Martinsried, Germany, **3** Bernstein Center for Computational Neuroscience, Munich, Germany

Abstract

Associative learning relies on event timing. Fruit flies for example, once trained with an odour that precedes electric shock, subsequently avoid this odour (punishment learning); if, on the other hand the odour follows the shock during training, it is approached later on (relief learning). During training, an odour-induced Ca^{++} signal and a shock-induced dopaminergic signal converge in the Kenyon cells, synergistically activating a Ca^{++}-calmodulin-sensitive adenylate cyclase, which likely leads to the synaptic plasticity underlying the conditioned avoidance of the odour. In *Aplysia*, the effect of serotonin on the corresponding adenylate cyclase is bi-directionally modulated by Ca^{++}, depending on the relative timing of the two inputs. Using a computational approach, we quantitatively explore this biochemical property of the adenylate cyclase and show that it can generate the effect of event timing on associative learning. We overcome the shortage of behavioural data in *Aplysia* and biochemical data in *Drosophila* by combining findings from both systems.

Citation: Yarali A, Nehrkorn J, Tanimoto H, Herz AVM (2012) Event Timing in Associative Learning: From Biochemical Reaction Dynamics to Behavioural Observations. PLoS ONE 7(3): e32885. doi:10.1371/journal.pone.0032885

Editor: Björn Brembs, Freie Universitaet Berlin, Germany

Received August 19, 2011; **Accepted** February 5, 2012; **Published** March 30, 2012

Funding: This work was supported by the Bundesministerium fuer Bildung und Forschung (BMBF) through the Bernstein Focus Neural Basis of Learning (H.T. and A.V.M.H.). The funders had no role in study design, data collection and analysis, decision to publish, or preparation of the manuscript.

Competing Interests: The authors have declared that no competing interests exist.

* E-mail: yarali@neuro.mpg.de

Introduction

Predicting future events is a key to survival. For example, if a sensory stimulus typically precedes an aversive event, this relationship will be learned to trigger anticipatory behaviour, such as avoidance [1]. On the other hand, a stimulus that occurs after an aversive event has subsided will be learned as a predictor for relief [2,3] or safety [4,5] and will induce approach. Event timing, therefore, determines which of the two opposite learned behaviours is established, as shown in various species including man [6–12]. *Drosophila* olfactory associative learning is well-suited for studying this phenomenon (Fig. 1) [11,13–17]: Flies learn to avoid an odour that precedes electric shock during training (i.e. punishment learning); whereas an odour that follows the shock is subsequently approached (i.e. relief learning).

In an attempt to explain punishment and relief learning in fruit flies, Drew and Abbott [18] propose a model circuit where the odour activates a large number of pre-synaptic neurons; while the shock impinges upon a common post-synaptic neuron that mediates the conditioned avoidance. For both types of neuron, the authors assume high firing rates that decay over several seconds upon the termination of the respective stimuli. Within this model circuit, a spike-timing-dependent plasticity (STDP) rule operating at the millisecond-scale can account for the effect of relative odour-shock timing on the conditioned behaviour, which occurs at the scale of several seconds. While demonstrating that slowly decaying spiking activity can enable STDP to function over long intervals, this model does not capture fruit fly olfactory learning, as the corresponding empirically measured odour responses in the Kenyon cells are sparse and short-lasting [19–21], violating the model's key assumption.

Here, we propose an alternative model motivated by cellular and biochemical data. In the *Drosophila* brain, individual odours activate small, specific groups of Kenyon cells increasing their intracellular Ca^{++} concentration [22–24]; whereas shock induces a dopaminergic reinforcement signal, which is also delivered to the Kenyon cells [25–29]. These two inputs likely converge on the Ca^{++}-calmodulin-sensitive adenylate cyclase, *rutabaga*; this process seems necessary and sufficient in the Kenyon cells for olfactory learning [30–33]. Thus, during punishment training, this adenylate cyclase is synergistically activated in the specific trained odour-responding Kenyon cells [34,35]; the resulting cAMP signalling then likely strengthens the output from these cells to the conditioned avoidance circuit (Fig. 2) [36]. Those Kenyon cells that respond to a control odour that is presented sufficiently before or after the shock also receive both inputs, but separated in time; consequently, less cAMP is produced [34] and the output of these Kenyon cells is strengthened less, if at all. Then, at test, flies are typically given the choice between the trained odour, which, due to the strengthened output of the respective Kenyon cells, can trigger conditioned avoidance, and the control odour, which does not trigger conditioned avoidance, as the output of the corresponding Kenyon cells has remained weak. To summarize, with respect to punishment learning, a particular, Ca^{++}-calmodulin-sensitive adenylate cyclase seems to be the critical detector of the odour-shock convergence.

The biochemical properties of the corresponding Ca^{++}-calmodulin-sensitive adenylate cyclase in *Aplysia* (AC-AplA, [37]) have been analyzed in detail. During gill withdrawal reflex conditioning, a Ca^{++} influx due to siphon-touch and a tail-shock-induced serotonergic signal converge on this adenylate cyclase (Fig. 2) [38–40], which is

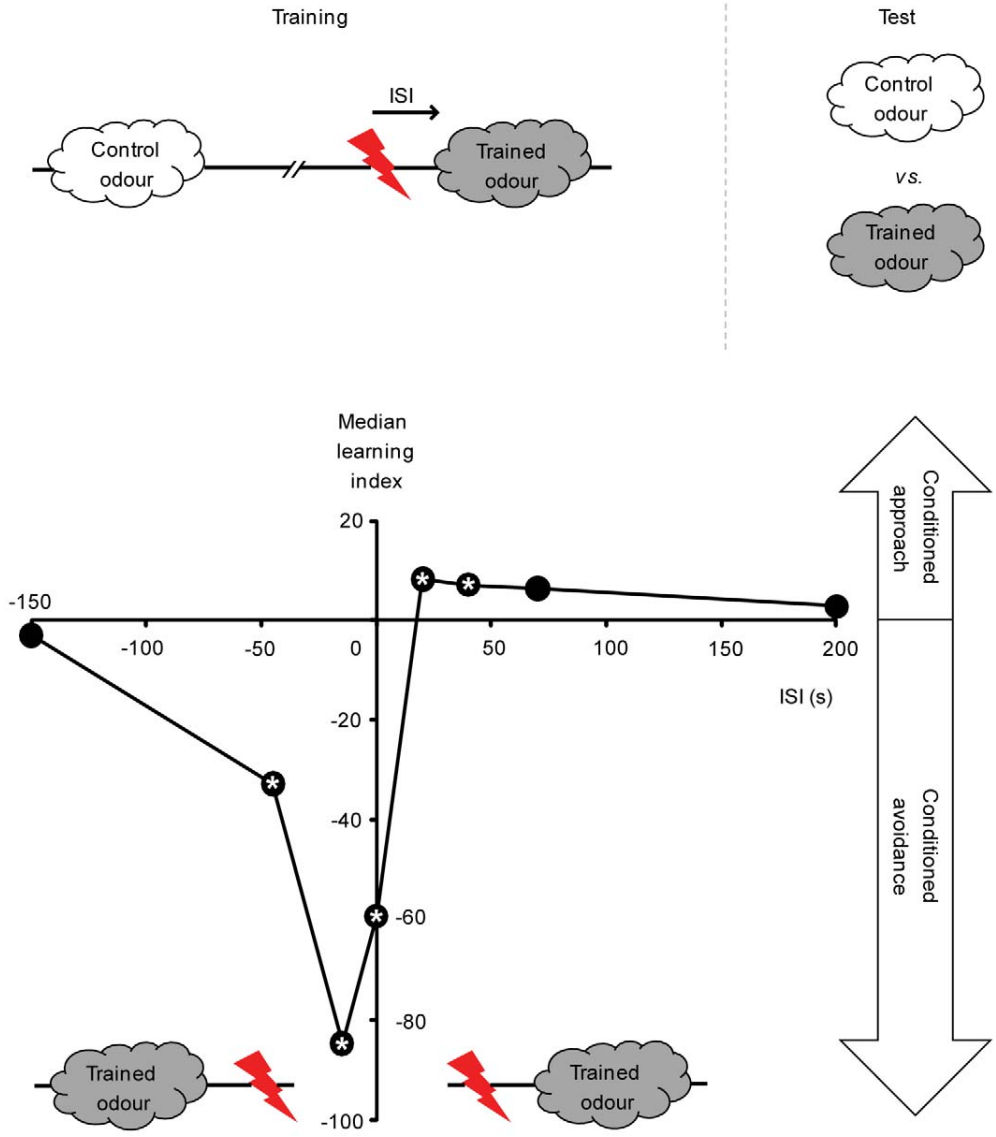

Figure 1. Event timing affects associative learning. Fruit flies are trained such that a control odour is presented alone, whereas a trained odour is paired with pulses of electric shock as reinforcement. Across groups, the inter-stimulus interval (ISI) between the onsets of the trained odour and shock is varied. Here, ISI is defined such that for negative ISI values, the trained odour precedes shock; positive ISI values mean that the trained odour follows shock. For each ISI, two fly subgroups are trained with switched roles for two odours (not shown). During the test, each subgroup is given the choice between the two odours; the difference between their preferences is taken as the learning index. Positive learning indices indicate conditioned approach to the trained odour, negative values reflect conditioned avoidance. Very long training ISIs support no significant conditioned behaviour. If the odour shortly precedes or overlaps with shock during training (ISI = −45 s, −15 s or 0 s), it is strongly avoided in the test (punishment learning). If the odour closely follows the shock-offset during training (ISI = 20 s or 40 s), flies approach it in the test (relief learning). *: $P<0.05/8$ while comparing to zero in a sign test. Sample sizes are N = 8, 24, 34, 47, 24, 35, 12 and 12. Data from [15], with permission from Informa healthcare.
doi:10.1371/journal.pone.0032885.g001

sensitive to the relative timing of the two inputs [41–43] (see Results for details). We test whether this biochemical phenomenon observed in *Aplysia* (and in rats [44]) can serve as a mechanism for the effect of event timing on associative learning as found in *Drosophila*. A computational approach allows us to overcome the shortage of behavioural data in *Aplysia* and biochemical data in *Drosophila* by combining findings from both systems.

Results

In an *Aplysia in vitro* neural membrane preparation [41–43], a transient serotonin input activates the adenylate cyclase; upon cessation of serotonin, the adenylate cyclase activity returns to the base-line. This effect of serotonin is modified by Ca^{++}. If Ca^{++} precedes serotonin by a short time, the adenylate cyclase is activated more rapidly so that the cAMP production exceeds the serotonin-only situation. If, however, Ca^{++} closely follows serotonin, the adenylate cyclase is deactivated faster, resulting in a cAMP production below the serotonin-only case. We implement this property of the adenylate cyclase in two alternative models [45,46]. This makes it possible to quantitatively explore whether and how far this biochemical phenomenon can explain the effect of event timing on learning; to this end, we simulate a key *Drosophila* experiment (Fig. 1). In addition, we test *in silico* for the

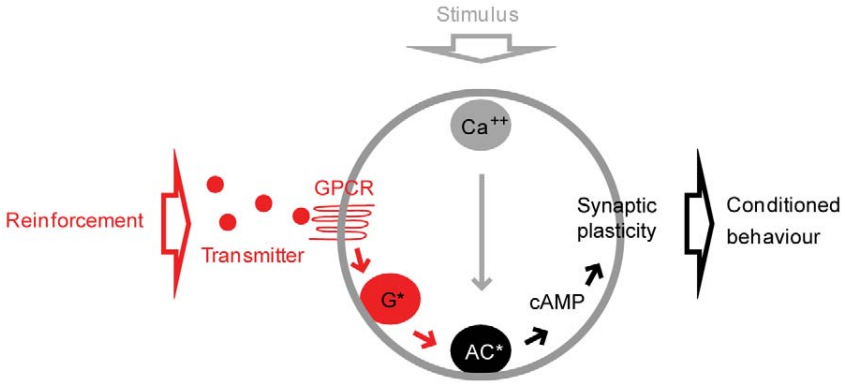

Figure 2. Adenylate cyclase as a molecular coincidence detector. In a variety of associative learning systems, a potential coincidence between the trained stimulus and the reinforcement is detected at the pre-synapse by a particular kind of adenylate cyclase. The stimulus acts on the respective neurons, raising the intracellular Ca^{++} concentration. The reinforcement induces the release of a transmitter that binds to its respective G protein coupled receptors (GPCR) on the very same neurons and activates the G protein (G*). If stimulus and reinforcement are appropriately timed, the two types of input act synergistically on the adenylate cyclase (AC*), triggering cAMP signalling, and thus lead to the strengthening of the output from these neurons to the respective conditioned behaviour pathway.
doi:10.1371/journal.pone.0032885.g002

effects of parameter changes and relate our results to behavioural findings in *Drosophila*.

Stimulation of the adenylate cyclase by the transmitter

We use the model by Rospars et al. [46] as a general framework to describe post-receptor G protein signalling. Adapting this model to our case (Fig. 3A), the shock-induced transmitter (Tr) binds to the G protein coupled receptor (GPCR) to form a complex (Tr/GPCR), resulting in receptor activation (GPCR*). GPCR* then dissociates the trimeric G protein ($G\alpha\beta\gamma$) into an activated α-subunit ($G\alpha^*$) and the $\beta\gamma$-subunits ($G\beta\gamma$). $G\alpha^*$ either spontaneously deactivates ($G\alpha$) to reassemble with $G\beta\gamma$, or it interacts with the adenylate cyclase (AC) to form an enzymatically active complex ($G\alpha^*/AC^*$), which is prone to dissociation into inactive AC and $G\alpha$. The concentration of the $G\alpha^*/AC^*$ complex, i.e. the activated adenylate cyclase, serves as the output variable of the system.

We stimulate this model with a transient transmitter input (Fig. 3B, left; see the Materials and Methods for details), which mimics the *in vitro* experiments in *Aplysia* (Fig. 1A of [42]). When the reaction rate constants k_5 and k_{-5} are appropriately adjusted (for a detailed sensitivity-analysis, see Fig. 5A), the concentration of $G\alpha^*/AC^*$ first rises to a peak within ~20 s and then decays back to zero within the next ~100 s (Fig. 3B, left), closely matching the corresponding *Aplysia* data (Fig. 4A of [42]); the deactivation of the adenylate cyclase in the model is slightly slower than the experimental observations.

Effect of Ca^{++}

As discussed above, in *Aplysia*, a brief serotonin input results in cAMP production; Ca^{++} in turn bi-directionally modulates the amount of this cAMP production, depending on its timing relative to serotonin [41–43]. Critically, at the steady state, Ca^{++} and serotonin have no synergistic effect on cAMP production [41–43]. In these biochemical experiments, Ca^{++}, bound to calmodulin, seems to interact with the adenylate cyclase [43] and the Ca^{++}-effect on adenylate cyclase is delayed by 2–3 s relative to the effect of serotonin [42,43]. As a simple way to account for all these findings in our model, we allow Ca^{++} to transiently increase the rate constants for both the formation and the dissociation of the $G\alpha^*/AC^*$ complex (k_5 and k_{-5}) with a delay of 2.5 s (Fig. 3A; see the Materials and Methods for details). For simplicity we exclude from our model the biochemical step(s) leading to the Ca^{++}-calmodulin interaction (see below for a discussion). We indeed find that if a Ca^{++} input (Fig. 3B, middle; see the Materials and Methods for details), fashioned after *Aplysia in vitro* experiments (Fig. 1A of [42]), arrives immediately before the transmitter, it accelerates the rise in $G\alpha^*/AC^*$ concentration, as at this time point, $G\alpha^*/AC^*$ formation is the dominant reaction. Consequently the area under the $G\alpha^*/AC^*$ curve is increased. Assuming that the amount of cAMP production is proportional to the concentration of active adenylate cyclase, this translates into more cAMP production. If, however, Ca^{++} arrives once the transmitter has been reduced, it accelerates the fall of $G\alpha^*/AC^*$ concentration (Fig. 3B, right), since at this time point, dissociation of $G\alpha^*/AC^*$ is dominant. The area under the resulting $G\alpha^*/AC^*$ curve is then smaller, meaning less cAMP production.

Effect of the relative timing of the transmitter and Ca^{++}

In the *Drosophila* learning experiment shown in Fig. 1, a control odour is given 210 s before electric shock; whereas a trained odour is paired with shock with varying inter-stimulus intervals (ISI). To simulate this experiment we represent the odour by the Ca^{++} input and the shock by the transmitter input. We neglect the very short time delays between the delivery of these stimuli and the resulting Ca^{++} influx into and transmitter release onto the Kenyon cells. Thus, in the control condition (Fig. 4, left), Ca^{++} arrives 210 s before the transmitter. We assume that the area under the resulting $G\alpha^*/AC^*$ concentration curve reflects the total amount of cAMP produced. This can be thought of as the cAMP production in those Kenyon cells that are responsive to the control odour (i.e. 'control' Kenyon cells). During associative training (Fig. 4, right), Ca^{++} follows or leads the transmitter by a variable ISI. Again, the time integral of the respective $G\alpha^*/AC^*$ concentration curve is taken as an estimate of cAMP production. Applied to the fly learning experiment in Fig. 1, this would be the amount of cAMP produced in those Kenyon cells that respond to the trained odour (i.e. 'trained' Kenyon cells). We plot the difference in cAMP production between the control condition and the associative training as percent of the control condition (Fig. 4, bottom: Percent associative effect). This reflects the test situation in the behavioural experiment in Fig. 1, where flies are given the

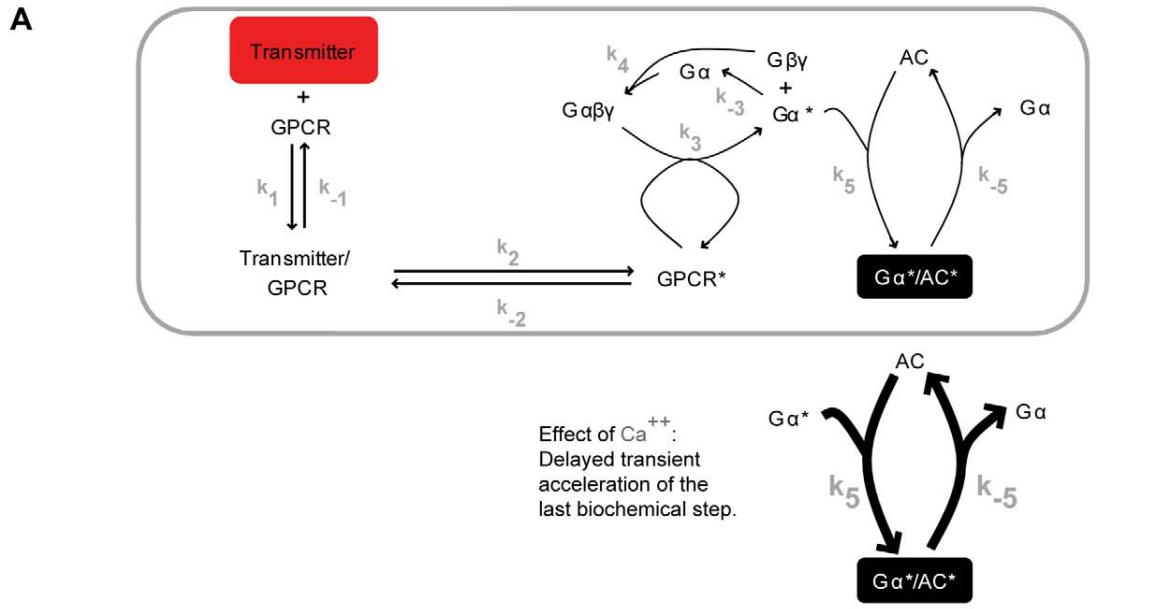

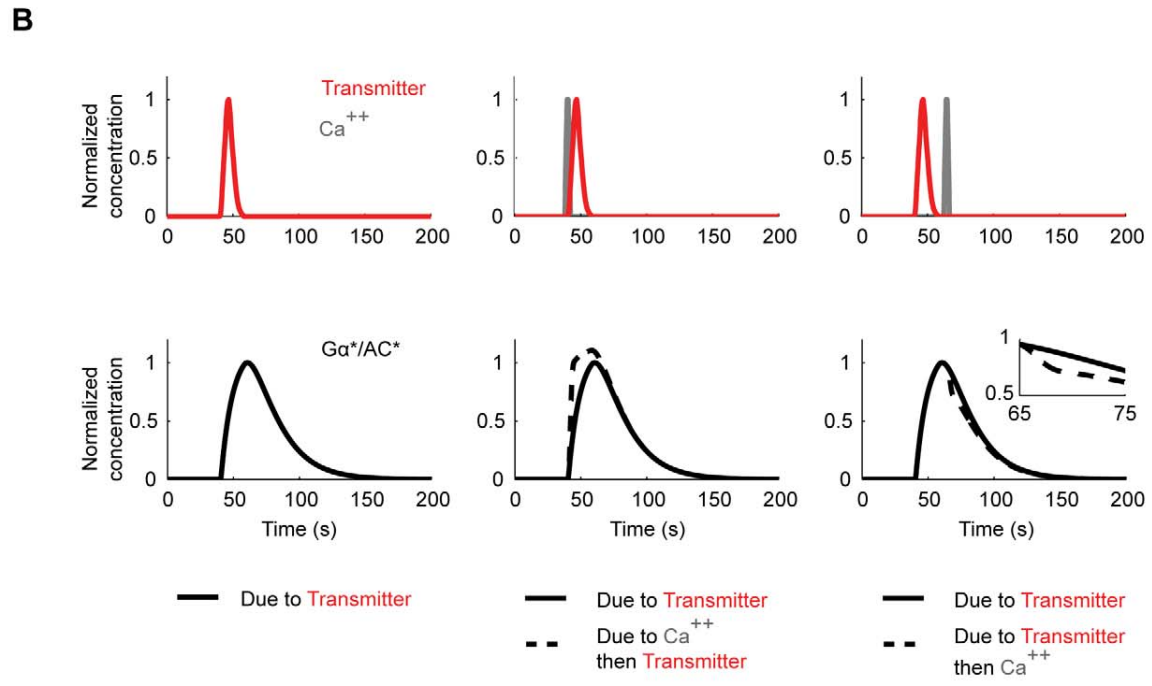

Figure 3. Regulation of the adenylate cyclase by the transmitter and Ca^{++}. A. Adapting the model of Rospars et al. [46], the transmitter reversibly binds to its respective G protein coupled receptor (GPCR) to form a complex, resulting in reversible receptor activation (GPCR*). GPRC* catalyzes the dissociation of the trimeric G protein ($G\alpha\beta\gamma$) into an activated α-subunit ($G\alpha^*$) and the β- and γ-subunits ($G\beta\gamma$). $G\alpha^*$ spontaneously deactivates ($G\alpha$) and reassembles with $G\beta\gamma$, or it reversibly interacts with the adenylate cyclase (AC) to form an enzymatically active complex ($G\alpha^*$/AC*), which serves as the output. Following data from *Aplysia* [41–43], Ca^{++} in turn transiently increases the rate constants for both the formation and the dissociation of the $G\alpha^*$/AC* complex (represented by the thickened arrows). The $k_{subscript}$ denote the rate constants of the respective reactions. B. When this model is stimulated with a transmitter input alone the $G\alpha^*$/AC* concentration rises to a peak of $\sim$0.42 molecules/μm^2 in $\sim$20 s after stimulus onset, and decays back to zero within the next $\sim$100 s (left). If a Ca^{++} input immediately precedes the transmitter, the build-up of the $G\alpha^*$/AC* concentration is transiently accelerated (middle). If on the other hand the Ca^{++} input follows the transmitter, the decay of the $G\alpha^*$/AC* concentration is transiently accelerated (right). For graphical reasons, normalized concentrations are calculated by dividing with the peak $G\alpha^*$/AC* concentration given transmitter input alone. The transmitter concentration reaches a peak of $\sim 6.7 \cdot 10^4$ molecules/μm^2 in $\sim$7 s and decays back to zero within $\sim$18 s; the Ca^{++} concentration starts rising $\sim$4.5 s after the onset, reaches a peak value of $5.6 \cdot 10^{-4}$ moles/L at $\sim$6 s and decays back to zero within $\sim$8.5 s after the onset. Also these inputs are plotted as normalized concentrations.
doi:10.1371/journal.pone.0032885.g003

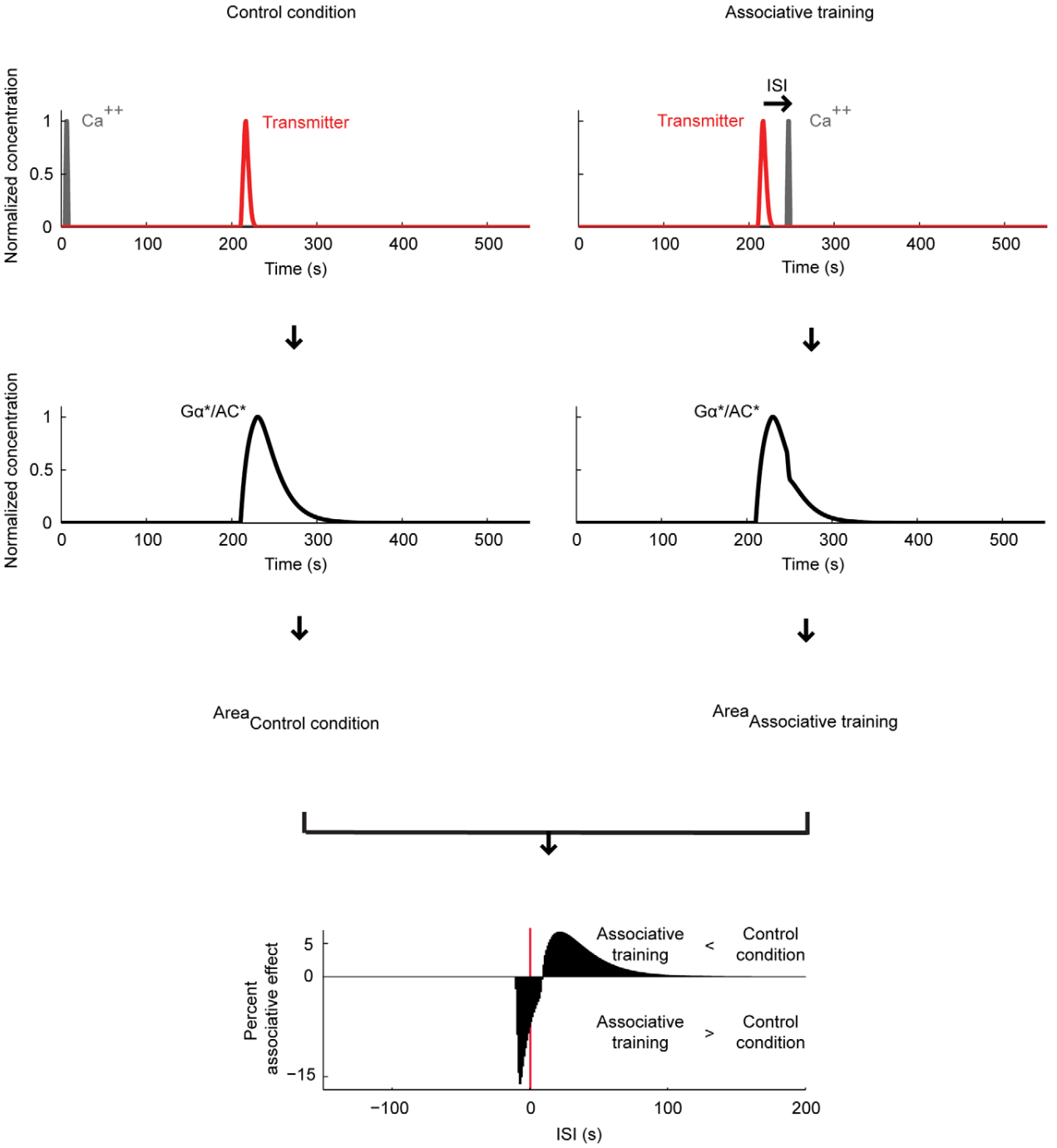

Figure 4. Relative timing of the transmitter and Ca^{++} affects the adenylate cyclase. We stimulate the model with transmitter and Ca^{++} (see Fig. 3B for the details). In the 'control condition' (left), Ca^{++} precedes the transmitter by an onset-to-onset interval of 210 s. In 'associative training' (right), the two inputs follow each other with an inter-stimulus interval (ISI), which is varied across experiments. Negative ISIs indicate training with first Ca^{++} and then the transmitter; positive ISIs mean the opposite sequence of inputs. For either condition, we take the area under the respective Gα*/AC* concentration curve as a measure of cAMP production. For each ISI, we calculate an 'associative effect', by subtracting the amount of cAMP produced during the respective associative training from that in the control condition. We then express the associative effect as percent of the area under the Gα*/AC* concentration curve in the control condition. These percent associative effects are plotted against the ISIs. For very large ISIs, we find no associative effect. If the Ca^{++} is closely paired with the transmitter, we find negative associative effects; the strongest negative associative effect (−15.5%) is obtained when using ISI ~−3 s. If on the other hand Ca^{++} follows the offset of the transmitter during training, we find positive associative effects; the largest positive associative effect (6.3%) is obtained for ISI ~26 s. Thus, depending on the relative timing of Ca^{++} and transmitter during training, opposing associative effects come about, closely matching the behavioural situation in Fig. 1.
doi:10.1371/journal.pone.0032885.g004

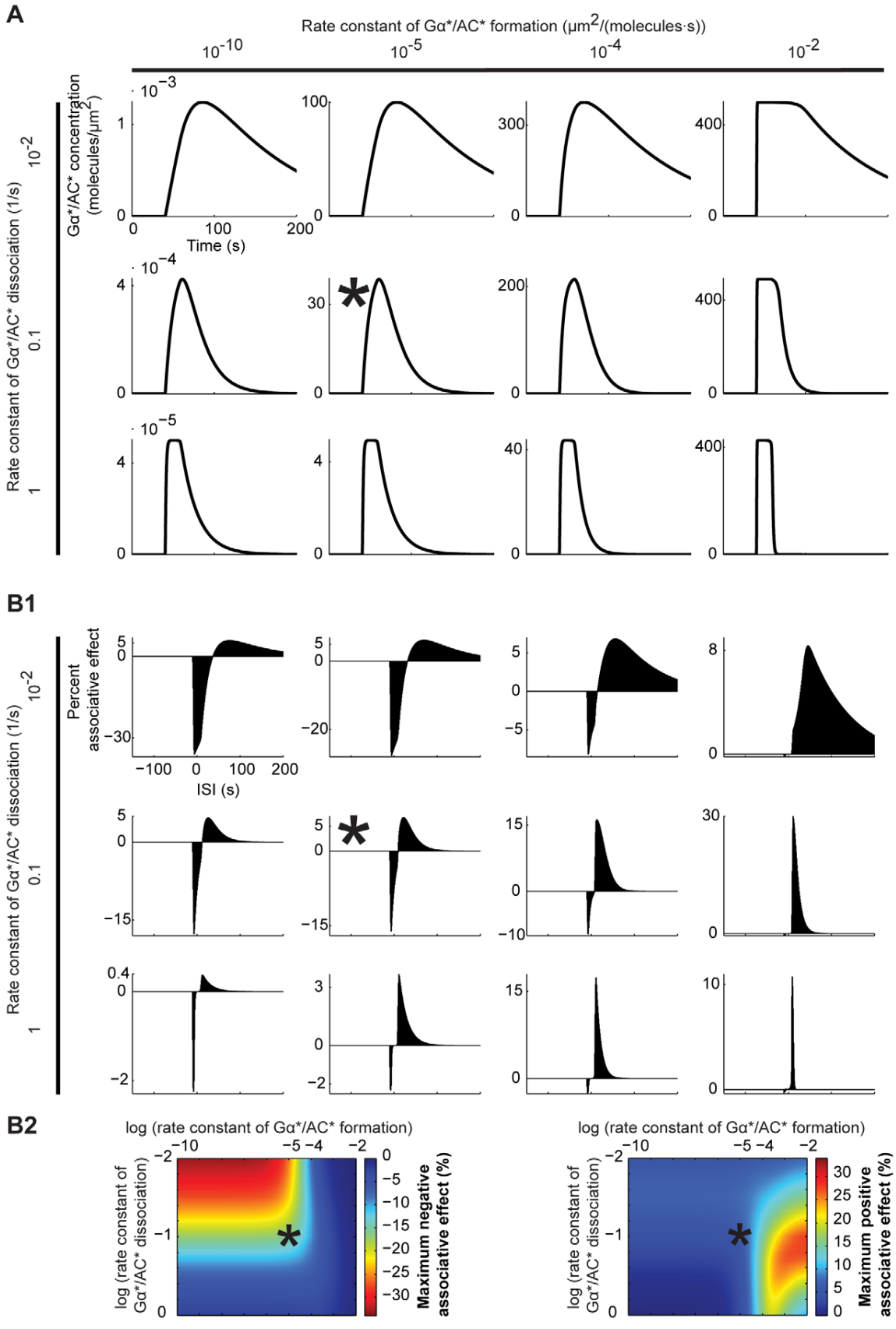
A
Rate constant of Gα*/AC* formation (μm²/(molecules·s))
10^-10
10^-5
10^-4
10^-2
Rate constant of Gα*/AC* dissociation (1/s)
Gα*/AC* concentration (molecules/μm²)
Time (s)
B1
Percent associative effect
ISI (s)
B2
log (rate constant of Gα*/AC* formation)
log (rate constant of Gα*/AC* dissociation)
Maximum negative associative effect (%)
Maximum positive associative effect (%)

Figure 5. Influence of the rate constants for Gα*/AC* formation and dissociation. A. Time course of the Gα*/AC* concentration, following a stimulation of the model with transmitter (see Fig. 3B for the details). B1. ISI-dependent associative effects, as explained in Fig. 4. B2. Color-coded representation of the size of the peak negative (left) and positive (right) associative effects. In (A), (B1) and (B2), we systematically change the rate constants for Gα*/AC* formation and dissociation (k_5 and k_{-5} in Fig. 3A). Using the default values of both rate constants, we obtain associative effects fitting the behavioural situation in Fig. 1 (B1, B2: marked with asterices). Notably, this fit is stable over more than five orders of magnitude of the formation rate constant, but is more sensitive to changes in the dissociation rate constant (B1, B2). The size (B2) and ISI-dependency (B1) of the associative effects are dictated by the dynamics of adenylate cyclase activation/deactivation (A). Particularly, the negative associative effect depends on the rising phase of the Gα*/AC* concentration: When either the formation or the dissociation rate constants are increased beyond their default values, the rising of the Gα*/AC* concentration becomes too fast to be further improved by Ca^{++}; the negative associative effect is thus attenuated. Also, in this case, the short rising phase of Gα*/AC* concentration limits the window of ISI values appropriate for the negative associative effect. In turn, decreasing both rate constants below their default values slows down the rise of Gα*/AC* concentration, leaving more space for improvement by Ca^{++}, thus boosting and -due to the longer rising phase- 'widening' the negative associative effect. As for the positive associative effect, the falling phase of the Gα*/AC* concentration matters: When both rate constants are moderately increased beyond their default values, the fall of Gα*/AC* concentration gets faster, that is, the dissociation of Gα*/AC* better dominates over its formation, boosting the positive associative effect. Critically, when the rate constants are increased too much, the drop of Gα*/AC* concentration is accelerated to its limit; thus, both the size and the 'width' of the positive associative effect suffer. To summarize, the negative associative effect is favoured by small values of both rate constants, whereas the positive associative effect needs moderately high values of these. Consequently, the overall effect size cannot be improved much beyond the default case, without compromising the relative sizes of the two associative effects with respect to each other and thus the fit to the behavioural situation.
doi:10.1371/journal.pone.0032885.g005

choice between the control odour and the trained odour. Note that in the control condition, a non-zero amount of cAMP is produced; when applied to the learning experiment this would mean a basic amount of cAMP in all Kenyon cells, possibly causing a basic strengthening of their output. Indeed in flies, mere exposure to the shock modifies the olfactory behaviour; interestingly, the resulting non-associatively modified odour responses are less aversive upon loss of cAMP signalling or Kenyon cell function [47,48].

Despite the overall simplicity of our approach, the simulation results (Fig. 4) agree strikingly well with the behavioural situation (Fig. 1). First, short negative or short positive ISIs result in negative associative effects; in other words, associative training with close Ca^{++} and transmitter pairing produces more cAMP than the control condition. Translating this to the learning experiment, *more* cAMP will be produced in the trained Kenyon cells than in the control Kenyon cells. Consequently, the output from the trained Kenyon cells to the downstream conditioned avoidance circuit will be strengthened more than that of the control Kenyon cells, resulting, at a choice situation, in relative avoidance of the trained odour (i.e. punishment learning). Next, for intermediate positive ISIs, the model produces positive associative effects, indicating *less* cAMP production during associative training than in the control condition. Applying this to the learning experiment, the output from the trained Kenyon cells to the downstream conditioned avoidance circuit will be strengthened less than the output from the control Kenyon cells. Consequently, given the choice between the two odours, the net behaviour will be conditioned approach towards the trained odour (i.e. relief learning). Finally, for very large (positive as well as negative) ISIs, the model shows no associative effect, as in the behavioural setting.

Other features of the simulation results are also reminiscent of the behavioural data in Fig. 1. First, the negative associative effect is larger than the positive associative effect. Second, the strongest negative associative effects are found when the onset of Ca^{++} precedes that of the transmitter; overlapping onsets result in a less pronounced negative associative effect. Note that, in behaviour, even an ISI of −45 s supports learning (Fig. 1); whereas in the model, negative ISIs longer than 5 s are not effective; this discrepancy is likely due to the properties of the Ca^{++} input in the present simulation (see Fig. 8 for a detailed analysis). Finally, in both behaviour and model, the strongest positive associative effects are obtained when the odour or Ca^{++} closely follows the offset of the shock or the transmitter.

Even with a single training trial, the negative and positive associative effects respectively reach up to ~16% and 6% of the control, measured at the level of cAMP production. More intense Ca^{++} inputs (see Fig. 8 for details) and repetitive training will boost these effects significantly, as will the high amplification factors often seen in signal transduction cascades [49].

Relationship between the adenylate cyclase dynamics and the associative effects

We next test how the agreement between model and behavioural data is influenced by changes in key model parameters. To this end, we first vary the rate constants for Gα*/AC* formation and dissociation (k_5 and k_{-5}). The dynamics of adenylate cyclase activation/deactivation (Fig. 5A) dictates both the ISI-dependency and the size of the associative effects (Figs. 5B1 and 5B2). Particularly, the duration of the rising and the falling phases of active adenylate cyclase concentration determine the window of ISI values appropriate for the negative and the positive associative effects, respectively. The sizes of the associative effects also depend on the dynamics of active adenylate cyclase concentration; intermediate speeds for build up and decay are best suited (see the legend of Fig. 5 for details). Notably, both the adenylate cyclase dynamics (Fig. 5A) and the associative effects (Figs. 5B1 and 5B2) remain stable over more than five orders of magnitude of the formation rate constant; whereas changes in the dissociation rate constant have much stronger influence.

The associative effects are influenced little by varying the rate constants of GPCR (Fig. 6A) or G protein (Fig. 6B) activation and deactivation within a certain range. But when the respective forward rate constants are increased beyond the shown values, the associative effects abruptly decrease (see the legend of Fig. 6 for a detailed explanation). These findings agree with a previous, more systematical sensitivity-analysis [50] of the model proposed by Rospars et al. [46].

Effects of the duration and intensity of the transmitter

To what extent do the observed associative effects depend on the specific properties of the inputs used?

We first study the effect of changes in the duration of the transmitter (Fig. 7), keeping the Ca^{++} input the same as in the previous experiments. For a fixed rise time of the transmitter, increasing its decay time constant from 0.1 s to 1 s hardly changes the size of the associative effects (Fig. 7, the first two cases). A more slowly decaying transmitter input on the other hand, due to a much higher control level of cAMP production, allows only for smaller percent associative effects (Fig. 7, the last case). A

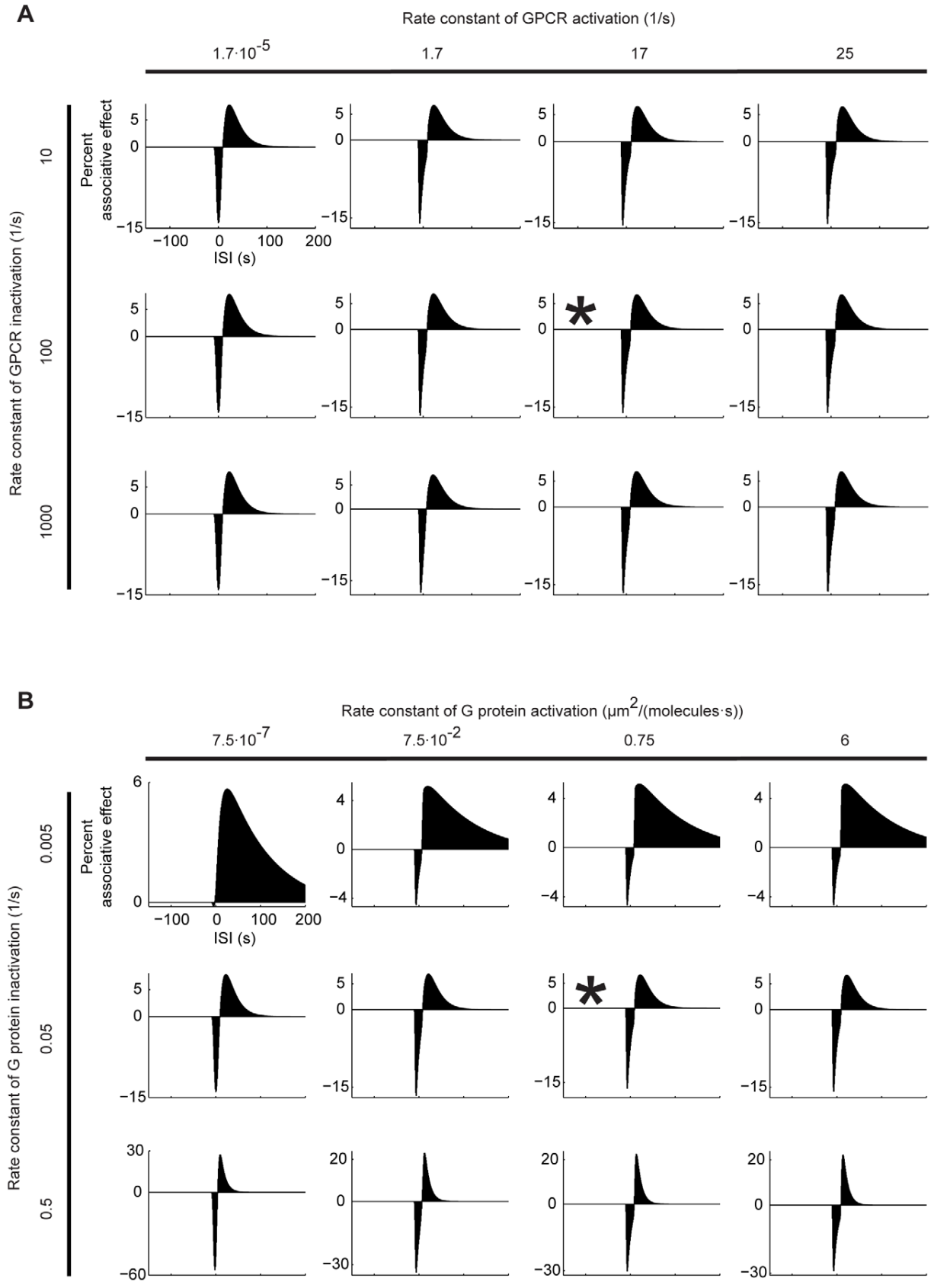
A
Rate constant of GPCR activation (1/s)
1.7·10^-5
1.7
17
25
Rate constant of GPCR inactivation (1/s)
10
100
1000
Percent associative effect
ISI (s)
B
Rate constant of G protein activation (μm^2/(molecules·s))
7.5·10^-7
7.5·10^-2
0.75
6
Rate constant of G protein inactivation (1/s)
0.005
0.05
0.5
Percent associative effect
ISI (s)

Figure 6. Dependence upon the activation and inactivation rate constants of GPCR and G protein. The percent associative effect is shown as a function of the ISI, as detailed in Fig. 4. Asterices mark the default conditions. A. Varying the rate constants for GPCR activation and inactivation hardly affects the size, or the 'shape' of the associative effects. B. Varying the rate constant of G protein activation also has nearly no bearings on the associative effects. As for the rate constant for G protein inactivation, higher values result in overall larger associative effects; this is because, both the rise and the fall of active adenylate cyclase concentration become moderately faster (not shown, see the legend of Fig. 5 for a more detailed explanation). In both (A) and (B), increasing the respective forward rate constants beyond the depicted range immediately recruits all available adenylate cyclase molecules, precluding any effect of Ca^{++} and thus any associative effect (not shown).
doi:10.1371/journal.pone.0032885.g006

corresponding effect of shock duration on the strength of learning remains to be probed for in fly learning experiments. As for the ISI-dependence of the associative effects, short transmitter inputs give good fit to the behavioural situation in Fig. 1 (Fig. 7, the first two cases). For more slowly decaying transmitter inputs, the positive associative effect only occurs for longer ISIs due to the broadened dynamics of adenylate cyclase activation/deactivation (Fig. 7, the last case). Quantitatively, we cannot provide a detailed comparison between these effects and those found at the behavioural level, since the dynamics of dopamine availability in the synaptic cleft upon shock stimulation is not known. It is however noteworthy that also in *Drosophila* behavioural experiments shock duration affects the window of ISIs appropriate for relief learning. For example, in Fig. 1, the shock lasts for 15 s; accordingly, relief learning is possible with ISIs longer than 15 s. For a 1.5s-long shock stimulus, however, an ISI of 2 s already supports relief learning (Fig. 8C of [17]). This invites a more systematic behavioural analysis of the effect of shock duration on relief learning.

To test for the effects of varying the transmitter intensity, we use the intermediate time course shown in Fig. 7 and keep the Ca^{++} input as in the previous simulations. Scaling the transmitter input up and down over more than 10 orders of magnitude leaves the associative effects largely unchanged, both in terms of their percent size and their ISI-dependencies (data not shown). Only, unrealistically large transmitter inputs ($\geq 10^7$ molecules/μm^2), immedi-

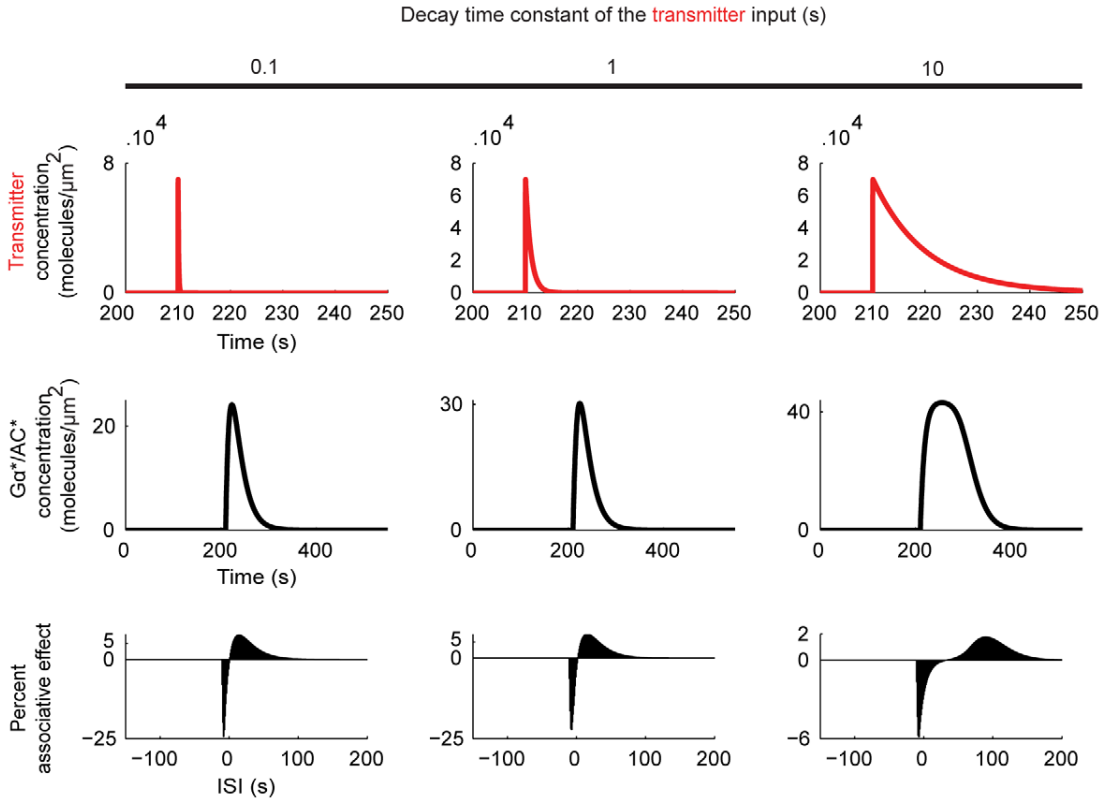

Figure 7. Influence of the transmitter duration. With a fixed Ca^{++} input, three different transmitter inputs are tested (top). They are all initiated at 210 s, rise to a peak of $7 \cdot 10^4$ molecules/μm^2 within 40 ms after the onset, but decay with different time constants as indicated above the panels. We plot the resulting adenylate cyclase dynamics (middle) and the ISI-dependent associative effects (bottom). In terms of the percent sizes of associative effects, changing the transmitter decay time constant from 0.1 to 1 (the first two cases) hardly makes a difference. A slower decaying transmitter input (the last case) broadens the dynamics of adenylate cyclase activation/deactivation, resulting in much higher cAMP production in the control condition; thus, the percent associative effects remain small. As for the ISI-dependence of the associative effects, short transmitter inputs (the first two cases) give good fits to the situation in Fig. 1; when a slower decaying transmitter input is used (the last case), the positive associative effect only occurs for large positive ISIs, due to the broadened adenylate cyclase activation/deactivation dynamics.
doi:10.1371/journal.pone.0032885.g007

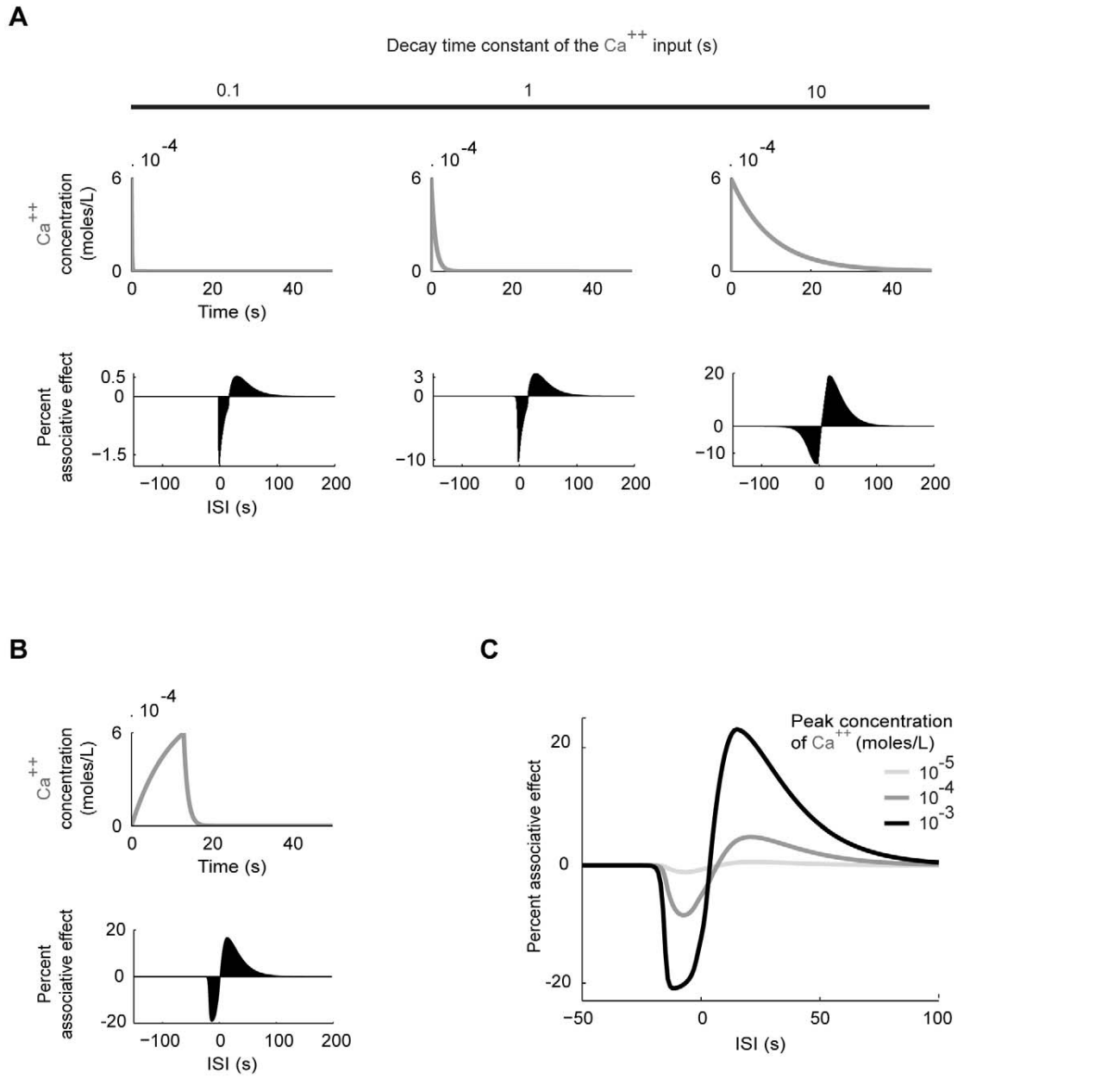

Figure 8. Influence of Ca^{++} duration and intensity. Complementing the analysis shown in Fig. 7 we now vary the Ca^{++} input while keeping the transmitter input fixed. In all three examples shown in (A), the Ca^{++} input rises to a peak of $6{\cdot}10^{-4}$ moles/L within 40 ms after the Ca^{++} onset, but decays with different time constants, chosen as 0.1 s, 1 s and 10 s (A, top). In this scenario, the associative effects increase with increasing Ca^{++} duration (A, bottom). In addition, a large decay constant causes a long tail of the Ca^{++} input that enables negative associative effects for longer ISIs (A, the last case). In (B) we provide an exemplary Ca^{++} input (B, top) which gives good fit to the behavioural results in Fig. 1 in terms of the ISI-dependency of the associative effects but not in terms of their sizes relative to each other (B, bottom). In this case, the Ca^{++} concentration rises to a peak of $6{\cdot}10^{-4}$ moles/L within 13 s after the onset, comparing well with the 15s- long odour presentation in Fig. 1. Note that the best negative associative effect occurs with ISI = −13 s, similar to the behavioural situation in Fig. 1. Finally, in (C), we study the effects of the intensity of the Ca^{++} input. We fix the transmitter input and use the Ca^{++} input depicted in (B), but scaled up and down by one order of magnitude. The intensity of Ca^{++} strongly influences the sizes of both the negative and the positive associative effects; the balance between the two is however somewhat compromised with increasing Ca^{++} intensity.
doi:10.1371/journal.pone.0032885.g008

ately activate all the available adenylate cyclase; this abolishes the possibility of modulation by Ca^{++} and precludes any associative effect (data not shown). These findings only partially reflect the situation in the fruit fly learning experiments, where intermediate shock intensities work best [13,51].

Effect of Ca^{++}duration and intensity

In Fig. 1, given a 15s-long odour presentation, even an ISI of −45 s supports punishment learning. When adhesion of residual odour substance to the experimental setup is excluded, a 10s-long odour presentation enables punishment learning with an ISI of up

to −25 s [52]. That is, a brief gap between the offset of the odour and the onset of the shock is readily tolerated. As an attempt to account for such 'trace conditioning' in our model, we vary the decay time constant of the Ca^{++} input, keeping constant its rise time and peak (Fig. 8A, top). In fact, implementing the biochemical steps of Ca^{++}-calmodulin interaction would likely have the same effect (Fig. 1 of [53]). In any case, more slowly decaying Ca^{++} inputs lead to larger associative effects (Fig. 8A, bottom); and enable longer ISIs to lead to negative associative effects (Fig. 8A, the last case). As exemplified in Fig. 8B, the shape of the Ca^{++} input is indeed a critical parameter for reproducing the behavioural situation in Fig. 1 (see the respective figure legend for details). In short, a long tail of odour-induced Ca^{++} (or Ca^{++}-calmodulin complex) increase in the Kenyon cells could bridge over at least part of the temporal gap between odour offset and shock onset. This could then be used by the Ca^{++}-calmodulin-dependent adenylate cyclase or likely also other signalling molecules [54] to enable 'trace conditioning'. Studies using genetically encoded Ca^{++} sensors to monitor the Kenyon cell odour responses neither rule out nor confirm the existence of such long tails in the Ca^{++} concentration [22–24].

Next, we look at the effects of the intensity of the Ca^{++} input. To investigate a scenario that mimics the behavioral situation as closely as possible, we use Ca^{++} inputs shaped as in Fig. 8B. We scale their size up or down by one order of magnitude. As shown in Fig. 8C, this strongly influences both the negative and the positive associative effects. In the fruit fly, too, learning is typically improved with increasing odour concentration; beyond a certain concentration, however, further increase deteriorates learning [13], which is not explained by our model.

Alternative model for the adenylate cyclase regulation

Finally, we test the generality of our results using an alternative model for the regulation of the adenylate cyclase by the transmitter [45]. This model (Fig. 9) includes only a single biochemical step for the GPCR activation and it ignores the trimeric nature of the G protein. In addition to its reduced complexity (i.e. five instead of nine differential equations), it differs from the first model (Fig. 3A) in terms of the initial concentrations of the molecules, as well as the reaction rate constants (see Materials and Methods for details).

In response to a transmitter input, the alternative model generates time courses for the active adenylate cyclase concentration (Fig. 10A) and associative effects (Fig. 10B) whose salient features are strikingly similar to those of the first model (Fig. 5). Most importantly, the simplified model also clearly shows opposing associative effects that depend in the same qualitative manner on event timing and the adenylate cyclase dynamics.

Note that the two models we use are adapted from two different systems (i.e., olfactory transduction in moth [46] and actin polymerization in human neutrophils [45], respectively) and thus the parameter estimates come from different methods, processes and species. Having reconciled these, we are confident that our results capture the generic properties of Ca^{++}-calmodulin-sensitive adenylate cyclase regulation. We believe that this cross-species approach we use strengthens the proof of concept that the reaction dynamics of adenylate cyclase signalling could explain the effect of event timing on associative learning.

Discussion

Event timing critically affects associative learning. Fruit flies, for example, learn an odour as a signal for punishment or relief, depending on whether it precedes or follows shock during training (Fig. 1) [11,13–17]. We suggest a simple biochemical explanation for these two opposing kinds of learning. During punishment training, a Ca^{++}-calmodulin-sensitive adenylate cyclase in the Kenyon cells seems to detect the convergence of the odour and the shock signals (Fig. 2) [30–35] (see also [55] for a similar mechanism in striatal medium spiny neurons). Based on biochemical data from *Aplysia* [41–43], we implement a model where shock-induced transmitter activates the adenylate cyclase and the underlying reaction dynamics are bi-directionally regulated by odour-induced Ca^{++}, depending on the relative timing of the two inputs (Fig. 3). Using this model, we simulate the key fruit fly learning experiment for the effect of event timing (Fig. 1). To mimic the situation in the control Kenyon cells, we use Ca^{++} and transmitter inputs that are sufficiently separated in time,

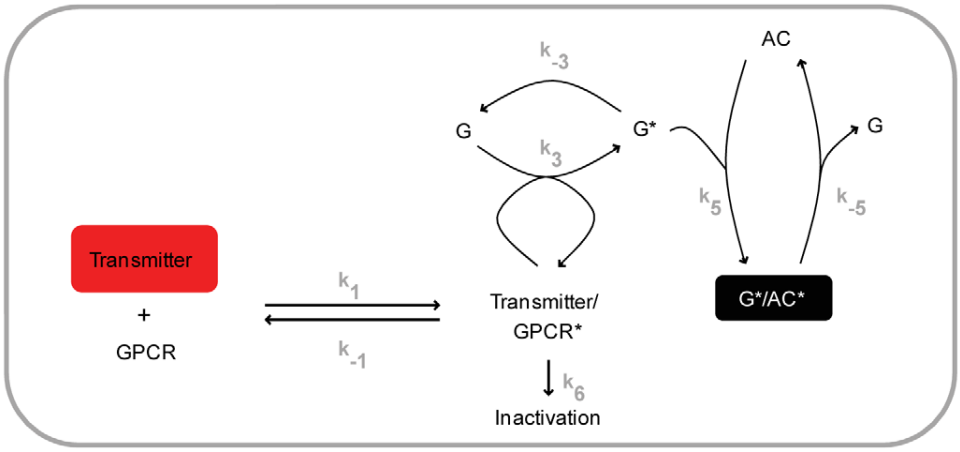

Figure 9. An alternative model for adenlyate cyclase regulation by the transmitter. To complement our main analysis based on the model adapted from [46] and shown in Fig. 3A, we finally use a simpler model variant [45]. Here, the transmitter reversibly binds to its respective G protein coupled receptor (GPCR) to form an active complex (Transmitter/GPCR*). This complex then dissociates, or it interacts with the G protein (G) to activate it (G*). The trimeric nature of the G protein is ignored (compare with Fig. 3A). G* on the one hand spontaneously deactivates (G), on the other hand it reversibly interacts with the adenylate cyclase (AC) to form an enzymatically active complex (G*/AC*), which serves as the system's output. The effect of Ca^{++} is implemented the same way as in Fig. 3A.
doi:10.1371/journal.pone.0032885.g009

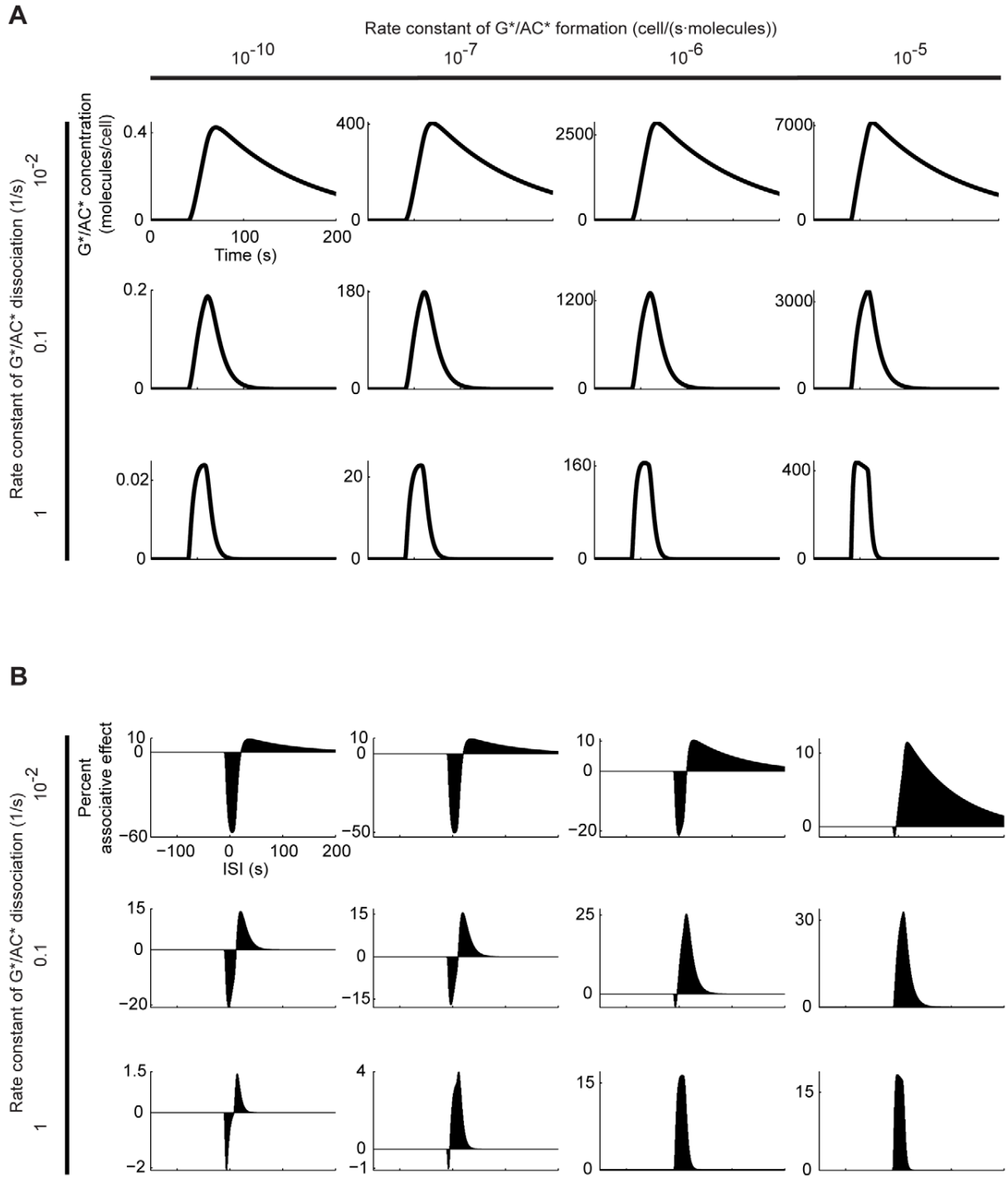

Figure 10. Alternative model: Influence of G*/AC* formation and dissociation rate constants. A. We stimulate the alternative model based on [45] with a transmitter input (details as in Fig. 3B) and plot the time course of the resulting G*/AC* concentration. B. Repeating the experiment in Fig. 4, we plot the percent associative effect as a function of the ISI. Comparison with Fig. 5 shows that despite their various differences both models generate rather similar associative effects.
doi:10.1371/journal.pone.0032885.g010

and assume that the resulting cAMP production will strengthen the output of these cells to the conditioned avoidance circuits to a certain level. To simulate the situation in the trained Kenyon cells, we use various inter-stimulus intervals (ISI) between the Ca^{++} and the transmitter. In this setting, the equivalent of punishment training leads to more cAMP than the control level (Fig. 4) so that the output of the trained Kenyon cells will be strengthened more than that of the control Kenyon cells, resulting in avoidance of the trained odour in a choice situation. The equivalent of relief training, in turn, results in a cAMP production below the control

level (Fig. 4); consequently, the output of the trained Kenyon cells will remain weaker than that of the control Kenyon cells, resulting in net approach to the trained odour. Despite its simple biochemical formulation, the model also recapitulates other salient features of punishment and relief learning (Fig. 4). This agreement between the simulation- and the behavioural data is robust with respect to changes in various model parameters within reasonably wide ranges (Figs. 5 and 6). Given the effects observed beyond these ranges however, it may be interesting to experimentally manipulate reaction rate constants, e.g., by changing ambient temperature, to then see the effects on the behavioural ISI-learning function. Importantly, our conclusions also hold for a rather different model for transmitter-mediated adenylate cyclase activation (Figs. 9 and 10).

The associative effects we report in Fig. 4 reach up to ~16% of the control condition; a stronger Ca^{++} input boosts these effects significantly (Fig. 8C); also, repetition of training will result in a cumulative increase. In addition, these effects will most likely be amplified through the downstream signal transduction cascade [49]. Note that a previous model based on spike-timing-dependent plasticity reports up to only ~0.7% change in synaptic strength in a single training trial (Fig. 1C of [18]), despite assuming unrealistically strong odour-induced activity. Experimentally, e.g., in vertebrate brain slices, no less than 20 pre-post synaptic action potential pairings are necessary to obtain only ~10% potentiation of synaptic strength [56]. Given these, the sizes of the associative effects we report seem reasonable. Critically, the quantitative relationship between synaptic plasticity and behavioural plasticity has not been characterized with respect to *Drosophila* olfactory learning; whereas few studies exist in other systems, e.g., [57] reports 10–20% strengthening in hippocampal synapses upon behavioural training. In general, the question of how much change in synaptic strength is *required* for making a difference in behaviour, is open.

The present model uses the amount of cAMP production as output. Clearly, much happens in reality between this step and the synaptic plasticity underlying learning. Implementing the following stages of signal transduction (e.g., activation of the cAMP-dependent protein kinase (PKA), phosphorylation of Synapsin [58]) may help understanding key features of associative learning, other than its sensitivity to event timing. For example, in the honey bee antennal lobe, a single olfactory reward training trial transiently activates PKA; repetitive training on the other hand results in prolonged PKA activation, which may be important for the formation of long-term memory [59] (see [60] for a computational model relying on this mechanism). Also, degradation of cAMP [35] and de-phosphorylation of key downstream proteins [61] is likely critical for restricting the effects of learning both during training and thereafter. All these downstream processes can be added to the model to explain the dynamics of memory acquisition or decay. In the current study however we focus on the effect of event timing on learning and provide a proof of concept that bi-directional regulation of adenylate cyclase can be the underlying mechanism. As a next step, one should experimentally test for a role of the Ca^{++}-calmodulin-sensitive adenylate cyclase, *rutabaga* in relief learning, using the available genetic tools, e.g., loss of function mutations [30,32,33], RNAi-knockdown [62]. Also the role of dopaminergic signalling in relief learning remains open. Blocking the neuronal output from two different, incomplete sets of dopaminergic neurons leaves relief learning intact [16]; however, given the caveats of the genetic techniques used in the respective study, the complementary approach of interfering with dopamine receptor function using genetic [27,63] and pharmacological [64] tools seems warranted. Note that for punishment learning, both the adenylate cyclase- and the dopamine roles are better established [25–33].

A previous model by Drew and Abbott [18] suggests that punishment learning strengthens the Kenyon cell output, whereas relief learning has a weakening effect, so that opposite kinds of conditioned behaviour result. As key mechanism the authors implement spike-timing-dependent plasticity (STDP) at the Kenyon cell output synapses [65,66]. To bridge the gap in time scales between STDP and behavioural event timing effects, they need to assume high and slowly decaying spiking activity in the Kenyon cells and postsynaptic neurons, following odour and shock, respectively. As these assumptions are experimentally not fulfilled [19–21], this particular, STDP-based model does not seem appropriate for olfactory learning in the fruit fly. This does however not exclude a role for STDP in insect olfactory learning: In the locust, specific Kenyon cell output synapses seem to be 'tagged' by the occurrence of temporally adjunct pre- and post-synaptic action potentials, mimicking the situation during odour presentation; only these tagged synapses are then modified upon delivery of a delayed neuromodulator [66]. Such a process could underlie punishment learning, including 'trace conditioning'; it can however not readily account for relief learning.

Both in Drew and Abbott's STDP-based model [18] and in the present adenylate cyclase-based model, punishment and relief training act on the same Kenyon cell output to the same downstream circuit, but in opposite ways. This scenario readily accounts for the observed diametrically opposite conditioned behaviours, i.e. avoidance *vs.* approach [11,13–17]. Further investigation into the repertoire of conditioned behaviours after punishment and relief training may well render this scenario short, e.g., if punishment learning can modulate kinds of behaviour that relief learning leaves unaffected and *vice versa*. In that case, an alternative scenario could be that punishment and relief learning strengthen the output from two distinct sets of Kenyon cells which redundantly encode the trained odour, but receive different kinds of reinforcement signal and send their output to different downstream circuits. In a related scenario, punishment and relief memory traces would be laid down within the same Kenyon cells, but at distinct sub-cellular sites, which receive different reinforcement signals and send output to different downstream circuits. In either case, it is not known how the reinforcement signal for relief is implemented at the neuronal level [16]. Finally, with respect to all scenarios discussed, the role of the Kenyon cells in relief learning awaits testing. Note that for punishment learning, this role is well-established [25,31–33].

To summarize, further experiments on the molecular, cellular and behavioural level are needed to elucidate the mechanism of relief learning. The present computational study may guide this process in that it identifies one plausible candidate scenario. More generally, our approach shows that even a simple biochemical process may help explain a non-trivial behavioural observation, such as the bi-directional effect of event timing on associative learning.

Materials and Methods

All simulations were done in MATLAB 7 (Mathworks, Natick, USA) on a PC. Except in Figs. 5B2, 8B and 8C, the differential equations were solved using the forward Euler method, where the time-dependent inputs and dynamical variables were discretized at 0.001 s. Variations of the temporal step size showed that this approach yielded a faithful yet simple numerical representation of the dynamics. In Figs. 5B2, 8B and 8C, we used the ordinary differential equation solver ode15 s, provided by MATLAB.

Regulation of the adenylate cyclase by the transmitter and Ca^{++}

We implemented two alternative models for the regulation of the adenylate cyclase by the transmitter and Ca^{++}. The first model was adapted from a previous model of G-protein-mediated insect olfactory signal transduction [46]. The alternative model was adapted from an implementation of G-protein signalling in actin polymerization in human neutrophils [45]. In what follows, we present in detail the first model; the alternative model is briefly explained at the end.

The transmitter (Tr) was the primary input to the model, as sketched in Fig. 3A. Unless stated otherwise, the time course of the Tr concentration was fashioned after biochemical experiments performed in *Aplysia*. To this end, we extracted the time-dependent serotonin concentration from Fig. 1A of [42] and used linear interpolation to generate the additional data points required for the simulations. Numerical values were converted from μmoles/L to molecules/μm^2 using a conversion factor.

$$\text{Conversion factor} = 10^{-21}\cdot\text{Avogadro's number}\cdot\frac{\text{Cell volume}}{\text{Cell surface area}} \quad (1)$$

Avogadro's number is $6.02\cdot10^{23}$ molecules/mol and, following [46], the cell volume was 2600 μm^3 and cell surface area was 426 μm^2, leading to a conversion factor of ~3700 molecules·μm/mol. The resulting Tr concentration reached a peak value of $6.7\cdot10^4$ molecules/μm^2 within ~7 s and decayed back to zero within ~18 s after stimulus onset.

For the simulations depicted in Fig. 7, the Tr concentration over time was taken as

$$[\mathrm{Tr}](t) = e^{-t/\tau 1} - e^{-t/\tau 2} \quad (2)$$

To cover different decay courses, the time constant τ1 was chosen as 0.1 s, 1 s and 10 s, respectively; with τ2 = 0.01 s, the peak concentration was reached within ~40 ms after transmitter onset. The resulting concentrations were normalized such that the peak was $7\cdot10^4$ molecules/μm^2 in each case. For varying Tr intensity, we used the time constants τ1 = 1 s and τ2 = 0.01 s and up- and down-scaled the respective function by division.

In each experiment, the desired Tr concentration time course was initiated at the specified point in time. In Figs. 3B and 4, for plotting reasons, concentrations were normalized relative to their peak values. For molecules other than Ca^{++} and Tr, concentrations were initiated with the values specified in Table 1.

The concentration of each kind of molecule was then updated according to the respective equation, below.

$$\frac{d[\mathrm{GPCR}]}{dt} = -k_1\cdot[\mathrm{Tr}]\cdot[\mathrm{GPCR}] + k_{-1}\cdot[\mathrm{Tr/GPCR}] \quad (3)$$

$$\frac{d[\mathrm{Tr/GPCR}]}{dt} = k_1\cdot[\mathrm{Tr}]\cdot[\mathrm{GPCR}] - (k_{-1}+k_2)\cdot[\mathrm{Tr/GPCR}] + k_{-2}\cdot[\mathrm{GPCR}^*] \quad (4)$$

$$\frac{d[\mathrm{GPCR}^*]}{dt} = k_2\cdot[\mathrm{Tr/GPCR}] - k_{-2}\cdot[\mathrm{GPCR}^*] \quad (5)$$

$$\frac{d[\mathrm{G}\alpha\beta\gamma]}{dt} = -k_3\cdot[\mathrm{G}\alpha\beta\gamma]\cdot[\mathrm{GPCR}^*] + k_4\cdot[\mathrm{G}\alpha]\cdot[\mathrm{G}\beta\gamma] \quad (6)$$

$$\frac{d[\mathrm{G}\beta\gamma]}{dt} = k_3\cdot[\mathrm{G}\alpha\beta\gamma]\cdot[\mathrm{GPCR}^*] - k_4\cdot[\mathrm{G}\alpha]\cdot[\mathrm{G}\beta\gamma] \quad (7)$$

$$\frac{d[\mathrm{G}\alpha^*]}{dt} = k_3\cdot[\mathrm{G}\alpha\beta\gamma]\cdot[\mathrm{GPCR}^*] - k_{-3}\cdot[\mathrm{G}\alpha^*] - k_5\cdot[\mathrm{G}\alpha^*]\cdot[\mathrm{AC}] \quad (8)$$

$$\frac{d[\mathrm{G}\alpha]}{dt} = k_{-3}\cdot[\mathrm{G}\alpha^*] - k_4\cdot[\mathrm{G}\alpha]\cdot[\mathrm{G}\beta\gamma] + k_{-5}\cdot[\mathrm{G}\alpha^*/\mathrm{AC}^*] \quad (9)$$

$$\frac{d[\mathrm{AC}]}{dt} = -k_5\cdot[\mathrm{G}\alpha^*]\cdot[\mathrm{AC}] + k_{-5}\cdot[\mathrm{G}\alpha^*/\mathrm{AC}^*] \quad (10)$$

$$\frac{d[\mathrm{G}\alpha^*/\mathrm{AC}^*]}{dt} = k_5\cdot[\mathrm{G}\alpha^*]\cdot[\mathrm{AC}] - k_{-5}\cdot[\mathrm{G}\alpha^*/\mathrm{AC}^*] \quad (11)$$

In these equations, the reaction rate constants (k) took the values listed in Table 2.

Table 1. Components and initial concentrations for the first model.

Abbreviation	Molecule	Initial concentration (molecules/μm^2)
GPCR	G protein coupled receptor	6000
Tr/GPCR	Complex of Tr and GPCR	0
GPCR*	Activated GPCR	0
Gαβγ	Trimeric G protein	1000
Gβγ	G protein β- and γ- subunits	0
Gα*	Active Gα	0
Gα	Inactive G protein α-subunit	0
AC	Adenylate cyclase	500
Gα*/AC*	Complex of Gα* and activated AC	0

All values were chosen according to [46] and were estimates from moth olfactory transduction (see [46] for further references).
doi:10.1371/journal.pone.0032885.t001

Table 2. Rate constants of the reactions for the first model.

Rate constant	Reaction	Value	Unit
k_1	Formation of the Tr/GPCR complex	$5.6 \cdot 10^{-5}$	μm^2/(molecules·s)
k_{-1}	Dissociation of the Tr/GPCR complex	8	1/s
k_2	Activation of GPCR	17	1/s
k_{-2}	Inactivation of GPCR	100	1/s
k_3	Dissociation of $G\alpha\beta\gamma$ into $G\alpha^*$ and $G\beta\gamma$	0.75	μm^2/(molecules·s)
k_{-3}	Deactivation of $G\alpha^*$ to $G\alpha$	0.05	1/s
k_4	Reassembly of $G\alpha$ and $G\beta\gamma$ into $G\alpha\beta\gamma$	2	μm^2/(molecules·s)
$k_5^{\text{base-line}}$	Formation of the $G\alpha^*$/AC* complex	10^{-5}	μm^2/(molecules·s)
$k_{-5}^{\text{base-line}}$	Dissociation of the $G\alpha^*$/AC* complex	0.1	1/s

Apart from k_5 and k_{-5}, all values were chosen according to [46]. Thus, k_1, k_{-1}, k_2, k_{-2} were estimates from moth olfactory transduction or vertebrate phototransduction (see [46] for further references). For the parameters k_5 and k_{-5} (see also Eqs. 13 and 14), the listed base-line values were chosen to mimic the experimentally measured dynamics of adenylate cyclase activation/deactivation in response to transmitter [42], for a detailed sensitivity-analysis, see Fig. 5A. k_5 and k_{-5} were sensitive to Ca^{++} (Eqs. 13 and 14).

doi:10.1371/journal.pone.0032885.t002

Ca^{++} was the second input to the model. Unless stated otherwise, its time-dependent concentration was modeled according to data from biochemical experiments carried out in *Aplysia* (Fig. 1A of [42]), using linear interpolation. The resulting Ca^{++} concentration started to rise at ~4.5 s, reached a peak value of $5.6 \cdot 10^{-4}$ moles/L within 6 s and decayed back to zero within ~8.5 s after stimulus onset. For Fig. 8A, the Ca^{++} concentration was calculated according to the Eq. (2), and then normalized such that the peak value was $6 \cdot 10^{-4}$ moles/L. In Figs. 8B and 8C, the Ca^{++} concentration over time was taken as

$$[Ca^{++}](t) = \begin{cases} 0 & t \le t_0, \\ [Ca^{++}_{peak}] \cdot \dfrac{e^{t\max/\tau 1}}{e^{t\max/\tau 1} - 1} \cdot \left(1 - e^{(t_0 - t)/\tau 1}\right) & t_0 < t \le t_{\max}, \\ [Ca^{++}_{peak}] \cdot e^{(-t + t_0 + t\max)/\tau 2} & t_{\max} < t \end{cases} \quad (12)$$

$[Ca^{++}{}_{peak}]$, the maximum value of $[Ca^{++}]$, was taken as $6 \cdot 10^{-4}$ moles/L in Fig. 8B and was varied as shown in Fig. 8C. t_0 was the onset of the Ca^{++} input; $t_{max} = 13$ s was the time it took the $[Ca^{++}]$ to reach its maximum; $\tau 1 = 10$ s and $\tau 2 = 1$ s were the time constants of $[Ca^{++}]$ rise and fall, respectively.

In order to account for the findings in *Aplysia* [41–43] (see Results for details), we assumed Ca^{++} to affect the reaction rate constants k_5 and k_{-5} with a delay of 2.5 s so that k_5 and k_{-5} became

$$k_5(t) = k_5^{\text{base-line}} \cdot \{1 + Ca^{++}\text{factor} \cdot [Ca^{++}](t - \Delta)\} \quad (13)$$

$$k_{-5}(t) = k_{-5}^{\text{base-line}} \cdot \{1 + Ca^{++}\text{factor} \cdot [Ca^{++}](t - \Delta)\}, \quad (14)$$

where the time-dependent input $[Ca^{++}](t)$ is replaced by $[Ca^{++}](t-\Delta)$ and $\Delta = 2.5$ s. We used Ca^{++} factor = 10 000 L/(moles·s).

Effect of event timing on the adenylate cyclase

The model system was stimulated with a transmitter input, as described above, delivered at time t = 210 s. For the control condition, a Ca^{++} input was given at t = 0 s. For the associative training, the Ca^{++} input was separated from the transmitter input with an inter-stimulus interval (ISI), which was varied across experiments between −150 s and 200 s in steps of 1 s, except in Fig. 5B2, where the range was −100 s to 200 s. Here, negative ISIs indicated that Ca^{++} preceded the transmitter; positive ISIs meant that Ca^{++} followed the transmitter. The timing of stimuli was fashioned after the behavioural experiment in Fig. 1. During the 550s- long simulation, the area under the $G\alpha^*$/AC* concentration curve was taken as a measure of cAMP production. For each ISI, we then calculated the percent associative effect as

$$\text{Percent associative effect} = \frac{\text{Area}_{\text{Control condition}} - \text{Area}_{\text{Associative training}}}{\text{Area}_{\text{Control condition}}} \cdot 100 \quad (15)$$

Negative values thus indicated that associative training with the particular ISI resulted in more cAMP production than the control

Table 3. Components and initial concentrations for the alternative model.

Abbreviation	Molecule	Initial concentration (molecules/cell)
GPCR	G protein coupled receptor	55 000
Tr/GPCR*	Complex of Tr and activated GPCR	0
G*	Activated G protein	0
AC	Adenylate cyclase	100 000
G*/AC*	Complex of G* and activated AC	0
G	G protein	100 000

Apart from the initial concentrations of AC and G*/AC*, values were as in [45] and thus estimates from neutrophil actin polymerization (see [45] for further references).

doi:10.1371/journal.pone.0032885.t003

Table 4. Rate constants of the reactions for the alternative model.

Rate constant	Reaction	Value	Unit
k_1	Formation of the Tr/GPCR* complex	$8.4 \cdot 10^7$	L/(moles·s)
k_{-1}	Dissociation of the Tr/GPCR* complex	0.37	1/s
k_6	Internalization of the Tr/GPCR* complex	0.0065	1/s
k_3	Activation of G	10^{-7}	cell/(molecules·s)
k_{-3}	Deactivation of G	0.2	1/s

All parameter values were as in [45] and thus measured or estimates from neutrophil actin polymerization (see [45] for further references). k_5 and k_{-5}, which are not included in the table, changed upon stimulation with Ca^{++} (Eqs. 13 and 14); their base-line values were varied in Fig. 10.
doi:10.1371/journal.pone.0032885.t004

condition; positive values meant less cAMP production compared to control.

Alternative model

The alternative model for the dual control of the adenylate cyclase by the transmitter (Tr) and Ca^{++} was based on [45] and is sketched in Fig. 9. The Tr and Ca^{++} concentrations were chosen according to the experiments performed in *Aplysia* (Fig. 1A of [42]), as already explained in the context of the first model, except that Tr concentration was measured in moles/L. Model components and initial concentrations are given in Table 3. The dynamical variables were updated according to the Eqs. (16) to (21) and the reaction rate constants are given in Table 4. The effect of Ca^{++} and the percent associative effect were defined as in the first model.

$$\frac{d[GPCR]}{dt} = -k_1 \cdot [Tr] \cdot [GPCR] + k_{-1} \cdot [Tr/GPCR^*] \quad (16)$$

$$\frac{d[Tr/GPCR^*]}{dt} = k_1 \cdot [Tr] \cdot [GPCR] - (k_{-1} + k_6) \cdot [Tr/GPCR^*] \quad (17)$$

$$\frac{d[G^*]}{dt} = k_3 \cdot [G] \cdot [Tr/GPCR^*] - k_{-3} \cdot [G^*] - k_5 \cdot [G^*] \cdot [AC] \quad (18)$$

$$\frac{d[AC]}{dt} = -k_5 \cdot [G^*] \cdot [AC] + k_{-5} \cdot [G^*/AC^*] \quad (19)$$

$$\frac{d[G^*/AC^*]}{dt} = k_5 \cdot [G^*] \cdot [AC] - k_{-5} \cdot [G^*/AC^*] \quad (20)$$

$$[G] + [G^*] + [G^*/AC^*] = 100000 \quad (21)$$

Acknowledgments

We would like to thank D. Reiff, E. Buchner, B. Gerber and A. Borst for discussions, and M. Stemmler for helpful comments on the manuscript.

Author Contributions

Conceived and designed the experiments: AY JN HT AVMH. Performed the experiments: AY JN. Analyzed the data: AY JN. Wrote the paper: AY JN HT AVMH.

References

1. Rescorla RA (1988) Behavioral studies of Pavlovian conditioning. Annu Rev Neurosci 11: 329–352.
2. Solomon RL, Corbit JD (1974) An opponent-process theory of motivation. I. Temporal dynamics of affect. Psychol Rev 81: 119–145.
3. Wagner AR (1981) SOP: A model of automatic memory processing in animal behavior. In: Spear NE, Miller RR, eds. Information Processing in Animals: Memory Mechanisms. Hillsdale, NJ: Erlbaum. pp 5–47.
4. Sutton RS, Barto AG (1990) Time-derivative models of pavlovian reinforcement. In: Gabriel M, Moore J, eds. Learning and computational neuroscience: Foundations of adaptive networks. Cambridge, MA: MIT Press. pp 497–537.
5. Chang RC, Blaisdell AP, Miller RR (2003) Backward conditioning: mediation by the context. J Exp Psychol Anim Behav Process 29: 171–183.
6. Moscovitch A, LoLordo VM (1968) Role of safety in the Pavlovian backward fear conditioning procedure. J Comp Physiol Psychol 66: 673–678.
7. Plotkin HC, Oakley DA (1975) Backward conditioning in the rabbit (Oryctolagus cuniculus). J Comp Physiol Psychol 88: 586–590.
8. Maier SF, Rapaport P, Wheatley KL (1976) Conditioned inhibition and the UCS-CS interval. Anim Learn Behav 4: 217–220.
9. Hellstern F, Malaka R, Hammer M (1998) Backward inhibitory learning in honeybees: a behavioral analysis of reinforcement processing. Learn Mem 4: 429–444.
10. Britton G, Farley J (1999) Behavioral and neural bases of noncoincidence learning in Hermissenda. J Neurosci 19: 9126–9132.
11. Tanimoto H, Heisenberg M, Gerber B (2004) Experimental psychology: event timing turns punishment to reward. Nature 430: 983.
12. Andreatta M, Muhlberger A, Yarali A, Gerber B, Pauli P (2010) A rift between implicit and explicit conditioned valence in human pain relief learning. Proc Biol Sci 277: 2411–2416.
13. Yarali A, Niewalda T, Chen Y-c, Tanimoto H, Duerrnagel S, et al. (2008) 'Pain relief' learning in fruit flies. Animal Behavior 76: 1173–1185.
14. Khurana S, Abu Baker MB, Siddiqi O (2009) Odor avoidance learning in the larva of Drosophila melanogaster. J Biosci 34: 621–631.
15. Yarali A, Krischke M, Michels B, Saumweber T, Mueller MJ, et al. (2009) Genetic distortion of the balance between punishment and relief learning in Drosophila. J Neurogenet 23: 235–247.
16. Yarali A, Gerber B (2010) A Neurogenetic Dissociation between Punishment-, Reward-, and Relief-Learning in Drosophila. Front Behav Neurosci 4: 189.
17. Murakami S, Dan C, Zagaeski B, Maeyama Y, Kunes S, et al. (2010) Optimizing Drosophila olfactory learning with a semi-automated training device. J Neurosci Methods 188: 195–204.
18. Drew PJ, Abbott LF (2006) Extending the effects of spike-timing-dependent plasticity to behavioral timescales. Proc Natl Acad Sci U S A 103: 8876–8881.
19. Ito I, Ong RC, Raman B, Stopfer M (2008) Olfactory learning and spike timing dependent plasticity. Commun Integr Biol 1: 170–171.
20. Murthy M, Fiete I, Laurent G (2008) Testing odor response stereotypy in the Drosophila mushroom body. Neuron 59: 1009–1023.
21. Turner GC, Bazhenov M, Laurent G (2008) Olfactory representations by Drosophila mushroom body neurons. J Neurophysiol 99: 734–746.
22. Wang Y, Guo HF, Pologruto TA, Hannan F, Hakker I, et al. (2004) Stereotyped odor-evoked activity in the mushroom body of Drosophila revealed by green fluorescent protein-based Ca2+ imaging. J Neurosci 24: 6507–6514.

23. Yu D, Akalal DB, Davis RL (2006) Drosophila alpha/beta mushroom body neurons form a branch-specific, long-term cellular memory trace after spaced olfactory conditioning. Neuron 52: 845–855.
24. Wang Y, Mamiya A, Chiang AS, Zhong Y (2008) Imaging of an early memory trace in the Drosophila mushroom body. J Neurosci 28: 4368–4376.
25. Schwaerzel M, Monastirioti M, Scholz H, Friggi-Grelin F, Birman S, et al. (2003) Dopamine and octopamine differentiate between aversive and appetitive olfactory memories in Drosophila. J Neurosci 23: 10495–10502.
26. Riemensperger T, Voller T, Stock P, Buchner E, Fiala A (2005) Punishment prediction by dopaminergic neurons in Drosophila. Curr Biol 15: 1953–1960.
27. Kim YC, Lee HG, Han KA (2007) D1 dopamine receptor dDA1 is required in the mushroom body neurons for aversive and appetitive learning in Drosophila. J Neurosci 27: 7640–7647.
28. Claridge-Chang A, Roorda RD, Vrontou E, Sjulson L, Li H, et al. (2009) Writing memories with light-addressable reinforcement circuitry. Cell 139: 405–415.
29. Aso Y, Siwanowicz I, Bräcker L, Ito K, Kitamoto T, et al. (2010) Specific dopaminergic neurons for the formation of labile aversive memory. Curr Biol 20: 1445–1451.
30. Livingstone MS, Sziber PP, Quinn WG (1984) Loss of calcium/calmodulin responsiveness in adenylate cyclase of rutabaga, a Drosophila learning mutant. Cell 37: 205–215.
31. Connolly JB, Roberts IJ, Armstrong JD, Kaiser K, Forte M, et al. (1996) Associative learning disrupted by impaired Gs signaling in Drosophila mushroom bodies. Science 274: 2104–2107.
32. Zars T, Fischer M, Schulz R, Heisenberg M (2000) Localization of a short-term memory in Drosophila. Science 288: 672–675.
33. Blum AL, Li W, Cressy M, Dubnau J (2009) Short- and long-term memory in Drosophila require cAMP signaling in distinct neuron types. Curr Biol 19: 1341–1350.
34. Tomchik SM, Davis RL (2009) Dynamics of learning-related cAMP signaling and stimulus integration in the Drosophila olfactory pathway. Neuron 64: 510–521.
35. Gervasi N, Tchenio P, Preat T (2010) PKA dynamics in a Drosophila learning center: coincidence detection by rutabaga adenylyl cyclase and spatial regulation by dunce phosphodiesterase. Neuron 65: 516–529.
36. Séjourné J, Plaçais PY, Aso Y, Siwanowicz I, Trannoy S, et al. (2011) Mushroom body efferent neurons responsible for aversive olfactory memory retrieval in Drosophila. Nat Neurosci 14: 903–910.
37. Lin AH, Cohen JE, Wan Q, Niu K, Shrestha P, et al. (2010) Serotonin stimulation of cAMP-dependent plasticity in Aplysia sensory neurons is mediated by calmodulin-sensitive adenylyl cyclase. Proc Natl Acad Sci U S A 107: 15607–15612.
38. Abrams TW (1985) Activity-dependent presynaptic facilitation: an associative mechanism in Aplysia. Cell Mol Neurobiol 5: 123–145.
39. Ocorr KA, Walters ET, Byrne JH (1985) Associative conditioning analog selectively increases cAMP levels of tail sensory neurons in Aplysia. Proc Natl Acad Sci U S A 82: 2548–2552.
40. Abrams TW, Karl KA, Kandel ER (1991) Biochemical studies of stimulus convergence during classical conditioning in Aplysia: dual regulation of adenylate cyclase by Ca2+/calmodulin and transmitter. J Neurosci 11: 2655–2665.
41. Yovell Y, Abrams TW (1992) Temporal asymmetry in activation of Aplysia adenylyl cyclase by calcium and transmitter may explain temporal requirements of conditioning. Proc Natl Acad Sci U S A 89: 6526–6530.
42. Abrams TW, Yovell Y, Onyike CU, Cohen JE, Jarrard HE (1998) Analysis of sequence-dependent interactions between transient calcium and transmitter stimuli in activating adenylyl cyclase in Aplysia: possible contribution to CS–US sequence requirement during conditioning. Learn Mem 4: 496–509.
43. Onyike CU, Lin AH, Abrams TW (1998) Persistence of the interaction of calmodulin with adenylyl cyclase: implications for integration of transient calcium stimuli. J Neurochem 71: 1298–1306.
44. Lin AH, Onyike CU, Abrams TW (1998) Sequence-dependent interactions between transient calcium and transmitter stimuli in activation of mammalian brain adenylyl cyclase. Brain Res 800: 300–307.
45. Adams JA, Omann GM, Linderman JJ (1998) A mathematical model for ligand/receptor/G-protein dynamics and actin polymerization in human neutrophils. J Theor Biol 193: 543–560.
46. Rospars JP, Lucas P, Coppey M (2007) Modeling the early steps of transduction in insect olfactory receptor neurons. Biosystems 89: 101–109.
47. Preat T (1998) Decreased odor avoidance after electric shock in Drosophila mutants biases learning and memory tests. J Neurosci 18: 8534–8538.
48. Acevedo SF, Froudarakis EI, Tsiorva A-A, Skoulakis EMC (2007) Distinct neuronal circuits mediate experience-dependent, non-associative osmotactic responses in Drosophila. Mol Cell Neurosci 34: 378–389.
49. Alberts B, Johnson A, Levis J, Raff M, Roberts K, et al. (2002) Molecular Biology of the Cell. 4th ed. New York: Garland Science. pp 868–869.
50. Halnes G, Ulfhielm E, Ljunggren EE, Kotaleski JH, Rospars J-P (2009) Modelling and sensitivity analysis of the reactions involving receptor, G-protein and effector in vertebrate olfactory receptor neurons. J Comput Neurosci 27: 471–491.
51. Tully T, Quinn WG (1985) Classical conditioning and retention in normal and mutant Drosophila melanogaster. J Comp Physiol A 157: 263–277.
52. Galili DS, Lüdke A, Galizia CG, Szyszka P, Tanimoto H (2011) Olfactory trace conditioning in Drosophila. J Neurosci 31: 7240–7248.
53. Dougherty DP, Wright GA, Yew AC (2005) Computational model of the cAMP-mediated sensory response and calcium-dependent adaptation in vertebrate olfactory receptor neurons. Proc Natl Acad Sci U S A 102: 10415–10420.
54. Shuai Y, Hu Y, Qin H, Campbell RA, Zhong Y (2011) Distinct molecular underpinnings of Drosophila olfactory trace conditioning. Proc Natl Acad Sci U S A 108: 20201–20206.
55. Lindskog M, Kim M, Wikström MA, Blackwell KT, Kotaleski JH (2006) Transient calcium and dopamine increase PKA activity and DARPP-32 phosphorylation. PLoS Comp Biol 2: e19.
56. Zhang J, Lau P, Bi G (2009) Gain in sensitivity and loss in temporal contrast of STDP by dopaminergic modulation at hippocampal synapses. Proc Natl Acad Sci U S A 106: 13028–13033.
57. Whitlock JR, Heynen AJ, Shuler MG, Bear MF (2006) Learning induces long-term potentiation in the hippocampus. Science 313: 1093–1097.
58. Michels B, Chen YC, Saumweber T, Mishra D, Tanimoto H, et al. (2011) Cellular site and molecular mode of synapsin action in associative learning. Learn Mem 18: 332–344.
59. Muller U (2000) Prolonged activation of cAMP-dependent protein kinase during conditioning induces long-term memory in honeybees. Neuron 27: 159–168.
60. Aszodi A, Muller U, Friedrich P, Spatz HC (1991) Signal convergence on protein kinase A as a molecular correlate of learning. Proc Natl Acad Sci U S A 88: 5832–5836.
61. Pagani MR, Oishi K, Gelb BD, Zhong Y (2009) The phosphatase SHP2 regulates the spacing effect for long-term memory induction. Cell 139: 186–198.
62. Pan Y, Zhou Y, Guo C, Gong H, Gong Z, et al. (2009) Differential roles of the fan-shaped body and the ellipsoid body in Drosophila visual pattern memory. Learn Mem 16: 289–295.
63. Selcho M, Pauls D, Han KA, Stocker RF, Thum AS (2009) The role of dopamine in Drosophila larval classical olfactory conditioning. PLoS One 4: e5897.
64. Seugnet L, Suzuki Y, Vine L, Gottschalk L, Shaw PJ (2008) D1 receptor activation in the mushroom bodies rescues sleep-loss-induced learning impairments in Drosophila. Curr Biol 18: 1110–1117.
65. Cassenaer S, Laurent G (2007) Hebbian STDP in mushroom bodies facilitates the synchronous flow of olfactory information in locusts. Nature 448: 709–713.
66. Cassenaer S, Laurent G (2012) Conditional modulation of spike-timing-dependent plasticity for olfactory learning. Nature 482: 47–52.

3

A MODEL FOR NON-MONOTONIC INTENSITY CODING

3.1 SUMMARY

Flies are able to associate the intensity of an olfactory stimulus with an electric shock. When trained at an intermediate intensity, they show a smaller conditioned response both for higher and lower odor intensities presented during the test, despite the fact that learning performance generally increases with increasing odor intensity.

This is particularly striking when regarding the representation of odor intensity in the first layers of olfactory processing in the fly olfactory system. Neuronal activity increases monotonically with increasing stimulus intensity. The activity pattern of a smaller intensity is always a subset of active units of the higher intensity. This representation is therefore not suitable for intensity specific learning.

We propose a minimalistic circuit motif that resolves this problem of nestedness by introducing a layer of intensity specific units. A balance of excitatory and inhibitory synapses combined with self-regulating homeostatic weights leads to neurons that respond strongest at an intermediate odor intensity. By incorporating a learning mechanism we show that the proposed circuit motif replicates the behavioral results obtained in the experiment. We further show numerical stability of the model under parameter variations, emphasizing the generality of the motif.

By relating the proposed model units in the circuit motif to the known anatomy of the fruit fly, we are able to suggest dedicated experiments that test the model assumptions.

3.2 REFERENCE

This work was performed in collaboration with A. Yarali, H. Tanimoto and A. V. M. Herz.

The paper has been published in the Royal Society Open Science under the reference

A model for non-monotonic intensity coding.
Johannes Nehrkorn, Hiromu Tanimoto, Andreas V. M. Herz, Ayse Yarali. R. Soc. open sci. 2015 2 150120;
http://dx.doi.org/10.1098/rsos.150120.
Published 6 May 2015

ROYAL SOCIETY OPEN SCIENCE

rsos.royalsocietypublishing.org

Research

Cite this article: Nehrkorn J, Tanimoto H, Herz AVM, Yarali A. 2015 A model for non-monotonic intensity coding. *R. Soc. open sci.* **2**: 150120.
http://dx.doi.org/10.1098/rsos.150120

Received: 23 March 2015
Accepted: 9 April 2015

Subject Category:
Biology (whole organism)

Subject Areas:
behaviour/neuroscience/computational biology

Keywords:
associative learning, homeostatic plasticity, neural coding, olfaction, stimulus intensity

Authors for correspondence:
Andreas V. M. Herz
e-mail: herz@bio.lmu.de
Ayse Yarali
e-mail: ayse.yarali@lin-magdeburg.de

Electronic supplementary material is available at http://dx.doi.org/10.1098/rsos.150120 or via http://rsos.royalsocietypublishing.org.

THE ROYAL SOCIETY PUBLISHING

A model for non-monotonic intensity coding

Johannes Nehrkorn[1,2], Hiromu Tanimoto[2,3], Andreas V. M. Herz[1] and Ayse Yarali[2,4,5]

[1]Department of Biology II, Bernstein Center for Computational Neuroscience Munich and Graduate School of Systemic Neurosciences, Ludwig-Maximilians-Universität München, Martinsried 82152, Germany
[2]Max Planck Institute of Neurobiology, Martinsried 82152, Germany
[3]Tohoku University Graduate School of Life Sciences, Sendai 980-8577, Japan
[4]Research Group Molecular Systems Biology of Learning, Leibniz Institute for Neurobiology, Magdeburg 39118, Germany
[5]Center for Brain and Behavioural Sciences, Magdeburg, Germany

1. Summary

Peripheral neurons of most sensory systems increase their response with increasing stimulus intensity. Behavioural responses, however, can be specific to some intermediate intensity level whose particular value might be innate or associatively learned. Learning such a preference requires an adjustable transformation from a monotonic stimulus representation at the sensory periphery to a non-monotonic representation for the motor command. How do neural systems accomplish this task? We tackle this general question focusing on odour-intensity learning in the fruit fly, whose first- and second-order olfactory neurons show monotonic stimulus–response curves. Nevertheless, flies form associative memories specific to particular trained odour intensities. Thus, downstream of the first two olfactory processing layers, odour intensity must be re-coded to enable intensity-specific associative learning. We present a minimal, feed-forward, three-layer circuit, which implements the required transformation by combining excitation, inhibition, and, as a decisive third element, homeostatic plasticity. Key features of this circuit motif are consistent with the known architecture and physiology of the fly olfactory system, whereas alternative mechanisms are either not composed of simple, scalable building blocks or not compatible with physiological observations. The simplicity of the circuit and the robustness of its function under parameter changes make this computational motif an attractive candidate for tuneable non-monotonic intensity coding.

2. Introduction

Varying a sensory stimulus can influence behaviour in two fundamentally different ways. First, the map from stimulus to behaviour can be one-to-one. For example, the reaction time of

human beings to a light stimulus decreases steadily with increasing light intensity [1]. At the neuronal level, monotonic stimulus–response curves suffice to explain this phenomenon. Second, a particular behaviour may only be triggered by a certain range of intermediate stimulus values; for instance, rats and fruit flies prefer weak, but not strong, salt solutions over plain water [2,3]. In this case, the brain needs to represent the stimulus in a non-monotonic way to generate the appropriate behaviour.

For some stimulus attributes, bell-shaped tuning curves at the sensory periphery solve this task. The peaked frequency tuning of hair cells [4], for example arises because the basal membrane of the vertebrate cochlea vibrates most strongly at a location determined by the frequency of the presented sound. For other stimulus dimensions, such as sound amplitude [5], sensory neurons have monotonic input–output curves, raising the question of how non-monotonic stimulus dependencies of behavioural responses are generated.

A suitable system to study this general question is odour-intensity learning. Odour intensity is typically encoded in a monotonic way by the first- and second-order olfactory neurons; consequently, the neuronal population activated by an odour grows with increasing odour intensity and the representation of a lower intensity is nested within that of a higher intensity (e.g. [6–8]). The overall increase in neuronal activation with rising odour intensity can be useful to explain the ability to detect odour gradients (as argued, e.g. in [9–11]) as well as the improvement of olfactory detection, associative learning and memory retrieval at higher intensities (e.g. [12]). Changes in the hedonic value of an odour with increasing intensity can arise if neurons with different sensitivities are connected to opponent downstream pathways (e.g. [13]). Finally, changes in discriminability across odours with rising intensity are consistent with growing odour representations (e.g. [14]). However, a key behavioural observation remains unexplained: animals form associative memories specific to trained odour intensities such that later on, neither lower nor higher intensities release as strong a conditioned behaviour, as shown in the fruit fly [12,15–17], honeybee [18] and mouse [19]. This intensity specificity of learning suggests that along the olfactory pathway, downstream of the initial monotonic encoding, odour intensity must be re-coded in a non-monotonic manner.

We present a simple, biologically plausible neuronal circuit motif that does just this. We quantitatively compare the intensity coding ability of this model to the intensity specificity of olfactory memories, as assayed in the fruit fly and discuss how this circuit may be implemented in the fly olfactory system, thus leading to experimentally testable hypotheses. The circuit motif found may also be relevant for other cases where stimulus intensity must be encoded in a non-monotonic fashion to enable intensity-specific behaviours (for an example in the auditory modality, see [5]).

3. Material and methods

3.1. Input layer

The activity of excitatory and inhibitory input neurons (figure 2*b*) are described by logistic input–output functions:

$$\mathrm{exc}_k(i) = \frac{1}{\mathrm{e}^{-4b(i-a_k)}+1} \quad \text{and} \quad \mathrm{inh}(i) = \frac{\mathrm{inh}_{\max}}{\mathrm{e}^{-4b_{\mathrm{inh}}(i-a_{\mathrm{inh}})}+1}, \tag{3.1}$$

where i is the odour intensity in logarithmic units. Thus, a_k and a_{inh} are the odour intensities at the turning points of the respective logistic sensitivity functions, i.e. a large negative a-value implies a high sensitivity. The factor 4 in the exponents is chosen so that b and b_{inh} are the slopes at the turning points, where $b > b_{\mathrm{inh}}$. The parameter $\mathrm{inh}_{\max} > 1$ scales the sensitivity function of the inhibitory input neuron. For simplicity, only three excitatory input neurons are considered. Their a_k values are shifted in steps of one logarithmic unit.

3.2. Intermediate layer

The activity of the intermediate-layer neurons (figure 2*c*) are calculated as rectified weighted sums of the input activities as

$$\mathrm{inter}_k(i) = \mathrm{Rect}(w_{\mathrm{exc}}\,\mathrm{exc}_k(i) + w_{\mathrm{inh}}\,\mathrm{inh}(i)), \tag{3.2}$$

where w_{exc} and w_{inh} are the weights of the respective excitatory and inhibitory inputs. The rectifying function $\mathrm{Rect}(x)$ is defined as $\mathrm{Rect}(x<0)=0$ and $\mathrm{Rect}(x\geq 0)=x$, and results in a threshold neuronal activation function.

3.3. Homeostatic plasticity

We consider two scenarios for homeostatic plasticity. In both cases, we do not model how the synaptic strength changes in response to each individual stimulus presentation but rather calculate the resulting mean effect of homeostatic plasticity under the assumption that already prior to the specific associative odour-shock training, the system has been exposed to odours drawn from a broad range of concentrations.

In the first scenario (figure 3*a*(i)), the weights of the inhibitory synapses to the intermediate layer are set uniformly to be $w_{\text{inh}} = -1$; whereas each excitatory synapse (w_{exc}) is subject to homeostatic plasticity. To implement the mean effect of this regulatory process, the weights w_{exc} are adjusted based on the sensitivity of the respective excitatory input neurons: the more sensitive an input neuron is (more negative a-value), the higher its mean activation and, consequently, the mean rate at which it drives the downstream intermediate-layer neuron. This effect will be balanced by homeostatic plasticity. As a measure of the input neuron's sensitivity, we take the integral of the input–output function $\text{exc}_k(i)$ over a concentration range $[c_0, c_1]$:

$$s = \int_{c_0}^{c_1} \text{exc}(i)\,\mathrm{d}i = \frac{1}{4b} \ln\left\{\frac{1+\mathrm{e}^{4b(c_1-a)}}{1+\mathrm{e}^{4b(c_0-a)}}\right\} = s(a). \tag{3.3}$$

The sensitivity function $s(a)$ approaches c_1–c_0 for $a \to -\infty$ and zero for $a \to \infty$. For intermediate values $c_0 < a < c_1$, $s(a)$ scales roughly linear in a. Then, based on $s(a)$, we adjust the respective excitatory output weight as

$$w_{\text{exc}}(a) = -\alpha(s(a) - d), \tag{3.4}$$

where α is a scaling factor and d is set such that $w_{\text{exc}}(a) > 0$ (see inset in figure 3*a*(i)). Thus, in the spirit of homeostatic plasticity, the more sensitive an excitatory input neuron is, the weaker its synapse to the intermediate layer will be. Mechanistically, this could either be implemented through 'local' homeostatic plasticity [20,21] acting directly at this excitatory synapse, or through classical homeostatic plasticity [22], as we only consider a single excitatory input to each intermediate-layer neuron.

In the second scenario (figure 3*b*(i)), the weights of all excitatory synapses are set to $w_{\text{exc}} = 1$. Implementing the mean effect of homeostatic plasticity, the weight of each inhibitory synapse is scaled according to the sensitivity of the cognate excitatory input neuron as

$$w_{\text{inh}}(a) = -\tilde{\alpha}s(a), \tag{3.5}$$

where $\tilde{\alpha}$ is a scaling factor (see inset in figure 3*b*(i)). Thus, the smaller the excitatory drive of an intermediate neuron, the weaker is also its inhibitory input, in accordance with experimental findings on homeostatic plasticity at inhibitory synapses [21,23,24].

3.4. Output neuron and associative plasticity

The activity of the output neuron is calculated as the weighted sum of the intermediate-layer neuron activities:

$$\text{out}(i) = \sum_k w_{\text{training},k}\text{inter}_k(i). \tag{3.6}$$

Initially, the weights $w_{\text{training},k}$ are all zero. During associative odour-shock training (e.g. figures 2*d*, 3*a*(iii),*b*(iii)), these weights change proportional to the odour-induced activity in the respective intermediate neuron, owing to the delivery of a concurrent reinforcement signal as

$$\Delta w_{\text{training},k} = \Theta(\text{shock})\,\text{inter}_k(i_{\text{training}}), \tag{3.7}$$

where $\theta(x)$ is the Heaviside function, defined as 0 if $x \leq 0$ and 1 otherwise, representing the presence versus absence of shock and i_{training} is the odour intensity at training.

4. Results

4.1. Olfactory memories of flies are odour-intensity specific

The intensity specificity of fruit fly olfactory memories has been reported in several studies using different developmental stages, experimental rationale and reinforcers ([12,15–17,25,26]; for a comparative discussion see [12]). We start with a meta-analysis of three experiments that apply a common paradigm to three odours [12]. In each experiment, flies are trained *en masse*, with pairings of a chosen intensity of the respective odour and electric shock. Different groups of flies are then tested for their avoidance of this odour at the trained, a lower or a higher intensity (figure 1*a*). In each case, conditioned avoidance is scored by comparing the behaviour of flies trained as explained with paired presentation of odour and shock versus flies trained with temporally unpaired presentation of the same stimuli; thus, the scores refer to effects of associative learning and not to innate odour-responsiveness. Across all three experiments, flies show the strongest conditioned avoidance when the testing and training intensities match (figure 1*b*). For better comparison across experiments, we align the three datasets along the stimulus and the response axes and find similar Gaussian fits, despite the diversity of odours (figure 1*c*). Results from an appetitive olfactory learning assay in *Drosophila* larvae [17] paint a similar picture (see the legend of figure 1*c*).

4.2. A simple circuit motif for odour-intensity-specific memories

Fruit fly olfactory sensory neurons (OSNs) and projection neurons (PNs) increase their activity with rising odour intensity at the single-cell level, as exemplified in figure 1*e*,*f* (see also [8,10,27,29–32] for demonstration of this property using a variety of methods). As a direct consequence of such monotonic input–output curves, an odour at low intensity excites relatively few neurons, whereas the same odour at a higher intensity recruits not only these but also additional neurons. Based on such a nested representation of odour intensities alone, the memory trace of a low-intensity odour would be activated at least as strongly by a higher intensity of the same odour. However, olfactory associative memories in flies are intensity specific (figure 1*a*–*c*). This implies that non-monotonic intensity responses must emerge in downstream layers of the olfactory pathway. The following model accomplishes this task.

The input layer of the model harbours multiple excitatory neurons (figure 2*a*, blue) with different, monotonic responses, represented by logistic functions that are shifted by different offsets along the stimulus axis (figure 2*b*, blue). These functions are inspired by fly OSN- and PN-electrophysiology (e.g. [27] and [29]; figure 1*e*,*f*), as well as computational models of olfactory transduction (e.g. [33]). The modelled excitatory input neurons are connected one-to-one with neurons of the intermediate layer (figure 2*a*, green). In addition, a single inhibitory neuron with monotonic input–output function (figure 2*a*,*b*, red) provides input to all intermediate neurons. The convergence of excitation and inhibition endows each intermediate neuron with a bell-shaped tuning curve (figure 2*c*). The relative shift of sensitivity across the excitatory input neurons (figure 2*b*, blue) and the shallower sensitivity curve of the inhibitory neuron as compared with the excitatory neurons cause the intermediate neurons to differ in their tuning curves (figure 2*c*) but the nestedness of these tuning curves rules out that memories are intensity specific.

To illustrate this important limitation we introduce an output neuron, onto which all intermediate neurons converge (figure 2*a*, black). Prior to any training, the synaptic weights are set to zero so that the output neuron does not respond to even the most intense odour (note that the innate olfactory behaviour pathway is not represented in the model). When we train the circuit by pairing a given odour intensity with electric shock (figure 2*d*, training), each intermediate neuron is activated to a certain degree, which depends on its tuning curve and the intensity of the presented odour. In addition, a reinforcement signal, induced by the electric shock is delivered to the output synapse of each intermediate neuron (figure 2*a*, yellow). Owing to this reinforcement signal, each output synapse is strengthened proportional to the respective level of odour-induced activity (figure 2*d*, training). This potentiation of output synapses is the trace for the odour-shock memory. To read out this trace at test, we present the circuit with various odour intensities and measure the activity of the output neuron (figure 2*d*, test). If the circuit mimics the flies' intensity-specific learning (figure 1*a*–*c*), the output neuron will respond most strongly when the training and testing intensities match. This is not the case (figure 2*d*, test): although after all three kinds of training, the output neuron activity depends on the odour intensity with a bell-shaped function, the peaks do not correspond to the respective odour intensities used at training.

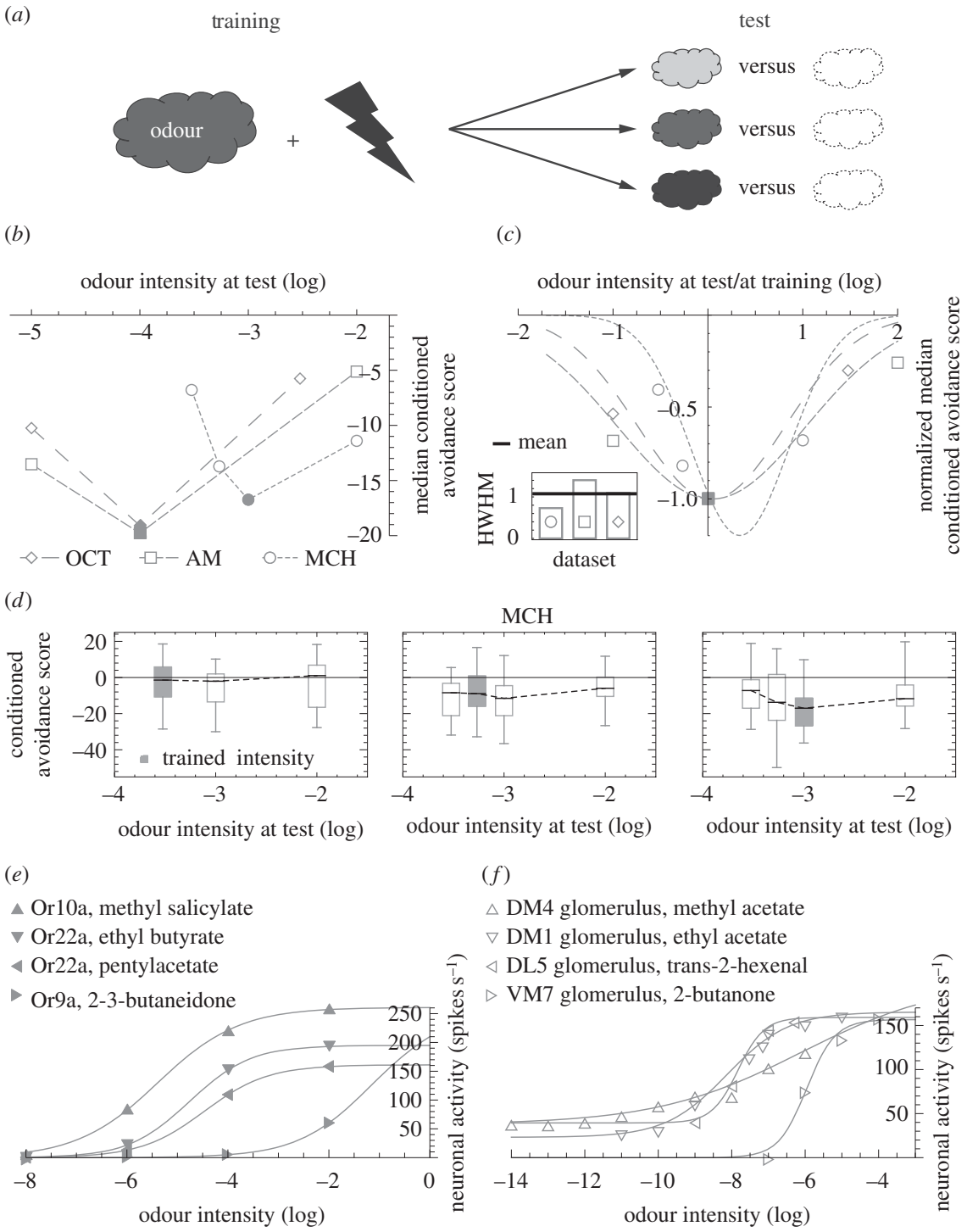

Figure 1. (*Caption overleaf.*)

To solve this problem, we enrich the circuit shown in figure 2*a* with homeostatic synaptic plasticity, which maintains the activity level of intermediate-layer neurons within a certain range by boosting weak signals, while suppressing strong ones [20–24]. Indeed, homeostatic regulation has been shown on different levels of the fly olfactory system [34–36]. Accordingly, we assume that the animal is exposed to a wide range of odours at various concentrations prior to the associative odour-shock training, and that this leads to homeostatic plasticity, which we describe at the level of time-averaged effects in our model. First, we implement this mechanism at the excitatory input synapses projecting onto the intermediate layer (figure 3*a*(i)). For simplicity, we calculate the resulting mean effect of homeostatic regulation instead of modelling the synaptic strength changes in response to each individual stimulus presentation. As expected, the more often an intermediate-layer neuron is activated on average (because of a more sensitive input neuron), the weaker the respective excitatory synapse becomes. In an alternative scenario (figure 3*b*(i)), we implement the homeostatic plasticity at the inhibitory synapses onto the intermediate layer. This means that the inhibitory synapses are adjusted such that the more often an intermediate-layer

Figure 1. (*Overleaf*.) Learned olfactory behaviour is intensity specific, unlike the response characteristics of sensory and projection neurons. (*a*) One subgroup of flies is trained *en masse* such that an odour is temporally paired with electric shock; whereas a second subgroup (not sketched) is presented with odour and shock in an unpaired fashion. Each subgroup is then tested for choice between the trained odour versus a non-odorous solvent and a preference index is calculated as $PI = (\#_{Odour} - \#_{Solvent}) \cdot 100/\#_{Total}$, where # is the number of flies on each side. A conditioned avoidance score is defined as $CAS = (PI_{Paired} - PI_{Unpaired})/2$, i.e. $PI_{Unpaired}$ acts as a baseline to which PI_{Paired} is compared. Negative CASs indicate conditioned avoidance. To probe for the intensity specificity of the conditioned behaviour, we compare CASs across groups, which are trained with one common odour intensity, but tested with different intensities (different grey shades). (*b*) In three different experiments, the design in (*a*) is applied to the odours 3-octanol (OCT), *n*-amylacetate (AM) and 4-methlycyclohexanol (MCH). Critically, odour intensities are chosen from the dynamic range of the respective dose–response curves of learning and retrieval [12]. The median CAS is shown as a function of the odour intensity at test. For filled symbols, the testing intensity equals training intensity. Sample sizes are left to right $N = 20, 20, 20$ for OCT, $N = 20, 24, 24$ for AM and $N = 24, 31, 24, 24$ for MCH, referring to the number of independent measurements. Data are from [12]. For a more detailed description of the methods, see [12]. (*c*) Data in (*b*) are normalized along the intensity axis by dividing test intensities by the training value; and along the CAS axis by dividing median CASs by values from matching training and testing intensities. The results are fitted with Gaussian distributions. Their half widths at half maximum (HWHM, inset) are similar (mean: 1.1, s.d.: 0.3) and close to results from odour-sugar associative learning experiments in larval *Drosophila* ([17], HWHM mean $\pm$ s.d. $= 1.5 \pm 0.4$). (*d*) In three different experiments, the design in (*a*) is applied to the odour MCH. In each experiment, a different MCH intensity is used for training. The box plots represent the median by the midline, 25 and 75% by the box boundaries and 0 and 100% by the whiskers. Grey filling indicates matching training and test intensities. Training with a very low MCH intensity (left panel) results in CASs that are not different from zero, no matter the testing intensity (Kruskal–Wallis test: $H = 1.04$, d.f. $= 2$, $p = 0.59$; one-sample sign test comparing pooled data to zero: $p = 0.90$; $N = 16, 24, 24$). When the training intensity is somewhat raised (middle panel), the CASs statistically do not depend on test intensity and when pooled indicate slight conditioned avoidance (Kruskal–Wallis test: $H = 4.65$, d.f. $= 3$, $p = 0.20$; one-sample sign test comparing pooled data to zero: $p < 0.05$; $N = 31, 33, 33, 33$). Finally, for a further raised training intensity (right panel), CASs depend on test intensity (Kruskal–Wallis test: $H = 9.27$, d.f. $= 3$, $p = 0.02$) and are strongest when training and test intensities resemble each other (Mann–Whitney *U* tests: test at 0.0003 versus 0.001: $U = 147.00$, $p < 0.05/3$; test at 0.00054 versus 0.001, $U = 290.00$, $p = 0.17$; test at 0.01 versus 0.001, $U = 159.00$, $p < 0.05/3$; $N = 24, 31, 24, 24$). Data in the right panel from [12]. Note that the training intensity used in this panel is chosen from the middle of the dynamic range of the dose–effect function for learning and retrieval [12]. (*e*) Monotonic intensity tuning of single olfactory sensory neurons (OSN) which ectopically express the specified olfactory receptor (Or) molecule, taken from [27]. For a comparison between the electrophysiology of such transgenic OSNs versus wild-type ones, see [28]. Note that monotonic intensity tuning has been documented also with respect to wild-type OSNs (e.g. [29]). (*f*) Monotonic intensity tuning of single olfactory projection neurons, innervating the indicated antennal lobe glomeruli, taken from [29]. In (*e*) and (*f*), the lines correspond to fitted logistic functions.

neuron is activated, the stronger the respective local inhibitory synapse becomes. Both scenarios result in non-monotonic and, critically, non-nested tuning curves across the intermediate layer (figure 3*a*(ii), *b*(ii)). Consequently, in either scenario, when we train the circuit with a given odour intensity paired with electric shock, the output neuron indeed responds most strongly to this very intensity at test (figure 3*a*(iii),*b*(iii)), mimicking the flies' odour-intensity-specific memories. Furthermore, with lower training intensities, the output neuron activity at test is smaller and more broadly tuned (especially pronounced in figure 3*a*(iii)), reflecting fly behavioural data, where lower training intensities result in weaker and less intensity-specific conditioned avoidance scores (figure 1*d*).

Within a biological implementation of the model, the sketched excitatory neurons of the input layer need to receive common olfactory input so that the rank order of sensitivities does not change with odour identity. This circuit property can be fulfilled if these neurons were, e.g. uni-glomerular projection neurons innervating a common antennal lobe glomerulus, or multi-glomerular projection neurons each innervating a large sum of glomeruli (see Discussion and figure 4 for details). Note also that the time scale on which the homeostatic plasticity occurs is long compared to the time scale of the training and testing of odour-intensity-specific memories. This is consistent with homeostatic adjustments taking place during development and/or early life in response to olfactory exposure.

Importantly, the ability of the model to mimic flies' intensity coding is robust across a large parameter space, as revealed by a detailed sensitivity analysis (electronic supplementary material, figure S1). This flexibility may render the model circuit attractive for a variety of neuronal systems.

5. Discussion

The early stages of most sensory systems encode stimulus intensity with monotonic response curves (see [42,43] for vision, [44] for hearing, [45] for somatosensation, [46] for taste, but [3] for an exception

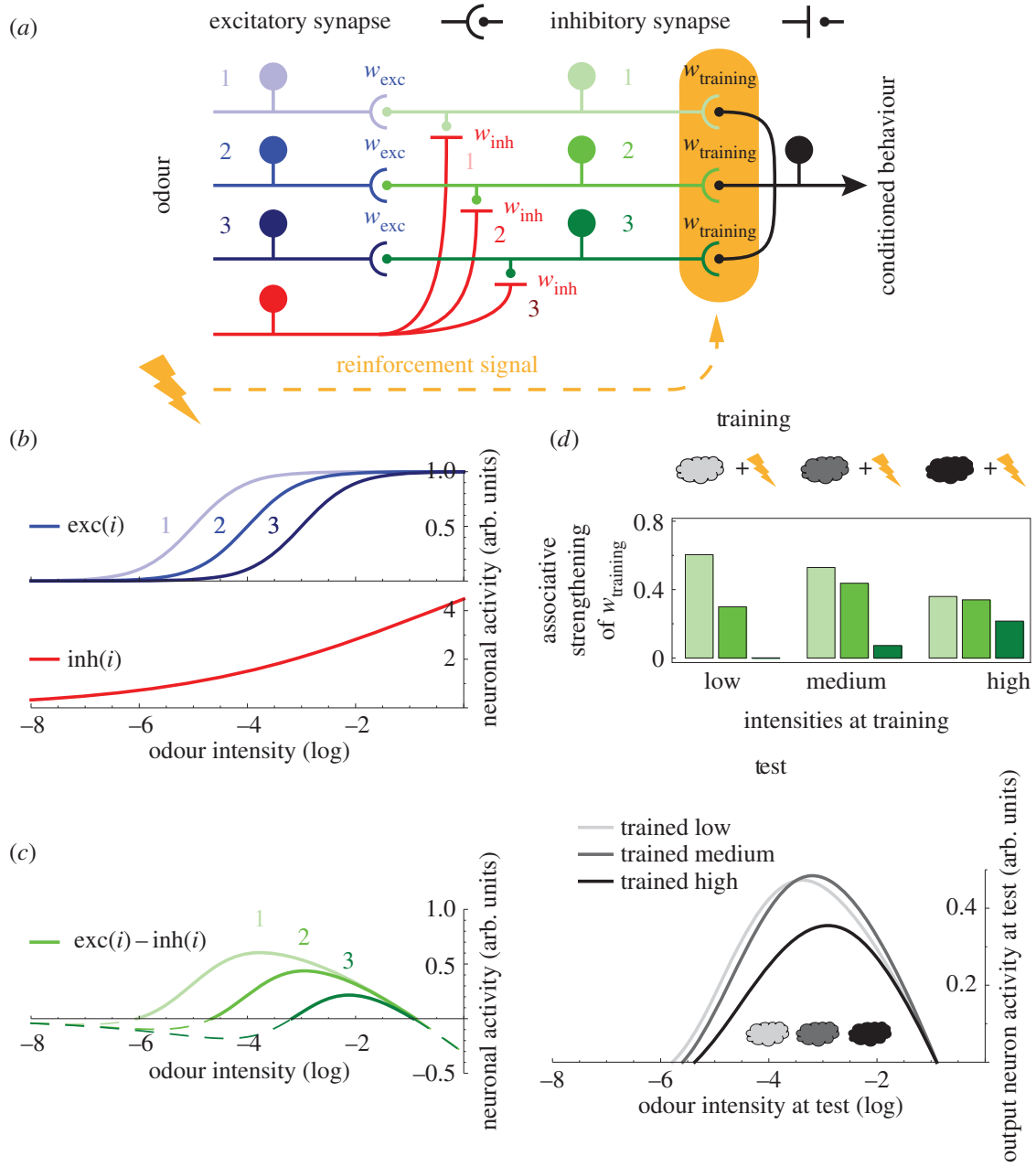

Figure 2. Convergence of excitatory and inhibitory inputs generates non-monotonic intensity tuning but does not allow intensity-specific memories. (*a*) Model circuit. The odour is feed-forwardly processed through three neuronal layers. For simplicity, the input layer consists of only three excitatory (blue) and one inhibitory neuron (red). The excitatory neurons connect one-to-one with three intermediate-layer neurons (green) with weights w_{exc}, the single inhibitory neuron provides input to all intermediate neurons with weights w_{inh}. Intermediate neurons converge onto one output neuron (black) with weights $w_{training}$. The output synapses of the intermediate layer also receive an electric shock-induced reinforcement signal (yellow). (*b*) The activity of input neurons increases with increasing odour intensity according to the logistic functions exc(*i*) (blue) and inh(*i*) (red), respectively. The different exc(*i*) share slope and asymptote, but are shifted along the intensity axis. Critically, the function inh(*i*) is less steep than the exc(*i*) functions. (*c*) The activity of each intermediate neuron is the weighted difference between its cognate excitatory input and the shared inhibitory input, i.e. exc(*i*)–inh(*i*) (green), as the weights of all inputs are adjusted to 1. The resulting bell-shaped tuning curves are nested. (*d*) Using this circuit, we simulate three experiments. Different odour intensities (differently shaded clouds) are paired with shock during training. Upon presentation of the respective odour intensity, each intermediate neuron is activated depending on its tuning. Upon the contingent delivery of shock, a reinforcement signal strengthens intermediate-layer output synapses, proportional to the pre-synaptic activity level (green bars). At test, we present the circuit with a series of odour intensities, including the trained ones, and measure the activity of the output neuron, which indeed depends non-monotonically on odour intensity in each experiment (grey lines). Critically, however, the activity peaks around the same intensity-range in all three experiments, despite the difference in the training intensities used.

regarding taste). The absence of non-monotonic intensity tuning in the initial processing steps is particularly striking in olfaction, because animals readily form odour-intensity-specific associative memories [12,15–19,25,26].

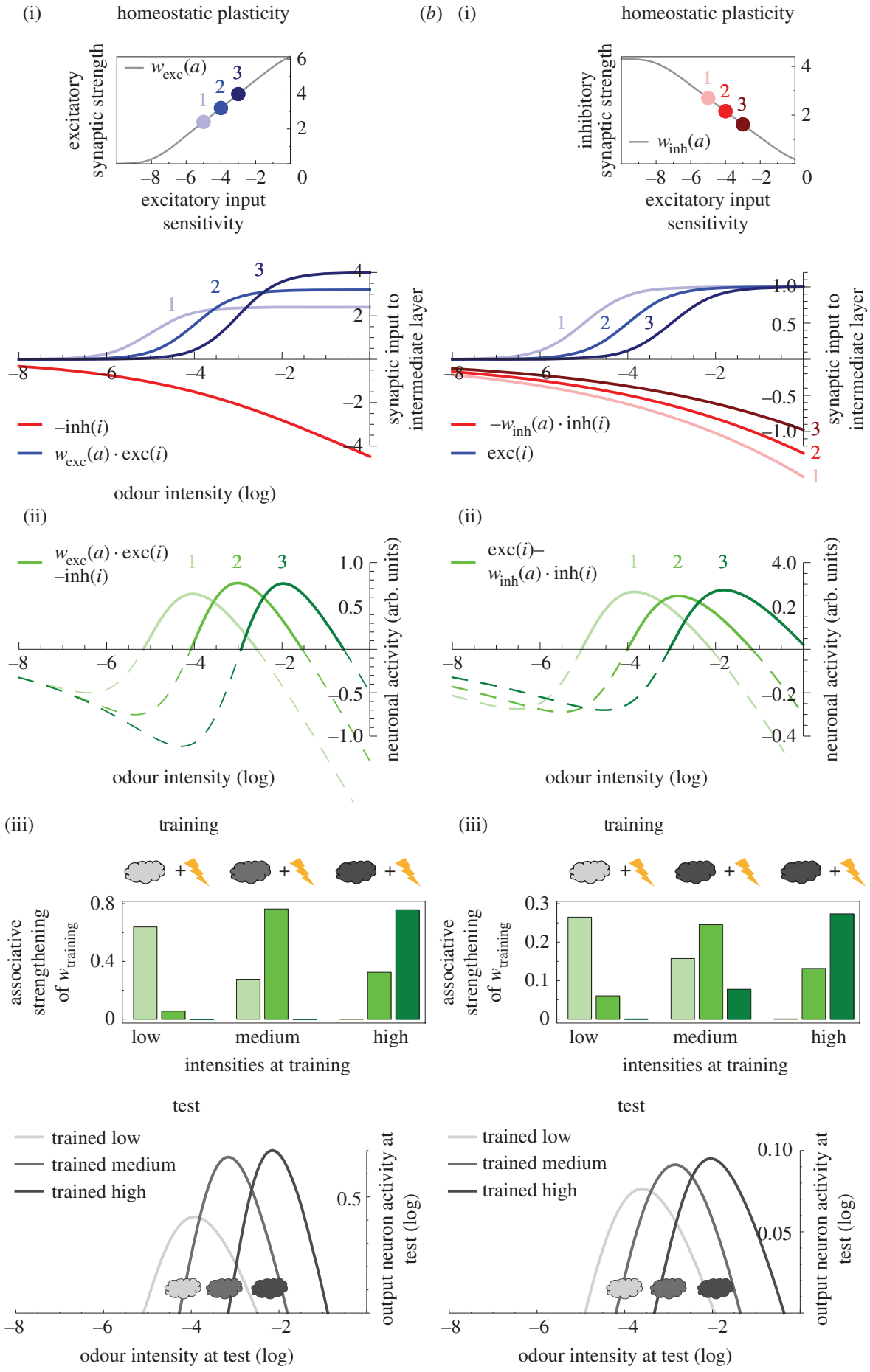

Figure 3. (*Caption opposite.*)

A suitable case to tackle this discrepancy is the fruit fly, where olfactory sensory and projection neurons (OSNs and PNs) have monotonic responses [8,10,27,29–32] (but see [9] for few examples of non-monotonic tuning at PN output sites). Peaked intensity tuning curves mainly emerge downstream, in

Figure 3. (*Opposite*.) Adding homeostatic plasticity enables intensity-specific memories. (*a*) Homeostatic plasticity is added to the circuit motif of figure 2: each excitatory synapse onto the intermediate layer is adjusted based on the respective input neuron's sensitivity. Thus, the weight w_{exc} becomes a function of a, which is the turning point of the logistic function exc(i), such that a large a-value (indicating a low neuronal sensitivity) is counterbalanced by a higher w_{exc} and vice versa (a(i) inset). (a(i)) Consequence of this homeostatic regulation on the excitatory synaptic inputs to the intermediate layer ($w_{exc}(a) \cdot$ exc(i), blue), together with the unadjusted inhibitory input ($-$inh(i), red). (a(ii)) The convergence of these inputs confer non-monotonic and non-nested intensity tuning to the intermediate neurons ($w_{exc}(a) \cdot$ exc(i)–inh(i), green). In (a(iii)), we apply the training and test design from figure 2*d*. Unlike in figure 2*d*, the output neuron at test responds most strongly to the respective intensity used at training. (*b*) With an alternative homeostatic plasticity rule, each inhibitory input synapse is adjusted based on the sensitivity of the cognate excitatory input. Thus, w_{inh} becomes a function of a as shown in the inset of (b(i)). In (b(i)), we plot the resulting, homeostatically regulated inhibitory inputs to the intermediate layer ($-w_{inh}(a) \cdot$ inh(i); red) and the excitatory inputs (exc(i), blue). (b(ii)) These converging inputs confer non-monotonic and non-nested tuning curves to the intermediate-layer neurons (exc(i)–$w_{inh}(a) \cdot$ inh(i), green). In (b(iii)), we apply the training-test design from figure 2*d* and obtain results similar to those in (a(iii)).

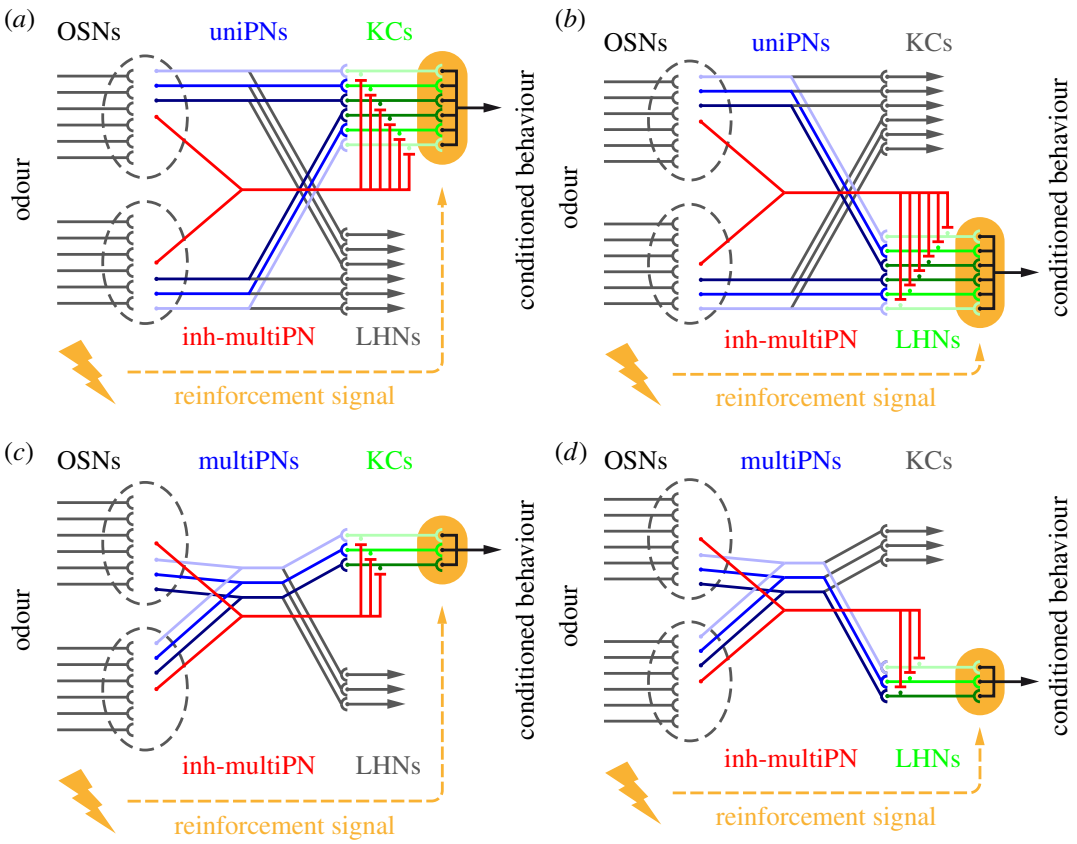

Figure 4. Scenarios for implementation in the fly olfactory system. We present four scenarios for implementing the circuit motif in figure 2*a* in the adult *Drosophila* olfactory system. In adult flies, approximately 1300 olfactory sensory neurons (OSNs) per hemisphere converge onto approximately 50 antennal lobe glomeruli, based on their olfactory receptor expression [37,38]. For simplicity, in each scenario, we depict only two glomeruli (grey dashed ellipsoids), each with six afferent OSNs. On average three homotypic uniPNs receive input at each glomerulus [39]. In (*a*) and (*b*), we use these 'sister' uniPNs as the excitatory input neurons (blue) and consider as the intermediate layer (highlighted in green) their post-synaptic partners, either the mushroom body Kenyon cells (KCs) in (*a*) or the lateral horn neurons (LHNs) in (*b*). For implementing the feed-forward inhibition from antennal lobe to the KCs (*a*) or to the LHNs (*b*), we propose anatomically described GABAergic multi-glomerular projection neurons (inh-multiPNs; red; see the main text for details). As the responses of uniPNs are partially odour identity-specific, an entanglement of identity and intensity coding is conceived in (*a*) and (*b*). Alternatively, the coding of identity and intensity may be segregated. Thus, in two further scenarios, we use multiPNs as the excitatory input neurons (multiPNs; blue; see the main text for anatomical references) and take as the intermediate layer their downstream partners the KCs (*c*) or the LHNs (*d*). The inhibitory channels are as proposed for (*a*) and (*b*), respectively. Note that these scenarios are based on adult *Drosophila* olfactory anatomy. At the larval stage, each antennal lobe glomerulus is innervated by a single uniPN [40] thus (*a*) or (*b*) would not apply; whereas (*c*) or (*d*) may be plausible as multi-glomerular projection neurons have been described in the larval olfactory system [41].

mushroom body (MB) Kenyon cells (KCs) [47,48], and, as recently found, in lateral horn neurons (LHNs) [49] (also see [50] for locust KCs). What kind of connectivity carries out this transformation?

5.1. Computational models of non-monotonic intensity coding

In a model suggested by Luo *et al.* [51], a layer of uni-glomerular projection neurons (uniPNs) gives randomly connected excitatory output to a layer of 2500 KCs and drives a global inhibitory neuron that also impinges upon the KCs. The synapses along the feed-forward inhibitory pathway are adjusted such that more sensitive uniPNs contribute stronger to inhibition, whereas those KCs with stronger excitatory input receive more inhibition. Although the model is concerned with the odour identity-tuned responses of third-order olfactory neurons, a substantial portion of the KCs also shows peaked intensity tuning. The large number of KCs in adult flies (e.g. [52]) fulfils the model's requirement. In flies, however, KCs display a heterogeneity of function in supporting short- versus long-term and perhaps even appetitive- versus aversive olfactory memories (e.g. [53,54]) and they support a variety of additional behavioural functions (e.g. context-generalization [55], regulation of sleep [56], decision-making [57]). It is thus not clear how many KCs would be 'available' for implementing this solution with respect to a given olfactory learning event. The randomness of the connectivity in Luo *et al.*'s model [51], despite being realistic (e.g. [58]), does not allow pinpointing an explicit minimal network structure that transforms monotonic responses to non-monotonic ones. Such information would be useful for generalizing to other developmental stages, species and modalities, where fewer neurons might be available. Technical implementations, too, would benefit from a design principle, which can be scaled according to need.

Here, different from Luo *et al*. [51] or the related framework of reservoir computing [59], we explicitly suggest a dedicated circuit motif transforming monotonic into non-monotonic responses. In this three-layer feed-forward circuit (figure 2), the input layer consists of multiple excitatory neurons with monotonic response curves reflecting different sensitivities and a single inhibitory neuron with a monotonic response function that is less steep than those of the excitatory neurons. Convergence of these elements onto the intermediate layer results in peaked tuning curves. To support intensity-specific memories, however, it is critical to have different neurons with non-nested tuning curves peaking at different values along the intensity axis (figures 2 versus 3). This property is generated through a homeostatic adjustment [20–24] of the excitatory versus inhibitory balance in the input to the intermediate neuron layer. Finally, all intermediate-layer neurons converge onto a single output neuron, with synapses that are subject to associative plasticity. In this scheme, the generation of peaked tuning curves in the intermediate layer resembles the mechanism by which mammalian auditory brainstem neurons encode sound amplitude with bell-shaped profiles [5]. The necessity of homeostatic plasticity, on the other hand, echoes a key ingredient of Luo *et al*.'s [51] model, where the feed-forward inhibitory pathway synapses are adjusted to balance out the effects of the excitatory pathway.

Could there be even simpler circuit motifs than those considered so far? Indeed, endowing intermediate-layer neurons with a resonate-and-fire mechanism [60] could achieve the required nonlinear transformation between stimulus intensity and circuit output. As in our model framework, odour intensity would be encoded monotonically in the frequency of periodic spike trains of input neurons (e.g. PNs). If their discharge frequency is too low or too high, the intermediate neuron would not fire. However, if the discharge frequency is close to (or matches) the resonance frequency of the intermediate neuron, this neuron would generate periodic spike trains, too.

Now consider a larger group of resonate-and-fire neurons with different resonance frequencies whose range covers the behaviourally relevant firing rates of the input neurons. In an odour-shock training episode with a given odour intensity, there would thus only be one neuron or a small group of neurons in resonance with the input. Different odour intensities would drive different subgroups. Owing to a reinforcement signal, the output synapses of these activated intermediate neurons would be associatively strengthened, laying down an intensity-specific memory trace. The larger the mismatch between input frequency and resonance frequency, the smaller the synaptic changes would be. After learning, only odour intensities close to the trained intensity would be transmitted; whereas lower or higher intensities would be filtered out, thus enabling intensity-specific conditioned behaviour.

A decisive ingredient of this alternative mechanism is the layer of resonate-and-fire neurons with cell-specific resonance frequencies. From each of these neurons, one would expect that during odour presentation, the inter-spike-intervals cluster around a particular value, reflecting the neuron's inverse resonance frequency. Neither fly [47,61], nor locust [50,62] KCs show this property; instead, KC inter-spike intervals vary significantly within a single response to one odour, across multiple responses to the

same odour and across responses to different odours. The data presented in [49] suggest that the same is true for LHNs.

A further alternative model [17] is conceptually similar to our approach but assigns to each intermediate neuron one excitatory and one inhibitory pre-synaptic partner, thus employing more neurons than the present model and requiring a rather specific circuit structure that may not match the fly olfactory system. The model proposed here is simpler and could be readily implemented in the fly olfactory system, where activity-dependent homeostatic plasticity has been observed at various neuropils [34–36].

5.2. Implementation of the present circuit motif in the *Drosophila* olfactory system

Given the scarceness of odour-intensity-resolved physiological data from the MB [47,48,50] and the LH [49] and the absence of behavioural studies that discriminatively test for the roles of these in intensity learning, we believe it too early to restrict the discussion to one or the other neuropil. We thus consider all known neuron types in the fly olfactory system to suggest four alternative implementations of the model, including detailed references to anatomy, thus pointing to testable hypotheses (figure 4).

In the first two scenarios (figure 4*a*,*b*), the excitatory input neurons for each antennal lobe glomerulus correspond to the homotypic uniPNs innervating that glomerulus [39]. UniPNs have monotonic response functions (see above for references). To accommodate our model, we assume different sensitivities for the different uniPNs innervating a common glomerulus; as these receive common OSN-input, the rank order of their sensitivities will be identical for all odours. As uniPNs project to both the MB and the LH, we consider either neuropil as the intermediate layer in figure 4*a*,*b*, respectively. Feed-forward inhibition from antennal lobe to MB is limited. The single identified type of likely GABAergic, multi-glomerular PN (inh-multiPN) projecting to the MB calyx ([39]; named 'mlPN4' in [63]) could implement the inhibition in figure 4*a*. Alternatively, inhibition could be carried out by the APL neuron, which provides feedback to the KCs [63,64] or by the MB-C1 neuron which connects LH to the MB [52] and has GABAergic counterparts in other insects [65,66]. For the inhibitory channel in figure 4*b*, several GABAergic inh-multiPN types projecting to the LH (e.g. 'mlPN2' and '-3' in [63]) are available as candidates. Interestingly, at least one of these neurons innervates almost the entire antennal lobe ('mlPN3' in [63]; also see [67]), providing a particularly elegant solution. Furthermore, some inh-multiPN types are known to have monotonic sensitivity functions, as required for a role in the present model [68–70]. Whether the detailed parametric properties of these sensitivity functions would enable non-monotonic intensity coding across the behaviourally relevant range remains to be investigated. As the responses of uniPNs are partially odour identity-specific, the scenarios in figure 4*a*,*b* conceive an entanglement of identity and intensity coding. This is especially true for the scenario in figure 4*a*, as a large body of evidence point to the MB KC output synapses as the site of the critical plasticity underlying learned olfactory behaviour (reviewed in [71,72]; also see e.g. [54,73,74] for neurogenetic analyses in *Drosophila* and e.g. [75,76] for electrophysiological accounts in other insects).

The extent to which animals should discriminate versus generalize along the odour intensity and the odour identity dimensions probably depends on the behavioural task at hand. In that sense, separating, instead of entangling the coding of these dimensions offers more degrees of freedom in regulating the balance between discrimination and generalization. Thus, in two further scenarios (figure 4*c*,*d*), we use multiPNs as the excitatory input neurons. Two anatomical candidates for such neurons project, respectively, to the MB and the LH and to only the LH ('mPN4' and 'lPN2' in [63]). Accordingly, we consider either neuropil for the intermediate layer in figure 4*c*,*d*, respectively, with the inhibitory channels as elaborated above. In these two scenarios, as the intensity coding circuit sums up activity across the antennal lobe glomeruli, it loses the information on odour identity and these two dimensions are coded separately. Whether and how these stimulus dimensions can be bound together to form a unitary percept of a particular odour at a particular intensity to enable an intensity- and identity-specific olfactory memory remains open.

The scenarios we propose can be directly tested because they are based on identified neuron types, as detailed above, and because transgenic tools for interfering with these neurons are available (e.g. [63]). The experimental design outlined in figure 1*a* can be used in conjunction with these tools to investigate the roles of specific neuron types. Particularly, the role of multi-glomerular projection neurons have so far been considered in the framework of innate olfactory behaviour, given their monotonic intensity sensitivity (e.g. [69,70]); a role for these neurons in enabling non-monotonic coding and associative learning of intensity is a novel suggestion.

Behavioural responses often depend in a bell-shaped fashion on certain stimulus attributes whose preferred value might be determined through associative learning. The present model demonstrates that an elementary circuit motif can achieve the required tuneable signal transformation. The model can be tested experimentally at a quantitative level. Owing to its simplicity, the underlying circuit motif could serve as an attractive candidate for tuneable non-monotonic intensity coding.

Data accessibility. The data plotted in figure 1*b*,*d* at Dryad: http://datadryad.org/ (doi:10.5061/dryad.qk0b0)

Acknowledgements. We are thankful to G. Galizia, B. Gerber, M. Heisenberg, V. Murthy, E. Pamir and A. Schaefer for fruitful discussions.

Funding statement. This work was supported by the Federal Ministry of Education and Research through the Bernstein Focus Neural Basis of Learning (H.T. and A.V.M.H.—BMBF 01GQ0932). In addition, LMU, MPG and LIN provided institutional support.

Author's contributions. J.N. carried out the implementation of the model. J.N., H.T., A.V.M.H. and A.Y. conceived the model and drafted the manuscript. All authors gave final approval for publication.

Conflict of interests. We have no competing interests.

References

1. Cattell JM. 1886 The influence of the intensity of the stimulus on the length of the reaction time. *Brain* **8**, 512–515. (doi:10.1093/brain/8.4.512)
2. Bare JK. 1949 The specific hunger for sodium chloride in normal and adrenalectomized white rats. *J. Comp. Physiol. Psychol.* **42**, 242–253. (doi:10.1037/h0057987)
3. Zhang YV, Ni J, Montell C. 2013 The molecular basis for attractive salt-taste coding in *Drosophila*. *Science* **340**, 1334–1338. (doi:10.1126/science.1234133)
4. Von Békésy G. 1960 *Experiments in hearing*. New York, NY: McGraw-Hill.
5. Zhou M, Tao HW, Zhang LI. 2012 Generation of intensity selectivity by differential synaptic tuning: fast-saturating excitation but slow-saturating inhibition. *J. Neurosci.* **32**, 18 068–18 078. (doi:10.1523/JNEUROSCI.3647-12.2012)
6. Duchamp-Viret P, Duchamp A, Chaput MA. 2000 Peripheral odor coding in the rat and frog: quality and intensity specification. *J. Neurosci.* **20**, 2383–2390.
7. Kajiya K, Inaki K, Tanaka M, Haga T, Kataoka H, Touhara K. 2001 Molecular bases of odor discrimination: reconstitution of olfactory receptors that recognize overlapping sets of odorants. *J. Neurosci.* **21**, 6018–6025.
8. Wang JW, Wong AM, Flores J, Vosshall LB, Axel R. 2003 Two-photon calcium imaging reveals an odor-evoked map of activity in the fly brain. *Cell* **112**, 271–282. (doi:10.1016/S0092-8674(03)00004-7)
9. Yamagata N, Schmuker M, Szyszka P, Mizunami M, Menzel R. 2009 Differential odor processing in two olfactory pathways in the honeybee. *Front. Syst. Neurosci.* **3**, 16. (doi:10.3389/neuro.06.016.2009)
10. Asahina K, Louis M, Piccinotti S, Vosshall LB. 2009 A circuit supporting concentration-invariant odor perception in *Drosophila*. *J. Biol.* **8**, 9. (doi:10.1186/jbiol108)
11. Slater G, Levy P, Chan KL, Larsen C. 2015 A central neural pathway controlling odor tracking in *Drosophila*. *J. Neurosci.* **35**, 1831–1848. (doi:10.1523/JNEUROSCI.2331-14.2015)
12. Yarali A, Ehser S, Hapil FZ, Huang J, Gerber B. 2009 Odour intensity learning in fruit flies. *Proc. R. Soc. B* **276**, 3413–3420. (doi:10.1098/rspb.2009.0705)
13. Semmelhack JL, Wang JW. 2009 Select *Drosophila* glomeruli mediate innate olfactory attraction and aversion. *Nature* **459**, 218–223. (doi:10.1038/nature07983)
14. Cleland TA, Narla VA. 2003 Intensity modulation of olfactory acuity. *Behav. Neurosci.* **117**, 1434–1440. (doi:10.1037/0735-7044.117.6.1434)
15. Xia S, Tully T. 2007 Segregation of odor identity and intensity during odor discrimination in *Drosophila* mushroom body. *PLoS Biol.* **5**, e264. (doi:10.1371/journal.pbio.0050264)
16. Masek P, Heisenberg M. 2008 Distinct memories of odor intensity and quality in *Drosophila*. *Proc. Natl Acad. Sci. USA* **105**, 15 985–15 990. (doi:10.1073/pnas.0804086105)
17. Mishra D, Chen YC, Yarali A, Oguz T, Gerber B. 2013 Olfactory memories are intensity specific in larval *Drosophila*. *J. Exp. Biol.* **216**, 1552–1560. (doi:10.1242/jeb.082222)
18. Wright GA, Thomson MG, Smith BH. 2005 Odour concentration affects odour identity in honeybees. *Proc. R. Soc. B* **272**, 2417–2422. (doi:10.1098/rspb.2005.3252)
19. Cleland TA, Chen SY, Hozer KW, Ukatu HN, Wong KJ, Zheng F. 2011 Sequential mechanisms underlying concentration invariance in biological olfaction. *Front. Neuroeng.* **4**, 21. (doi:10.3389/fneng.2011.00021)
20. Hou Q, Zhang D, Jarzylo L, Huganir RL, Man HY. 2008 Homeostatic regulation of AMPA receptor expression at single hippocampal synapses. *Proc. Natl Acad. Sci. USA* **105**, 775–780. (doi:10.1073/pnas.0706447105)
21. Turrigiano G. 2012 Homeostatic synaptic plasticity: local and global mechanisms for stabilizing neuronal function. *Cold Spring Harb. Perspect. Biol.* **4**, a005736. (doi:10.1101/cshperspect.a005736)
22. Turrigiano GG, Nelson SB. 2000 Hebb and homeostasis in neuronal plasticity. *Curr. Opin. Neurobiol.* **10**, 358–364. (doi:10.1016/S0959-4388(00)00091-X)
23. Nusser Z, Hajos N, Somogyi P, Mody I. 1998 Increased number of synaptic $GABA_A$ receptors underlies potentiation at hippocampal inhibitory synapses. *Nature* **395**, 172–177. (doi:10.1038/25999)
24. Kilman V, van Rossum MC, Turrigiano GG. 2002 Activity deprivation reduces miniature IPSC amplitude by decreasing the number of postsynaptic $GABA_A$ receptors clustered at neocortical synapses. *J. Neurosci.* **22**, 1328–1337.
25. DasGupta S, Waddell S. 2008 Learned odor discrimination in *Drosophila* without combinatorial odor maps in the antennal lobe. *Curr. Biol.* **18**, 1668–1674. (doi:10.1016/j.cub.2008.08.071)
26. Borst A. 1983 Computation of olfactory signals in *Drosophila melanogaster*. *J. Comp. Physiol.* **152**, 373–383. (doi:10.1007/BF00606242)
27. Hallem EA, Carlson JR. 2006 Coding of odors by a receptor repertoire. *Cell* **125**, 143–160. (doi:10.1016/j.cell.2006.01.050)
28. Hallem EA, Ho MG, Carlson JR. 2004 The molecular basis of odor coding in the *Drosophila* antenna. *Cell* **117**, 965–979. (doi:10.1016/j.cell.2004.05.012)
29. Olsen SR, Bhandawat V, Wilson RI. 2010 Divisive normalization in olfactory population codes. *Neuron* **66**, 287–299. (doi:10.1016/j.neuron.2010.04.009)
30. Ng M, Roorda RD, Lima SQ, Zemelman BV, Morcillo P, Miesenbock G. 2002 Transmission of olfactory information between three populations of neurons in the antennal lobe of the fly. *Neuron* **36**, 463–474. (doi:10.1016/S0896-6273(02)00975-3)
31. Bhandawat V, Olsen SR, Gouwens NW, Schlief ML, Wilson RI. 2007 Sensory processing in the *Drosophila* antennal lobe increases reliability and separability of ensemble odor representations. *Nat. Neurosci.* **10**, 1474–1482. (doi:10.1038/nn1976)
32. Root CM, Semmelhack JL, Wong AM, Flores J, Wang JW. 2007 Propagation of olfactory information in *Drosophila*. *Proc. Natl Acad. Sci. USA* **104**, 11 826–11 831. (doi:10.1073/pnas.0704523104)
33. Rospars JP, Lansky P, Tuckwell HC, Vermeulen A. 1996 Coding of odor intensity in a steady-state deterministic model of an olfactory receptor neuron. *J. Comput. Neurosci.* **3**, 51–72. (doi:10.1007/BF00158337)
34. Sachse S, Rueckert E, Keller A, Okada R, Tanaka NK, Ito K, Vosshall LB. 2007 Activity-dependent plasticity in an olfactory circuit. *Neuron* **56**, 838–850. (doi:10.1016/j.neuron.2007.10.035)
35. Kremer MC *et al.* 2010 Structural long-term changes at mushroom body input synapses. *Curr. Biol.* **20**, 1938–1944. (doi:10.1016/j.cub.2010.09.060)
36. Kazama H, Wilson RI. 2008 Homeostatic matching and nonlinear amplification at identified central

synapses. *Neuron* **58**, 401–413. (doi:10.1016/j.neuron.2008.02.030)

37. Stocker RF. 2001 *Drosophila* as a focus in olfactory research: mapping of olfactory sensilla by fine structure, odor specificity, odorant receptor expression, and central connectivity. *Microsc. Res. Tech.* **55**, 284–296. (doi:10.1002/jemt.1178)
38. Laissue PP, Reiter C, Hiesinger PR, Halter S, Fischbach KF, Stocker RF. 1999 Three-dimensional reconstruction of the antennal lobe in *Drosophila melanogaster*. *J. Comp. Neurol.* **405**, 543–552. (doi:10.1002/(SICI)1096-9861(19990322)405:4<543::AID-CNE7>3.0.CO;2-A)
39. Stocker RF, Lienhard MC, Borst A, Fischbach KF. 1990 Neuronal architecture of the antennal lobe in *Drosophila melanogaster*. *Cell Tissue Res.* **262**, 9–34. (doi:10.1007/BF00327741)
40. Ramaekers A, Magnenat E, Marin EC, Gendre N, Jefferis GS, Luo L, Stocker RF. 2005 Glomerular maps without cellular redundancy at successive levels of the *Drosophila* larval olfactory circuit. *Curr. Biol.* **15**, 982–992. (doi:10.1016/j.cub.2005.04.032)
41. Thum AS, Leisibach B, Gendre N, Selcho M, Stocker RF. 2011 Diversity, variability, and suboesophageal connectivity of antennal lobe neurons in *D. melanogaster* larvae. *J. Comp. Neurol.* **519**, 3415–3432. (doi:10.1002/cne.22713)
42. Belusic G, Pirih P, Stavenga DG. 2010 Photoreceptor responses of fruitflies with normal and reduced arrestin content studied by simultaneous measurements of visual pigment fluorescence and ERG. *J. Comp. Physiol. A* **196**, 23–35. (doi:10.1007/s00359-009-0489-5)
43. Oesch NW, Diamond JS. 2011 Ribbon synapses compute temporal contrast and encode luminance in retinal rod bipolar cells. *Nat. Neurosci.* **14**, 1555–1561. (doi:10.1038/nn.2945)
44. Barbour DL. 2011 Intensity-invariant coding in the auditory system. *Neurosci. Biobehav. Rev.* **35**, 2064–2072. (doi:10.1016/j.neubiorev.2011.04.009)
45. Bensmaia SJ. 2008 Tactile intensity and population codes. *Behav. Brain Res.* **190**, 165–173. (doi:10.1016/j.bbr.2008.02.044)
46. Yamamoto T. 1984 Taste responses of cortical neurons. *Prog. Neurobiol.* **23**, 273–315. (doi:10.1016/0301-0082(84)90007-8)
47. Murthy M, Fiete I, Laurent G. 2008 Testing odor response stereotypy in the *Drosophila* mushroom body. *Neuron* **59**, 1009–1023. (doi:10.1016/j.neuron.2008.07.040)
48. Wang Y, Guo HF, Pologruto TA, Hannan F, Hakker I, Svoboda K, Zhong Y. 2004 Stereotyped odor-evoked activity in the mushroom body of *Drosophila* revealed by green fluorescent protein-based Ca^{2+} imaging. *J. Neurosci.* **24**, 6507–6514. (doi:10.1523/JNEUROSCI.3727-03.2004)
49. Fisek M, Wilson RI. 2013 Stereotyped connectivity and computations in higher-order olfactory neurons. *Nat. Neurosci.* **17**, 280–288 (doi:10.1038/nn.3613)
50. Stopfer M, Jayaraman V, Laurent G. 2003 Intensity versus identity coding in an olfactory system. *Neuron* **39**, 991–1004. (doi:10.1016/j.neuron.2003.08.011)
51. Luo SX, Axel R, Abbott LF. 2010 Generating sparse and selective third-order responses in the olfactory system of the fly. *Proc. Natl Acad. Sci. USA* **107**, 10 713–10 718. (doi:10.1073/pnas.1005635107)
52. Tanaka NK, Tanimoto H, Ito K. 2008 Neuronal assemblies of the *Drosophila* mushroom body. *J. Comp. Neurol.* **508**, 711–755. (doi:10.1002/cne.21692)
53. Trannoy S, Redt-Clouet C, Dura JM, Preat T. 2011 Parallel processing of appetitive short- and long-term memories in *Drosophila*. *Curr. Biol.* **21**, 1647–1653. (doi:10.1016/j.cub.2011.08.032)
54. Perisse E, Yin Y, Lin AC, Lin S, Huetteroth W, Waddell S. 2013 Different Kenyon cell populations drive learned approach and avoidance in *Drosophila*. *Neuron* **79**, 945–956. (doi:10.1016/j.neuron.2013.07.045)
55. Liu L, Wolf R, Ernst R, Heisenberg M. 1999 Context generalization in *Drosophila* visual learning requires the mushroom bodies. *Nature* **400**, 753–756. (doi:10.1038/23456)
56. Joiner WJ, Crocker A, White BH, Sehgal A. 2006 Sleep in *Drosophila* is regulated by adult mushroom bodies. *Nature* **441**, 757–760. (doi:10.1038/nature04811)
57. Zhang K, Guo JZ, Peng Y, Xi W, Guo A. 2007 Dopamine-mushroom body circuit regulates saliency-based decision-making in *Drosophila*. *Science* **316**, 1901–1904. (doi:10.1126/science.1137357)
58. Caron SJ, Ruta V, Abbott LF, Axel R. 2013 Random convergence of olfactory inputs in the *Drosophila* mushroom body. *Nature* **497**, 113–117. (doi:10.1038/nature12063)
59. Buonomano DV, Maass W. 2009 State-dependent computations: spatiotemporal processing in cortical networks. *Nat. Rev. Neurosci.* **10**, 113–125. (doi:10.1038/nrn2558)
60. Izhikevich EM. 2001 Resonate-and-fire neurons. *Neural Netw.* **14**, 883–894. (doi:10.1016/S0893-6080(01)00078-8)
61. Turner GC, Bazhenov M, Laurent G. 2008 Olfactory representations by *Drosophila* mushroom body neurons. *J. Neurophysiol.* **99**, 734–746. (doi:10.1152/jn.01283.2007)
62. Shen K, Tootoonian S, Laurent G. 2013 Encoding of mixtures in a simple olfactory system. *Neuron* **80**, 1246–1262. (doi:10.1016/j.neuron.2013.08.026)
63. Tanaka NK, Endo K, Ito K. 2012 Organization of antennal lobe-associated neurons in adult *Drosophila melanogaster* brain. *J. Comp. Neurol.* **520**, 4067–4130. (doi:10.1002/cne.23142)
64. Liu X, Davis RL. 2009 The GABAergic anterior paired lateral neuron suppresses and is suppressed by olfactory learning. *Nat. Neurosci.* **12**, 53–59. (doi:10.1038/nn.2235)
65. Nishino H, Mizunami M. 1998 Giant input neurons of the mushroom body: intracellular recording and staining in the cockroach. *Neurosci. Lett.* **246**, 57–60. (doi:10.1016/S0304-3940(98)00231-6)
66. Perez-Orive J, Mazor O, Turner GC, Cassenaer S, Wilson RI, Laurent G. 2002 Oscillations and sparsening of odor representations in the mushroom body. *Science* **297**, 359–365. (doi:10.1126/science.1070502)
67. Marin EC, Jefferis GS, Komiyama T, Zhu H, Luo L. 2002 Representation of the glomerular olfactory map in the *Drosophila* brain. *Cell* **109**, 243–255. (doi:10.1016/S0092-8674(02)00700-6)
68. Liang L, Li Y, Potter CJ, Yizhar O, Deisseroth K, Tsien RW, Luo L. 2013 GABAergic projection neurons route selective olfactory inputs to specific higher-order neurons. *Neuron* **79**, 917–931. (doi:10.1016/j.neuron.2013.06.014)
69. Wang K, Gong J, Wang Q, Li H, Cheng Q, Liu Y, Zeng S, Wang Z. 2014 Parallel pathways convey olfactory information with opposite polarities in *Drosophila*. *Proc. Natl Acad. Sci. USA* **111**, 3164–3169. (doi:10.1073/pnas.1317911111)
70. Strutz A *et al.* 2014 Decoding odor quality and intensity in the *Drosophila* brain. *eLife* **3**, e04147. (doi:10.7554/eLife.04147)
71. Heisenberg M. 2003 Mushroom body memoir: from maps to models. *Nat. Rev. Neurosci.* **4**, 266–275. (doi:10.1038/nrn1074)
72. Gerber B, Tanimoto H, Heisenberg M. 2004 An engram found? Evaluating the evidence from fruit flies. *Curr. Opin. Neurobiol.* **14**, 737–744. (doi:10.1016/j.conb.2004.10.014)
73. Sejourne J *et al.* 2011 Mushroom body efferent neurons responsible for aversive olfactory memory retrieval in *Drosophila*. *Nat. Neurosci.* **14**, 903–910. (doi:10.1038/nn.2846)
74. Aso Y *et al.* 2014 Mushroom body output neurons encode valence and guide memory-based action selection in *Drosophila*. *eLife* **3**, e04580. (doi:10.7554/eLife.04580)
75. Strube-Bloss MF, Nawrot MP, Menzel R. 2011 Mushroom body output neurons encode odor-reward associations. *J. Neurosci.* **31**, 3129–3140. (doi:10.1523/JNEUROSCI.2583-10.2011)
76. Cassenaer S, Laurent G. 2012 Conditional modulation of spike-timing-dependent plasticity for olfactory learning. *Nature* **482**, 47–52. (doi:10.1038/nature10776)

4

OLFACTORY TRACE CONDITIONING IN *DROSOPHILA* AS REVEALED BY MACHINE LEARNING TECHNIQUES AT THE SINGLE FLY LEVEL

4.1 SUMMARY

Animals are able to associate two stimuli even when these are presented discontinuously. During this temporal gap the animal needs to keep a trace of the stimulus in its nervous system. In an olfactory trace conditioning paradigm flies show their ability to bridge stimulus free intervals of a duration of up to five seconds.

So far it is not clear which units harbor this stimulus trace. We analyzed optical recordings of first, second and third order olfactory neurons (ORNS, PNs and KCs) from *Drosophila*. We performed both a correlation analysis and a machine learning approach based on support vector machines (SVMs) on a single fly level. We compared the direct stimulus response with the post-stimulus activity and found, consistent with previous studies, low correlation values on the level of ORNs and PNs. Classification with SVMs also failed for the first two layers of olfactory processing. The analysis for KCs however revealed high correlation values and successful classification of stimulus responses based on training of post-stimulus activity. This emphasizes the role of the KCs in olfactory learning not only as convergence site but also as place for a stimulus trace that is kept for a time period of several seconds.

All data discussed in this paper was generously shared by Alja Lüdke, working at the University of Constance together with

Paul Szyszka and Giovanni Galizia. The research was conceived and planned by AVMH and JN. Results were discussed between JN, AL, PS, GG and AVMH. Analysis was performed by JN, the manuscript was written by AVMH and JN.

Olfactory trace conditioning in *Drosophila* as revealed by machine learning techniques at the single-fly level

Johannes Nehrkorn,[1,*] Alja Lüdke,[2] Paul Szyszka,[2] Giovanni Galizia,[2] and Andreas V.M. Herz[1]

[1] *Bernstein Center for Computational Neuroscience Munich, Graduate School of Systemic Neurosciences and Fakultät für Biologie, Ludwig-Maximilians-Universität München 82152 Martinsried, Germany*

[2] *Department of Biology, Neurobiology, University of Konstanz, Konstanz, Germany*

(Dated: August 22, 2015)

Both vertebrates and invertebrates are able to form associations between stimuli, even when the first stimulus ends before the second one starts, as demonstrated by trace conditioning. To form such an associative memory, some neural representation of the first stimulus has to be retained by the nervous system until the onset of the second stimulus. How and where this stimulus trace is encoded in insects has remained an open question. We analyze *Drosophila* olfactory neurons recordings from the first three layers of sensory processing — olfactory receptor neurons (ORNs), projection neurons (PNs), and Kenyon Cells (KCs) — and compare their internal calcium dynamics during stimulus representation with post-stimulus calcium responses. We show that the information in the post-stimulus responses of ORNs or PNs is not sufficient to correctly classify the identity of an odor. However, odor classification based on post-stimulus responses was successful at the KC level. This finding provides a strong indication that the calcium dynamics of Kenyon Cells encode olfactory stimulus traces and thus enable associations between temporally disconnected stimuli.

INTRODUCTION

Fruit flies and other animals can be trained to associate an odor with an electric shock [30], even if there is a stimulus-free interval between the offset of the odor and the onset of the shock [9, 12, 24, 26]. This variant of classical conditioning is called trace conditioning since the animal has to keep a trace of the past conditioned stimulus (CS) until the onset of the unconditioned stimulus (US). In rodents, the hippocampus is required for trace conditioning [33]. But where is the stimulus trace represented in an insect brain? To address this key question for learning and memory, we apply state-of-the-art data-analysis methods to data obtained by *in vivo* Calcium imaging in the fruit fly *Drosophila melanogaster*.

The olfactory system of *Drosophila* consists of several layers of neurons [16]. Odorant molecules bind to receptors expressed by olfactory receptor neurons (ORNs) in the two antennae, evoking odor-specific activity patterns [14, 19]. ORNs project to the antennal lobe (AL), where they form synapses with projection neurons (PNs) and local interneurons in distinct neuropils called glomeruli. Typically, ORNs express only one type of olfactory receptor and all ORNs expressing the same receptor type project to the same glomerulus; in addition the glomerular layout of the AL is stereotypic between flies [32].

Local excitatory and inhibitory interneurons in the AL transform the antennal odor representation [1, 21–23, 34–36] and PNs forward this new representation to the mushroom body (MB) and lateral horn (LH). Kenyon cells (KCs) in the MB respond sparsely to odors [3, 17, 31]. The connectivity between PNs and KCs has been suggested to be quasi random [4], unlike the more organized projection from AL to LH [10, 29]. Functionally, the MB is the convergence center for odor information and reinforcement signals [8, 15], whereas the LH is generally considered to be involved in innate odor responses; for an alternative functional interpretation, see Galizia [13].

Recently, Galili et al. [12] established a rigorous experimental paradigm to compare trace conditioning and delay conditioning (the first stimulus is still present when the second stimulus starts) at the behavioral level. In addition, these authors carried out *in vivo* calcium imaging of ORNs in search for the neural correlate of the stimulus trace. Averaging over responses of different flies, these authors performed a compound correlation analysis that suggests that the neural substrate of the trace is most likely downstream of the ORNs.

We extend this study and analyze the time-resolved response patterns obtained by *in vivo* Calcium imaging of populations of ORNs, PNs and KCs. Comparing the responses to different odorants we aim at finding and characterizing the neural correlate of the stimulus trace that the animal might use to form associative memories between odors and a reinforcing stimulus. In particular, we ask whether this trace simply reflects binding and unbinding processes at the ORN level or whether it is constructed *de novo* at the level of the antennal lobe or mushroom body.

RESULTS

Successful olfactory trace conditioning requires an odor-specific trace of neural activity that extends sufficiently beyond the termination of the CS presentation. To detect such a stimulus trace, we compared the patterns of calcium activity during the CS with the post-odor re-

sponse, the activity in the interstimulus-interval following the CS. To determine where this trace is formed in the insect brain, the analysis was done separately at the ORN-, PN- and KC-level. As a measure for the similarity of responses during odor stimulation and post-odor responses we calculated Pearson correlation coefficients at different time points (see Methods), both for two repetitions of the same stimulus and across stimuli. To test whether the post-odor response reliably encodes the preceding stimulus and thus enables trace conditioning, we asked whether this stimulus can be correctly classified using only its particular post-odor response.

Correlations – same odor

To measure the similarity of neural responses, we calculated the Pearson correlation coefficient individually for each stimulus and fly (auto-correlation) and between two repetitions of the same stimulus (cross-correlation). As an example, correlation matrices for Butanol stimulation are shown in Fig. 1 for ORNs, PNs, and KCs (top to bottom), with auto-correlations in the left-hand panels and cross-correlations in the right-hand panels. Each panel contains 175×175 pixels, corresponding to the 175 frames that were recorded at a frequency of 20 Hz, for a total duration of 35 seconds. The stimulus was presented from time $t = 0$ s until $t = 10$ s, as indicated by the gray bars, followed by a 20-second post-stimulus period. Each pixel shows the Pearson correlation coefficient between the two time points indicated on the x and y axes. Correlation values are color coded as explained in the color bar: Positive correlations are red, negative values blue, and low correlations are in pale colors.

The upper-right triangular part of Fig. 1A demonstrates that the ORN odor response is strongly correlated with itself during the entire stimulus duration (high correlation values for all time pairs between around $t = 0$ s and $t = 10$ s); the same holds for the first 10 to 15 seconds of the post-odor response, although the stripes indicate stronger temporal fluctuations in that period. Notably, the correlation between odor response and post-odor response is much lower (pale colors for in the upper right quadrant), suggesting that at the ORN-level post-odor responses do not provide suitable stimulus traces.

Apart from slightly higher similarities between odor and post-odor responses (in particular around $t = 25$ s), the correlation structure evoked by a repeated Butanol stimulus, ButL 2, (lower-left part of Fig. 1A) closely mimics that triggered by ButL 1. Indeed, the cross-correlation between the first and second repetition of ButL shows high values during the stimulus presentation (Fig. 1B, from $t = 0$ s to $t = 10$ s) but the correlation of the post-odor responses is rather weak (Fig. 1B, for $t > 10$ s).

PN responses (Figs. 1C and 1D) are similar to ORN

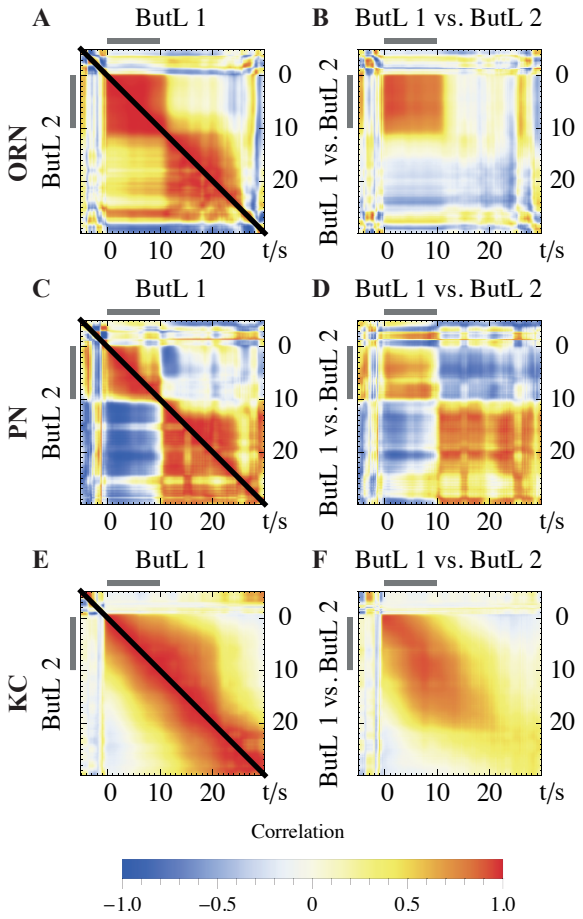

FIG. 1. Temporal evolution of response correlations. Each panel depicts time-dependent Pearson correlation coefficients between the glomerular responses at the times indicated on the x and y axis. gray bars represent stimulus presentation. **(A)** Auto-correlation of the activities of olfactory receptor neurons (ORNs) of one fly in response to two stimulus presentations of Butanol (upper-right triangle: 1^{st} presentation, lower-left triangle: 2^{nd} presentation). **(B)** Cross-correlation for the responses in (A). **(C, D)** As (A, B) but for projection neurons (PNs). **(E, F)** As (A, B) but for Kenyon cells (KCs).

responses in some aspects: Patterns of high correlation are visible for time periods during and after stimulus presentation for both repetitions of Butanol (Fig. 1C, upper and lower triangle for $t \sim 0s$ to $t \sim 10s$ and $t \sim 10s$ to $t \sim 30s$). However, the correlations between odor- and post-odor responses are now much lower, at times even negative. Temporal fluctuations are stronger, both during and after odor presentation, and generate the pronounced stripe-like patterns. This is also evident in the cross-correlations of PNs (Fig. 1D): During odor presentation, correlations are not as large as for ORNs and and vary strongly in time. After odor presentation, however, there is still an area of high correlation with temporal

fluctuation from $t \sim 10$ s to $t \sim 30$ s.

In stark contrast to these observations, there are no structured patterns in the KC responses (Figs. 1E, 1F). For both repetitions of Butanol (upper and lower triangle of Fig. 1E) a band of high correlation extends along the entire diagonal, indicating that irrespective of the stimulus offset the stimulus response changes slowly over time. The duration of high similarity (the width of the high-correlation band) varies between five and ten seconds. As for the ORN and PN responses, KC responses are also stereotypic between repetitions of the same stimulus (Fig. 1F). From stimulus onset until about 5 to 10 seconds after stimulus offset, a band of high correlation along the diagonal is clearly visible. This observation holds for most but not all KC recordings.

Correlations across odors

To successfully associate a particular odor trace with the shock stimulus, the post-stimulus responses triggered by different odors must be sufficiently different from each other, but similar enough to the stimulus response of the same odor. We therefore analyzed correlations across odors at the same points in time and across different points in time.

For mean correlation values close to one the variance has to be small, as demonstrated by the rightmost data points in all three panels of Fig. 3. However, at smaller mean correlation values across flies, the responses of ORNs, PNs, and KCs differ systematically. For ORNs, the smallest mean correlation values are close to zero. In this region, the variability between flies ranges from almost -1 to +1. With increasing mean correlation, the variability quickly drops to rather small values, with the most reliable response (high R values for all flies) occurring for a repeated presentation of the same odor (ButL). For PNs, the smallest mean correlation values are negative and far less variable than in ORNs. The variability then slightly increases and only slowly (and in a non-monotone fashion) approaches zero for the highest mean correlation values. Finally, for KCs, mean correlation values range from just below zero up to almost one, with one outlier fly that shows a completely different behavior. For all others, high values correspond also to the repetition of the same odor (Fig. 2). Unlike in ORNs, the variability between flies starts with very small values. Overall, the fly-to-fly variability at the KC level is smaller than at the PN level.

The correlation analysis shows that odor pairs can be separated into two complementary response classes at the ORN level. One class has low mean correlation values and a high fly-to-fly variability, the other has high correlation values that are consistent across flies (low variability). For PNs, only very few odor pairs yield high correlation values and the variation across flies is higher for

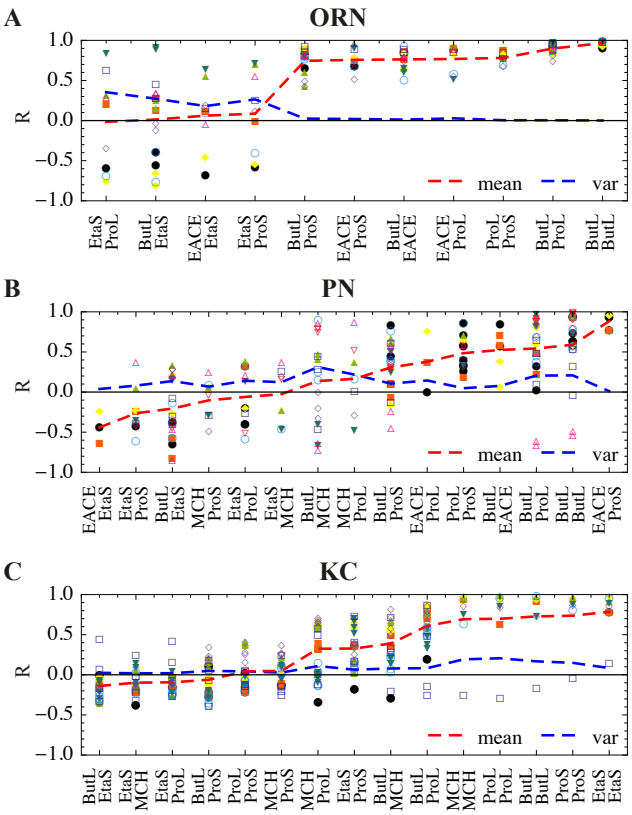

FIG. 2. Response correlations across odors for individual flies. Correlations between responses to the stimulus pairs indicated on the x-axis were calculated one second after stimulus onset ($t = 1$ s). In each panel, every color-symbol combination corresponds to one individual fly (but is re-used for different flies in the different panels). The dashed red line denotes the mean correlation over all flies for each odor pair, the dashed blue line depicts the corresponding variance. Results are shone in **(A)** for ORNs, in **(B)** for PNs and in **(C)** for KCs. The similarity of responses to different odors as well as the variability of responses between flies are clearly visible.

all odor pairs. In KCs, except for the pair (MCH, ProL), the variability between flies is consistently low. Correlation values are only high for repetitions of the same odor which indicates well separated representations of odors in KCs.

Analyzing correlation values averaged over flies supports this finding. During stimulus presentation, the similarity across odors decreases from ORNs to PNs to KCs (Fig. 3A, blue boxplots), indicating an increase in odor separation. Correlations for the same odor are high for all three layers of processing (Fig. 3A, yellow boxplots). For ORNs and PNs, however, values only represent the repetition of a single stimulus, butanol. Correlations for post-odor responses at $t = 15$ s are generally smaller (Fig. 3B). For ORNs and PNs however the correlation for the same odor is smaller than for KCs (Fig. 3B, yellow boxplots).

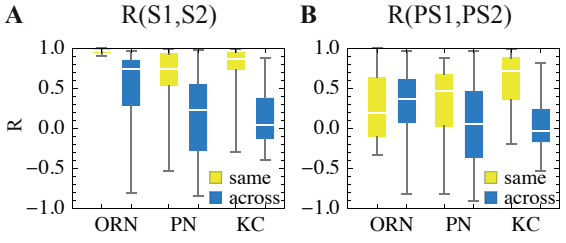

FIG. 3. Mean stimulus correlations. Boxplots show values across flies. Yellow symbols ("same") refer to correlations between two presentations of the same odor, blue symbols ("across") denote correlations between different odors. Boxplots show mean, upper and lower quartile and whiskers extreme values. For ORNs and PNs, only butanol was presented twice, hence the small variation for ORNs during stimulus presentation. **(A)** Responses during stimulus (S) presentation at $t = 1$ s. Mean correlations between the same stimuli are high, and lower across different stimuli. **(B)** Post-stimulus (PS) responses after $t = 15$ s. For ORNs, PNs and KCs, correlations across stimuli are similar to the stimulus correlations in A. Unlike the trend for across-odor correlations of stimulus and post-stimulus responses alike, same-odor correlations *increase* for post-odor responses from ORNs and PNs to KCs.

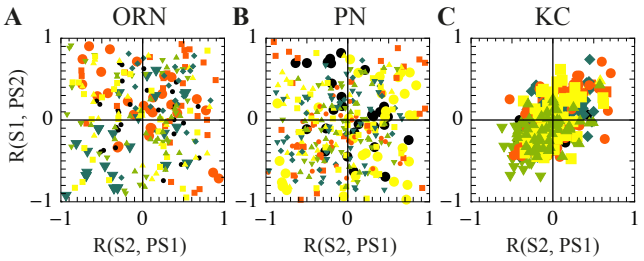

FIG. 4. Correlation between stimulus response of odor 1 (S1) and post-stimulus response of odor 2 (PS2) vs. correlation between stimulus response of odor 2 (S2) and post-stimulus response of odor 1 (PS1). **(A)** ORNs, **(B)** PN, **(C)** KC. Each point represents the value for one odor pair, and within one panel the same plot markers correspond to the same fly. For each fly, a correlation value was calculated and tested for significance. Significant correlations are highlighted with larger symbols. For ORNs, two flies show significant correlation (−0.55 and 0.40), for PNs three (−0.46, −0.18, 0.37) but all flies for KC (0.52, 0.61, 0.61, 0.28, 0.52, 0.61, 0.42, 0.37). This analysis shows that stimulus and post-stimulus responses are consistent only at the KC-level.

To analyze the consistency of post-stimulus responses we calculated the correlation between stimulus and post-stimulus responses across all odor pairs (Fig. 4). If the post-stimulus response contains information about the stimulus, it should do so consistently from trial to trial. We would then expect the correlation between stimulus response of odor 1 and post-stimulus response of odor 2 (we call this R(S1,PS2)) to be similar to the reversed case of post-stimulus response of odor 1 and stimulus response of odor 2 (R(S2,PS1)). For ORNs and PNs this is clearly not the case (Fig. 4A, B). Correlation values are scattered in all four quadrants and the correlation between R(S1,PS2) and R(S2,PS1) is significant only for two flies with values of −0.55 and 0.40 for ORNs and three flies for PNs with values −0.46, −0.18 and 0.37. For a consistent response we expect correlation values to be significant and similar across flies. This is the case for KCs (Fig. 4C). Correlation between R(S1,PS2) and R(S2,PS1) is significant for all flies and the values are $\sim 1/2$, indicating a consistent post-stimulus response across all odors and flies.

Classification

The correlation analysis provides a measure of response similarity over time for repetitions of the same odor and across different odors. Based on this analysis, we learned that the correlation between the odor response and the post-odor response is low at the level of ORNs and PNs. At the KC-level, however, the representation of the stimulus is slowly varying in time without an abrupt change after stimulus offset.

This observation hints at a possible neural substrate for the olfactory stimulus trace. We therefore tested whether the information contained in the stimulus responses at the ORN, PN and KC level can be used to recognize an odor during stimulus presentation based solely on the post-odor response. To do so, we first used support vector machines (SVMs), a classification model in machine learning which gains its power from projecting the data into a high-dimensional feature space. Next, we use a second approach, a linear discriminant analysis which is well established in analyzing data from olfactory experiments ([11], [3] and references therein) and can readily be implemented in a biological system using integrate-and-fire neurons. In this approach responses are classified based on the Euclidean distance between the multi-dimensional response vectors.

Support Vector Machines

For each fly, we trained one SVM at time $t = 15$ s (post-odor response) for each odor. We then classified responses for the same point in time and for $t = 1$s (stimulus response). Doing this for different parameter combinations, we find parameter sets for each fly giving the best classification performance.

For ORNs, PNs and KCs, training and testing at the same point in time ($15s$ s) revealed a reliable classification (Fig. 5, left of dashed line), with classification performance reaching unity in almost all cases. This holds for a broad range of parameters (not shown).

When testing against the stimulus response ($t = 1$ s), there is a clear difference between ORNs and PNs vs.

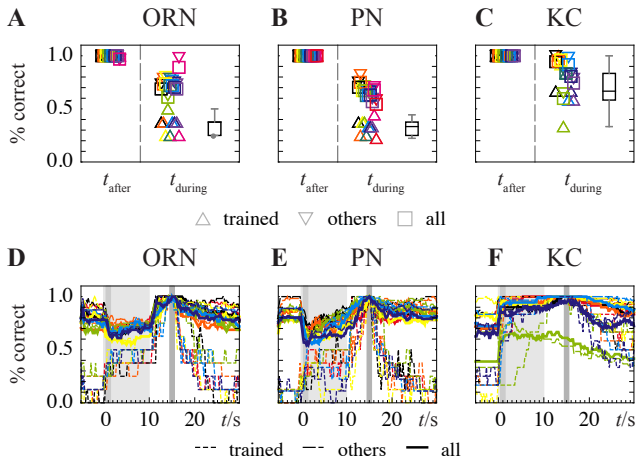

FIG. 5. Classification results for C-SVMs. **(A)** - **(C)** Each plot indicates the percentage of correct classifications. Within one panel, different flies are indicated by different colors. Triangles pointing upwards indicate a correct classification of the trained odor, downward pointing triangles correct classification of all other odors and squares the overall classification performance (see Fig. 6 for an illustration of the implications). In each plot, on the left hand side of the dashed line, the classification performance for training and testing at $t = 15s$ is indicated, on the right side when trained at $t = 15$ s and tested at $t = 1$ s. Box plots show the distribution of the classification performance for the trained odor across flies (upwards pointing triangles). Whiskers denote extreme values, the box upper and lower quartiles. Classification for ORNs and PNs fails mainly because trained odors are misclassified with mean values of $\sim 33\%$, (A) and (B). For KCs, the mean classification performance is $\sim 70\%$ (C). We conclude that the neural representation at the ORN and PN level is not sufficient for trace learning. Rather, the stimulus trace is represented at the KC level. **(D)** - **(F)** Temporal evolution of classification success. Each plot shows the classification result over the time course of the experiment for SVMs trained at $t = 15$ s (dark gray bar). Stimulus duration is indicated by a light gray background and the intermediate gray bar and the medium gray bar indicates the time used for classification in (A) - (C). Classification for ORNs and PNs is only good in close proximity to $t = 15$ s. For KCs classification performance is high both during stimulus presentation and for the post-stimulus response.

KCs (Fig. 5, right of dashed line). We decomposed the overall classification performance into classification of the trained odor, all others and overall classification due to the imbalance in the number of responses (trained: upwards triangle, other: downward triangle, squares: overall). As there are more other odors, overall classification might seem high, even though the trained odors were classified incorrectly (see Fig. 6 for an illustration of this problem). This is what we actually observe for ORNs and PNs: Trained odors are classified poorly, as illustrated by the box plots for the classification performance of trained odors. Medians are around 30 % and the spread is not very large. On the other hand, when classifying KC responses during the stimulus, classification of the trained odor is relatively high, with a median across flies over 60 %. The instances shown in Fig. 5 correspond to the parameter combinations with the best overall performance (see Methods). In this case, the results are more sensitive to the parameters used (not shown). We performed the same analysis with a different kind of support vector machine, called ν-SVM (see Methods). The results did not differ from the ones obtained with C-SVMs, which shows that the approach does not rely on a specific machine learning approach.

Classification performance over time revealed a high classification performance for ORNs and PNs only in close proximity of the trained time (Fig. 5D, E, grey bar at 15s); whereas classification performance for KCs remained high over a long period of time (Fig. 5F).

DISCUSSION

For trace conditioning, it is crucial to keep information of the CS until the arrival of the US. Fruit flies readily form an associative memory between an odor stimulus and an electric shock, even when these two stimuli are separated by a stimulus free interval of a few seconds [12]. In this study, we were interested in how and where in the nervous system this trace is kept.

Temporal evolution of stimulus representation

At the population level, Galili et al. [12] already found a strong correlation of ORN responses during stimulus presentation and after stimulus presentation, but not between the two. Their analysis was based on averaged responses across different flies. Due to the large response variability between different flies, the correlation of odor pairs varies also strongly form fly to fly (Fig. 2). At the ORN level odor responses fall in two different classes. For one class of odors, responses are similar across flies. For the other, similarity varies greatly between flies, and almost vanishes when averaged across flies. At the next processing layer, the PNs, odor responses are less similar and the variation between flies is greater. The largest change, however, happens from PNs to KCs. The similarity of different odor responses is consistently small across flies, only repeated presentations of the same odor reach high correlation values.

Taking mean correlation values across flies and odors emphasizes this sharpening and the reliability of the odor response (Fig. 3A). Correlation values for the same odor are high across the three processing layers, correlations across odors are, however, smallest at the KC level, indicating a well separated odor representation. This is in line with earlier work, both experimentally and theoretically. According to these studies, the AL sharpens the

odor representation by a non-linear transformation that enhances small ORN responses and saturates for strong ORN responses [18, 22]. The quasi-random connectivity pattern from AL to KCs leads to a sparse and well separated odor representation [3, 18, 20].

The temporal evolution from stimulus response to post-odor activity changes from ORNs to PNs to KCs. ORNs show a high level of correlation during odor presentation for all flies, both for the auto-correlation and the cross-correlation between two repetitions of the same stimulus. The correlation pattern of the post-stimulus response was mixed: In most cases, rather large auto-correlations could be observed, whereas cross-correlation were weak. So even though the post-odor response is similar to itself, it is not as stable as the odor responses to repetitions of the same stimulus. The correlation between odor presentation and post-odor response was generally weak, confirming that ORNs most likely do not harbor a trace of the stimulus.

The responses of PNs contain a richer temporal structure as the corresponding ORN responses. The correlation matrices show striped patterns on a temporal order of seconds. Similar to ORNs, the level of auto-correlation during stimulus presentation is high, although not as high as for ORNs and temporally less strongly separated. The calculated cross-correlations were not as large as for ORNs and not as prolonged in time. Post-odor responses showed a greater variability between flies, ranging from well correlated responses (both in terms of auto- and cross-correlations) to cases of no correlation at all. Interestingly, correlations between stimulus and post-stimulus responses was smaller and in most cases even negative for PNs. This strong difference between odor and post-odor response makes the PNs also an unlikely place for a stimulus trace.

The third level of olfactory processing, the KCs, showed a rich diversity of correlation patterns. In some cases, we found correlation patterns similar to ORNs and PNs, with rather clear separations between stimulus and post-stimulus responses. More interesting, however, were cases, where the correlation pattern did not abruptly change after stimulus onset, but rather changed slowly over a time period of five to ten seconds. This happened for auto-correlations as well as for cross-correlations. Such responses could harbor a stimulus trace, enabling flies to associate odor responses with a temporally separated electric shock.

Probing the information content of responses by machine learning approaches

The KCs in the mushroom body have already been suggested to harbor an olfactory stimulus trace [12]. To test the information content of an olfactory stimulus presentation, machine learning approaches are well suited and have been used before [3, 7, 28]. So far only stimulus responses have been classified, revealing a well-separated representation of different odors at the KC level and enabling predictions about the perceptual similarity of different odors.

Our findings of well separated odor responses are in line with these findings. Classification with SVMs performs well and is not sensitive to either the particular SVM model or a particular set of parameters. Given the high performance, we can not find a difference between ORN, PN and KC odor representation if we focus on single time points.

This changes, however, drastically as soon as the time of training and testing differs. The representation at the level of ORNs and PNs changes on a short timescale, such that a classification of responses outside a time-window of a few seconds fails (Fig. 5A, B and D, E). The information about the odor is not preserved between stimulus response and post-stimulus response. KC responses differ strongly in this respect: Reliable classification of odor identity is possible over a longer period of time, including the stimulus response when trained on the post-stimulus response. In this case the choice of parameters for the SVM becomes more critical, but again the particular model (C-SVM or ν-SVM) does not change the overall outcome.

Stimulus trace

The insect mushroom bodies are the associative center for olfactory learning of insects, especially for *Drosophila*. Th representation of different odors is odor specific and both appetitive and aversive reinforcement signals are projected to the Kenyon cells [8]. This makes these neurons a plausible substrate for the olfactory stimulus trace, as had already been suggested in the study of Galili et al. [12]. Using a combination of a correlation analysis and a machine learning approaches, we extended these findings to the single-fly level. We found that it is highly unlikely for the stimulus trace to be present in the first or second layer of olfactory processing. We could also show that odors can be successfully classified based on the post-odor KC activity, as is required for trace conditioning. The data analyzed were Ca^{++} recordings, indicating that the trace might be represented by the internal calcium dynamics of KCs. Whether the spiking activity of KCs also provides a suitable substrate for a stimulus trace remains an open question for further research.

METHODS

In vivo calcium imaging. Imaging data were recorded with a rate of 5 Hz for 35 seconds, resulting in 175 frames. Odors were presented for 10 seconds (frames 26 - 75) in

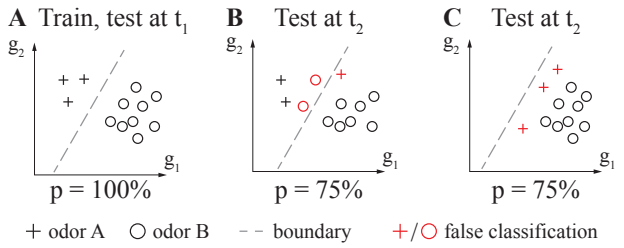

FIG. 6. Illustration of classification performance. **(A)** Responses of two glomeruli at time t_1 to a stimulus are plotted along the glomerular response axes g_1 and g_2, respectively. Crosses correspond to odor A, circles to odor B. A classifier calculates a separation boundary (dashed line). In this case, all responses on the left of the line are correctly classified as indicating the presence of odor A, all responses on the right as odor B. Accordingly, the performance of the classifier is $p = 100\%$. **(B)** At time t_2, the responses might differ from those in (A), as indicated by the shifted crosses and circles. When testing with the same classifier as in (A), the three responses indicated in red are misclassified, reducing the performance to $p = 75\%$. **(C)** In this example, there are also three misclassified responses (red), again resulting in $p = 75\%$. However, all responses to odor A are now misclassified, whereas all responses to odor B are correctly classified, so that $p_A = 0$ and $p_B = 100\%$. As there are many more responses to B than to A, the overall performance measure is still high, even though the classification fails completely. We therefore consider not only the overall performance p but also the subgroup performances when evaluating a particular classifier.

a pseudorandom order after 5 seconds of baseline recording. For each trial, time t is defined such that the stimulus presentation begins at $t = 0$. The identification of glomeruli was done as described in Silbering and Galizia [27] and Silbering et al. [28]. A relative change in fluorescence was calculated as $\Delta F(i)/F$, where $F(i)$ is the fluorescence signal of the ith frame, and F is the baseline fluorescence for frames 10 - 25. Bleach correction was applied. For a detailed description, see [12].

Neural responses. For the data analysis, the responses were represented as relative fluorescence changes for each frame of the whole recording time, sorted by fly and glomerulus for ORNs and PNs and identified areas for KCs. These responses were first temporally smoothed by taking running averages over one-second long windows. For one fly and at a given time t, the response vector r consists of the responses of all glomeruli (or MB areas which we consider as KCs) at that time, in response to one stimulus.

Correlations. We calculate the Pearson's correlation coefficient R between two response patterns$\mathbf{r}(t_1) = \{r_1(t_1), \ldots, r_N(t_1)\}$ and $\mathbf{r}(t_2) = \{r_1(t_2), \ldots, r_N(t_2)\}$ at times t_1 and t_2

$$R[\mathbf{r}(t_1), \mathbf{r}(t_2)] = \frac{\sum_{j=1}^{N} [r_j(t_1) - \overline{r(t_1)}\ ][r_j(t_2) - \overline{r(t_2)}\ ]}{\sqrt{\sum_{j=1}^{N} [r_j(t_1) - \overline{r(t_1)}\ ]^2 \sum_{j=1}^{N} [r_j(t_2) - \overline{r(t_2)}\ ]^2}},$$

where $\overline{r(t_1)}$ and $\overline{r(t_2)}$ denote the population-averaged responses at time t_1 and t_2, respectively, N is the number of glomeruli or areas, and $j \in \{1, \ldots, N\}$. R-values range from -1 (perfectly anti-correlated) to 1 (perfectly correlated).

Classification. In the first step, we train one classifier for each stimulus. The classifier separates one odor against all others odors at time $t_{\text{after}} = 15$s, i.e., five seconds after odor presentation ended. We then test the classifiers at time t_{after} and at a specific time-point during stimulus presentation, $t_{\text{during}} = 1$s. The performance p of the classifier is defined as the percentage of correct classifications. We discriminate between the performance for the trained odor (p_{trained}), other odors (p_{other}) and overall performance p to avoid misinterpretations arising from the imbalance in the number of responses for trained and other odors. This problem is illustrated in Fig. 6: When all responses are classified correctly, $p = 100\%$ (Fig. 6A). Figs. 6B and C show two cases with identical $p = 75\%$ but very different p_{trained} and p_{other}. In Fig. 6B, $p_{\text{trained}} = 2/3$ and $p_{\text{other}} = 7/9$, which we would consider a reasonable classification performance. In Fig. 6C however, $p_{\text{trained}} = 0\%$ and $p_{\text{other}} = 100\%$. As all trained odors were classified incorrectly, the classification failed completely despite a high overall "performance" measure.

Support Vector Machines (SVMs). Classifications based on SVMs were performed using the LIBSVM library [5] with the integrated interface to MATLAB. Calculations were carried out with MathWorks MATLAB R2014a. Classifications consisted of training a SVM for each stimulus at time $t = 15$ s and classifying responses over the whole recording time. Because of the anatomical stereotypy of the fly olfactory pathways up to the AL [32], this can be done at the level of ORNs and PNs for multiple flies at once by using the largest set of common glomeruli and treating recordings of different flies as repetitions of the same experiment. We considered two different implementations of SVMs, C-support vector classification (C-SVC) [2, 6] and ν-SVC [25] and tested various kernel functions; linear: $K(x, x') = x \cdot x'$, polynomial: $K(x, x') = (\gamma x \cdot x' + c)^3$, radial basis functions: $K(x, x') = \exp\left(-\gamma \|x - x'\|^2\right)$ and a sigmoidal function: $K(x, x') = \tanh(\gamma x \cdot x')$, where γ is a parameter that was adjusted together with the cost parameter C for C-SVC or the parameter ν for ν-SVC. To maximize the classification performance we scan a range of parameters. We define maximum classification performance when both p_{trained} and p_{other} are as large as possible, and p follows as a result of the two.

* johannes.nehrkorn@gmail.com

[1] Bhandawat, V., Olsen, S. R., Gouwens, N. W., Schlief, M. L., and Wilson, R. I. (2007). Sensory processing in the Drosophila antennal lobe increases reliability and separability of ensemble odor representations. *Nature neuroscience*, 10(11):1474–82.

[2] Boser, B., Guyon, I., and Vapnik, V. (1992). A training algorithm for optimal margin classifiers. In *Proceedings of the 5th Annual ACM Workshop on Computational Learning Theory*, pages 144 – 152. ACM Press.

[3] Campbell, R. a. a., Honegger, K. S., Qin, H., Li, W., Demir, E., and Turner, G. C. (2013). Imaging a population code for odor identity in the Drosophila mushroom body. *The Journal of neuroscience : the official journal of the Society for Neuroscience*, 33(25):10568–81.

[4] Caron, S. J. C., Ruta, V., Abbott, L. F., and Axel, R. (2013). Random convergence of olfactory inputs in the Drosophila mushroom body. *Nature*, 497(7447):113–7.

[5] Chang, C.-C. and Lin, C.-J. (2011). LIBSVM: A library for support vector machines. *ACM Transactions on Intelligent Systems and Technology*, 2:27:1–27:27. Software available at `http://www.csie.ntu.edu.tw/~cjlin/libsvm`.

[6] Cortes, C. and Vapnik, V. (1995). Support-vector networks. *Machine Learning*, 20(3):273–297.

[7] Cury, K. M. and Uchida, N. (2010). Robust Odor Coding via Inhalation-Coupled Transient Activity in the Mammalian Olfactory Bulb. *Neuron*, 68(3):570–585.

[8] Davis, R. L. (2005). Olfactory memory formation in Drosophila: from molecular to systems neuroscience. *Annual review of neuroscience*, 28:275–302.

[9] Dylla, K. V., Galili, D. S., Szyszka, P., and Lüdke, A. (2013). Trace conditioning in insects-keep the trace! *Frontiers in Physiology*, 4 AUG(August):67.

[10] Fişek, M. and Wilson, R. I. (2014). Stereotyped connectivity and computations in higher-order olfactory neurons. *Nature neuroscience*, 17(December):280–8.

[11] Fisher, R. A. (1936). The use of multiple measurements in taxonomic problems. *Ann. Eugen.*, 7(2):179–188.

[12] Galili, D. S., Lüdke, A., Galizia, C. G., Szyszka, P., and Tanimoto, H. (2011). Olfactory trace conditioning in Drosophila. *The Journal of Neuroscience*, 31(20):7240–8.

[13] Galizia, C. G. (2014). Olfactory coding in the insect brain: Data and conjectures. *European Journal of Neuroscience*, 39(February):1784–1795.

[14] Galizia, C. G. and Szyszka, P. (2008). Olfactory coding in the insect brain: molecular receptive ranges, spatial and temporal coding. *Entomologia Experimentalis et Applicata*, 128(1):81–92.

[15] Gerber, B., Tanimoto, H., and Heisenberg, M. (2004). An engram found? Evaluating the evidence from fruit flies. *Current opinion in neurobiology*, 14(6):737–44.

[16] Heisenberg, M. (2003). Mushroom body memoir: from maps to models. *Nature Reviews Neuroscience*, 4(April):266–275.

[17] Honegger, K. S., Campbell, R. a. a., and Turner, G. C. (2011). Cellular-Resolution Population Imaging Reveals Robust Sparse Coding in the Drosophila Mushroom Body. *Journal of Neuroscience*, 31(33):11772–11785.

[18] Luo, S. X., Axel, R., and Abbott, L. F. (2010). Generating sparse and selective third-order responses in the olfactory system of the fly. *Proceedings of the National Academy of Sciences of the United States of America*, 107(23):10713–8.

[19] Masse, N. Y., Turner, G. C., and Jefferis, G. S. X. E. (2009). Olfactory information processing in Drosophila. *Curr Biol*, 19(16):R700–13.

[20] Murthy, M., Fiete, I., and Laurent, G. (2008). Testing odor response stereotypy in the Drosophila mushroom body. *Neuron*, 59(6):1009–23.

[21] Olsen, S. R., Bhandawat, V., and Wilson, R. I. (2007). Excitatory interactions between olfactory processing channels in the Drosophila antennal lobe. *Neuron*, 54(1):89–103.

[22] Olsen, S. R., Bhandawat, V., and Wilson, R. I. (2010). Divisive normalization in olfactory population codes. *Neuron*, 66(2):287–99.

[23] Olsen, S. R. and Wilson, R. I. (2008). Lateral presynaptic inhibition mediates gain control in an olfactory circuit. *Nature*, 452(7190):956–60.

[24] Pavlov, I. P. (1927). An Investigation of the Physiological Activity of the Cerebral Cortex. *Oxford University Press*, 17:1574.

[25] Schölkopf, B. and Williamson, R. (1999). Support Vector Method for Novelty Detection. *NIPS*, pages 582–588.

[26] Shuai, Y., Hu, Y., Qin, H., Campbell, R. a. a., and Zhong, Y. (2011). Distinct molecular underpinnings of Drosophila olfactory trace conditioning. *Proceedings of the National Academy of Sciences of the United States of America*, 108(50).

[27] Silbering, A. and Galizia, C. (2007). Processing of odor mixtures in the Drosophila antennal lobe reveals both global inhibition and glomerulus-specific interactions. *The Journal of Neuroscience*, 27(44):11966–11977.

[28] Silbering, A. F., Okada, R., Ito, K., and Galizia, C. G. (2008). Olfactory information processing in the Drosophila antennal lobe: anything goes? *The Journal of neuroscience : the official journal of the Society for Neuroscience*, 28(49):13075–87.

[29] Strutz, A., Soelter, J., Baschwitz, A., Farhan, A., Grabe, V., Rybak, J., Knaden, M., Schmuker, M., Hansson, B. S., and Sachse, S. (2014). Decoding odor quality and intensity in the Drosophila brain. *eLife*, 3:1–21.

[30] Tully, T. and Quinn, W. G. (1985). Classical conditioning and retention in normal and mutant Drosophila melanogaster. *Journal of comparative physiology. A, Sensory, neural, and behavioral physiology*, 157(2):263–77.

[31] Turner, G. C., Bazhenov, M., and Laurent, G. (2008). Olfactory representations by Drosophila mushroom body neurons. *Journal of neurophysiology*, 99(2):734–46.

[32] Vosshall, L. B., Wong, A. M., and Axel, R. (2000). An Olfactory Sensory Map in the Fly Brain. *Cell*, 102(2):147–159.

[33] Wallenstein, G. V., Eichenbaum, H., and Hasselmo, M. E. (1998). The hippocampus as an associator of discontiguous events. *Trends Neurosci.*, 21(8):317–323.

[34] Wilson, R. I. (2013). Early Olfactory Processing in Drosophila : Mechanisms and Principles. *Annual Review of Neuroscience*, 36(1):217–241.

[35] Wilson, R. I., Turner, G. C., and Laurent, G. (2004). Transformation of olfactory representations in the Drosophila antennal lobe. *Science (New York, N.Y.)*, 303(5656):366–70.

[36] Yaksi, E. and Wilson, R. I. (2010). Electrical coupling between olfactory glomeruli. *Neuron*, 67(6):1034–47.

5

DISCUSSION

Learning is a key to survival. Using the experience of past events to make decisions for the future is crucial, for animals and humans alike. The underlying neural structures and mechanisms of learning have been the subject of intense studies for more than a century.

In this thesis we developed computational models adjusted to olfactory learning in the fruit fly *Drosophila melanogaster*. Our focus was on fundamental properties of stimulus representation and association, which gives the developed models also relevance beyond the scope of the chosen model animal.

In the first paper we present a model for the timing-dependent bi-directional change of a biochemical reaction product. In the model animal the bi-directional production of an activated complex changes the hedonic value of the CS, which changes its behavior from conditioned avoidance to conditioned approach. In the experiment, an odor was paired with an electric shock, which is a well established learning paradigm referred to as aversive olfactory conditioning. We found that a bi-directional modification of intra-cellular reaction dynamics in KCs is sufficient to account for the shift from aversive to attractive behavior after training only depending on the relative timing of odor and shock.

In the second paper we introduce a minimal circuit motif that transforms a monotonic stimulus representation into a non-monotonic one. The experimental and behavioral motivation is a phenomenon called intensity learning. Fruit flies are able to associate an intermediate odor intensity with an electric shock, which they express by showing a smaller conditioned avoid-

ance response to both lower and higher intensities of the same odor. In the first two olfactory processing layers, odor intensity is however encoded as monotonically increasing neuronal activity. The proposed circuit motif breaks the nestedness that is inherent in such a code by balancing excitation and inhibition and introducing homeostatic plasticity into the system. This transformation introduces units with peak responses at different intermediate intensities, which we could show to support intensity specific learning.

In the third study we aim to reveal the neuronal units that harbor an olfactory stimulus trace. Flies are able to bridge a stimulus free interval between an odor and shock in classical olfactory conditioning to form an associative memory of the odor. To this end they need to generalize from the post-stimulus odor representation that coincides with the shock to the stimulus representation of the same odor, which they are exposed to during the test at a later point in time. We apply advanced data analysis techniques to investigate the similarity of the combinatorial olfactory code during and after stimulus presentation. We analyzed optical recordings of *Drosophila* olfactory receptor neurons (ORNs), projection neurons (PNs) and KCs. Using machine learning algorithms we evaluated the probability to correctly classify odor identity given its post-odor representation. We could show that for ORN and PN responses post-odor response patterns are not likely to harbor a stimulus trace. For KCs however response patterns during and after odor presentation share similar features that allow for correct classification. This is a strong indication that KCs activity keeps a stimulus trace for a time, which is long enough to bridge a stimulus free interval on the order of seconds.

5.1 CLASSICAL CONDITIONING, LEARNING AND MEMORY

Ivan Pavlov highlighted classical conditioning as a form of associative learning in the beginning of the 20th century [122]. In his well-known experiments he trained dogs to associate the presentation of food with the sound of a bell. Behaviorally the

successful association between the two stimuli manifested itself in increased salivation when the dogs heard only the ring of the bell. Less known is the discovery of Edwin Twitmyer around the same time. He studied the human patellar tendon reflex. He warned his subjects by ringing a bell before giving them a tap to their patellar tendon. As a case of a coincidental discovery, he realized that after a number of repetitions the sound of the bell itself was enough to elicit the reflexive response of a knee jerk [123].

The neuronal basis of learning is an intensely investigated topic. In mammals it is studied in an eyeblink conditioning paradigm. An auditory or visual stimulus is paired with an air puff or weak electric shock to the eye (for an early example in rabbits, see [124, 125]). Mccormick et al. [126] showed in lesion studies the critical role of the cerebellum for the formation of associative memories for delay conditioning (see also [127, 128]), a form of associative training, where conditioned and US overlap in time. More recent studies could pinpoint the location within the cerebellum to the anterior interpositus nucleus [129]. Additionally the amygdala plays a role in memory consolidation, both for delay and trace conditioning [130, 131], where trace conditioning refers to associative training with a stimulus-free interval between conditioned and US. Trace conditioning requires also additional cerebral structures. Studies have shown the necessity of the hippocampus [132] and the anterior cingulate cortex [133–135]. In mice the involvement of the cerebellum in trace eyeblink conditioning is under debate [136].

Also invertebrates such as insects and mollusks [137] have the ability to associate two stimuli with each other. For the fruit fly and the honey bee *Apis mellifera* the paradigm of choice is olfactory conditioning. An odor serves as unconditioned stimulus (US) and is paired with either an aversive conditioned stimulus (CS) such as electric shock or an appetitive CS such as a sugar solution (for *Drosophila* see [3, 4]; for bees see [138, 139]). In particular *Drosophila melanogaster* has been and still is the prime model organism. Despite having a nervous system with a relatively small number of neurons on the order of 100.000 [140], it is able to show an impressively complex repertoire of

behaviors [141, 142]. Flies show delay and trace conditioning as well as relief learning, which is yet another variation of aversive classical conditioning. For relief learning, the order of CS and US is reversed, such that the CS follows the US, which leads to a change of the hedonic value of the US compared to trace and delay conditioning. The advantages of studying classical conditioning in *Drosophila* lie both in the in part easily accessible nervous system as well as in the vast array of genetic tools, which are readily available to target and manipulate specific neuronal populations [11]. This enables targeted testing of hypothesis by manipulating the processing part and measuring the behavioral performance of the fly through classical conditioning.

5.2 STIMULUS REPRESENTATION

To form an associative memory the animal first has to detect both stimuli and represent them in its nervous system in an appropriate way. A stimulus activates a first layer of sensory neurons. Along the sensory pathway to higher brain areas the stimulus representation undergoes a change, e.g., to enhance certain stimulus features and suppress others.

Neurons encode stimuli in different ways. Adrian [143] introduced the notion of rate coding. They measured spiking activity of muscular neurons in response to different forces applied to the muscle. They calculated mean firing rates of the muscular neurons and showed that increased weight leads to an increased firing rate. When neurons respond with few or only a single spike to a stimulus it is not possible to appropriately determine a firing rate. In this case the precise timing of the onset spike with respect to stimulus onset could encode a stimulus feature. Gollisch and Meister [144] showed such a temporal coding scheme for retinal ganglion cells. These cells encode spatial information through spike timing. If neurons fire in a background of oscillations, the relative phase of the spike could also carry information. This has been suggested, e.g., for the visual cortex [145] and for neurons in the entorhinal cortex [146].

Encoding complex stimuli with single neurons quickly requires a large number of neurons. Making use of the joint activity of a set of neurons increases the encoding capacity. In mammals position in space is encoded in two different ways. A place cell fires only in one specific location [147]. To encode a large space with a certain precision requires many cells. Grid cells however fire at multiple locations in a regular pattern [148]. The activity of a single cell leaves ambiguity to the position in space, but the combined activity of all cells determines the position precisely. The same precision requires fewer grid cells than place cells [149].

Coding of olfactory stimuli is another prominent example of such population codes. A large set of receptors is tuned broadly to odorant molecules. Many receptors are activated by a set of odorants and most odorants in turn activate a set of receptors. An odor identity is characterized by the joint activation pattern of all receptors. Given the large number of possible combinations of joint activation, already a relatively small number of receptors has a large encoding capacity (for references see chapter 1).

Simultaneous recordings of a large set of neurons are the basis to understand the combinatorial odor code, which changes from one processing layer to the next. Fdez Galán et al. [72] optically recorded ORN activity in the antennal lobe (AL) in response to a set of odors. They represent the response as a vector in a multi-dimensional odor space, which is spanned by glomerular activity. They reduced the complexity of the data by projecting it onto the first two or three principle components. In this reduced representation, they could show that the response to an odor quickly reaches an odor-specific fix point. The odor representation is stable during stimulus presentation and decays back to a resting state after stimulus offset.

Campbell et al. [150] investigated odor identity coding in *Drosophila* KCs. By imaging a population of neurons simultaneously, they could computationally classify neuronal responses and compare this to behavioral performance. They found that their

analysis based on KC activity could well predict the behavioral performance of odor discrimination.

When the animal is trained to form an associative memory, the reinforcing stimulus coincides with the current odor representation within the nervous system. Subsequently in the test, the odor representation alone triggers a conditioned response. For delay conditioning, this is straightforward. Thus the same receptors respond to the odor, the same glomerular activity pattern is active in the AL and the same KCs are active during formation of the association and retrieval.

For trace conditioning however CS and US are separated by a temporal gap during training. This means that the CS coincides with the post-stimulus response of the US instead of the direct stimulus representation. In the test already the direct stimulus response triggers the conditioned response. Therefore the animal has to be able to infer the stimulus from its post stimulus representation. If the two are too dissimilar, an association cannot be formed. Galili et al. [6] showed, that *Drosophlia* is able to form associative memories in an olfactory trace conditioning paradigm. Additionally they analyzed Ca^{++} recordings of ORNs in the AL in search for the stimulus trace. They calculated mean correlations across all experiments between odor and post-odor response as a measure of similarity. Correlation values between both were however low, and they suggested that the trace should be represented in one of the subsequent neuronal layers of olfactory processing. Szyszka et al. [151] performed a similar experiment with bees in an appetitive olfactory trace conditioning paradigm. Here the proboscis extension reflex in response to the touch of the antenna with a sugar solution serves as conditioned response. In the same analysis of PN responses in the AL they also were not able to find a sign of an olfactory stimulus trace in the post-odor activity.

Both Galili et al. [6] and Szyszka et al. [151] suggested the KCs as the next logical location of the stimulus trace. In chapter 4 we analyzed Ca^{++} recordings from *Drosophila* ORNs, PNs and KCs in search for an olfactory stimulus trace. In contrast to Galili et al. [6] and Szyszka et al. [151] we analyzed the data

from each fly individually. Especially for odors with low mean similarity scores the variability across flies was large. On the population level, our analysis confirmed findings from previous studies: Odor quality separability increased from ORNs to PNs to KCs. Correlation of repeated presentation of the same odors remained high through all three layers, but correlation across different odors decreased from ORNs to KCs. The correlation between stimulus and post-stimulus response was only high in KCs. Comparing the correlations between odor and post-odor responses between repeated measurements showed only in KCs consistent correlation values. We argue that this consistency of post-odor responses is a critical feature of a stimulus trace.

In a second step we employed a machine learning approach to classify odor and post-odor responses with support vector machines (SVMs). In contrast to correlation values, SVMs are sensitive to differences of responses in only a small subset of units. As first test we classified odor quality during stimulus presentation. As expected classification performance is high on all three levels of olfactory processing. We then trained the SVMs on the post-odor representation and tested it against the representation during odor stimulation. The performance for ORNs and PNs was poor, consistent with the findings from the correlation analysis. For KCs on the other hand classification performance was high for all odors and almost all flies. This finding shows that the representation and its temporal evolution on the level of KCs is suitable for olfactory trace conditioning. We therefore suggest that the trace of an olfactory stimulus is contained in the prolonged Ca^{++} signal within KCs.

5.3 STIMULUS TIMING

The timing of stimuli has a large impact on the learned behavior. For training with an aversive US, switching the order of stimuli changes also the hedonic value of the CS.

A modeling study by Drew and Abbott [81] suggests spike-timing dependent plasticity as underlying mechanism. Qualitatively the change in synaptic efficacy has a similar timing dependent shape as the behavioral learning experiment demonstrated by Yarali et al. [152]. However a key assumption of the model, prolonged firing at a high rate of third order olfactory neurons, is not met in the olfactory system of *Drosophila*.

We offer now a different explanation of the phenomenon on the level of the molecular reaction dynamics, which underlie memory formation in KC. *In vitro* experiments in *Aplysia* revealed a Ca^{++}-sensitivity of adyenylate cyclase activation by the transmitter serotonin. Depending on the timing of Ca^{++}, more or less activated adyenylate cyclase is produced. We incorporate this finding into a model of post-receptor G-protein signaling developed for olfactory transduction in moth. In the case of olfactory learning of *Drosophila*, the electric shock activates the transmitter, which is delivered to the KCs. The odor stimulus leads to a rise of Ca^{++} concentration in a subset of odor-identity specific KCs. We model this effect by transiently increasing the reaction constants for the formation and dissociation of the activated G-protein complex, depending on the Ca^{++} concentration. The amount of produced activated complex now depends on the relative timing between transmitter and Ca^{++} signal. When the dominant process is the formation of activated complex, increased reaction dynamics lead to an overall increased amount of activated complex. On the other hand, if Ca^{++} concentration increases when the dominant process is the dissociation of activated complex, overall less of the activated complex will be produced. We interpret the total amount of activated complex as proxy for synaptic strengthening onto the behavioral output circuit. Since the modification by Ca^{++} only takes place in odor-activated KCs, the behavioral response is specific to the trained odor.

The heart of the presented model is the symmetrical modification of the reaction rate as a result of a transient input. Despite the complexity of the reaction cascade, which was implemented for the transduction mechanism in the case of olfactory learning, the main building block is simple. Yet the result is a bi-

modally changed outcome controlled by the relative timing of both inputs.

5.4 STIMULUS PROPERTIES

We discussed stimulus representation in the nervous system above and focused on the aspect of odor quality. In general there is a second attribute we can assign to a stimulus, which we call "intensity". This holds for all sensory stimuli. Light is described in terms of its frequency or wavelength and its intensity or brightness. We characterize a sound by its frequency and its loudness or amplitude; an odor by the chemical compounds and the concentration, either in dilution or in air. How are these two different stimulus properties encoded in the nervous system?

In mammals, the detection of auditory stimuli is solved by the anatomical properties of the inner ear. Ossicles transmit oscillations from air to the perilymph in the cochlea. The movement of the perilymph is detected by hair cells on the basilar membrane. Mechanically opened ion channels in conjunction with voltage gated ion channels depolarize the hair cell. The cell releases neurotransmitters onto the second order nerve cell, which triggers action potentials. The detection of different sound frequencies happens along the cochlea in a tonotopic order. Given the diameter of the tube-shaped cochlea and stiffness of the basilar membrane, hair cells resonate at different frequencies in different locations. Detection of high frequencies happens at the front of the cochlea whereas lower frequencies are detected further down the tube. Sound loudness or sound level is encoded by the firing rate of the auditory nerves in a monotonic fashion [153, 154]. In short, stimulus quality is encoded by different neurons along a tonotopic axis and from there transferred to higher brain areas, conserving the spatial arrangement in the cochlea. Sound intensity is encoded monotonically by increasing firing rates of auditory neurons.

In the olfactory system of both mammals and invertebrates, odor quality is encoded in the first step by a set of olfactory receptors. Most receptors have overlapping response profiles, such that one chemical compound activates different receptors to a different degree and each receptor is activated by different chemical components. In this combinatorial code, the combined activity of all receptors represents an odor's quality. A combinatorial code vastly increases the capacity of the system compared to a labeled line code, where one receptor codes only for one specific odor[1]. Different to the auditory system, there is no obvious spatial organization in the olfactory bulb or AL, which would correspond to, e.g., chemical properties of odorants. Odor intensity on the other hand has a similar representation as auditory loudness in mammals. Receptor neurons and projection neurons monotonically increase their firing rates with increasing odor intensity.

What is the consequence of such an encoding scheme on subsequent behavior, especially associative learning? When the animal learns the link between CS and US, it associates the current neuronal representation of the stimulus with the reinforcing US, which triggers the behavioral response. The subsequent reactivation of the same neuronal representation then triggers the behavioral response without the US hence the name conditioned response. The animal might however generalize the conditioned response to different stimuli with a similar neuronal representation. This allows measuring the subjective similarity of different stimuli. In the case of olfactory stimuli, different combinations of neuronal units are activated by different odors. Even if two different odors activate the same subset of neurons, an animal will show a stronger conditioned response to the trained odor. If they are compared in the test, the conditioned response to the trained odor will be stronger. This case is even simpler for the auditory example with hair cells that are tuned to a certain frequency. A sound with different frequency will

1 For specific chemicals, the olfactory system does have a labeled line code. There might be an underlying balance between the optimization of the capacity of a system vs. the ability to reliably detect very specific stimuli. For flies, for example, certain pheromones and CO_2 are encoded by specific receptor neurons and directly trigger a behavioral response.

activate different neurons, therefore not driving a conditioned response.

For a monotonic stimulus representation, which is the case for sound and odor intensity, the situation is different. The code is nested, i.e., the representation of a lower intensity is always a subset of the neuronal representation of a higher intensity. When the animal forms an association with an intermediate intensity, the subsequent test with a higher intensity will trigger the same conditioned response. Moreover, when the higher intensity is tested against the lower, the higher intensity will drive the conditioned response at least as strong as the lower one, possibly even stronger. Such a coding scheme should therefore not support intensity specific learning. Nevertheless flies form olfactory memories specific to an intermediate intensity. They show a less strong conditioned avoidance to both lower and higher odor intensities. Here, the classical conditioning paradigm revealed an interesting capability of the system. Along the processing path of olfaction, units with intensity specific tuning have to arise.

Zhou et al. [155] investigated intensity selective neurons in the rat auditory system. Intensity selective cells appear along the auditory pathway first in the dorsal cochlear nucleus. Zhou et al. [155] performed *in vivo* recordings from pyramidal neurons, which showed non-monotonic response properties. Intensity selective cells received fast saturating excitatory input, but slow saturating inhibitory input. Thus, for higher sound intensities, inhibition dominates over excitation, effectively creating non-monotonic intensity tuning.

In a behavioral assay, Zhang et al. [156] showed a non-monotonic behavioral response to an increasing sensory stimulus in *Drosophila*. They investigated the perception of different salt concentrations, which revealed an attractive preference peak at an intermediate salt concentration. They argue that a certain amount of salt is beneficial to the animal whereas a too high concentration is harmful. They show that the coding of salt-concentration preference relies on two distinct sets of gustatory receptor neurons. One set codes for low salt concentrations

and drives attraction, the other for high concentration driving rejection. The competition between both receptors leads to a bi-directional non-monotonic response to increasing salt concentration.

In the olfactory system of *Drosophila* Yarali et al. [10] showed non-monotonic conditioned behavior to increasing odor intensity. Flies were conditioned in an aversive olfactory conditioning paradigm to an intermediate intensity of an odor. In the test they showed the strongest conditioned avoidance reaction to the same intermediate odor intensity. When tested against both lower and higher intensities, the conditioned avoidance scores were significantly lower. The underlying neuronal circuit of third order olfactory neurons was investigated by Fişek and Wilson [37]. Stereotyped connections from the AL convey olfactory information to the lateral horn. The combination of both inhibitory and excitatory projection neurons leads to non-monotonic responses of lateral horn neurons with increasing intensity. Even though the lateral horn is believed to be most important with respect to innate odor behavior rather than learned behavior, the emergence of intensity selective neurons along the olfactory pathway is a notable step towards understanding intensity specific behavior. In a modeling study Luo et al. [58] also investigated third order neuron responses in the mushroom body. As input to their model they use measured ORN responses from a study by Hallem and Carlson [43]. The AL is simplified as transformation of neuron activity, taking into account the local non-linear properties of AL synapses and lateral inhibition in the AL as described by Olsen et al. [54]. A quasi-random connectivity pattern transfers the olfactory representation to the KCs, which receive excitatory input from a subset of glomeruli and a global inhibition proportional to AL activity. Under these assumptions a subset of KCs shows a non-monotonic response probability to increasing odor intensity. In their approach the non-monotonic tuning of KCs emerged as a result of the large number of KCs and the randomized connectivity pattern with randomized weights and the associated inhibitory weight. It was however outside of the scope of their study to investigate this phenomenon in detail.

In contrast to the model by Luo et al. [58], we propose a dedicated minimal circuit motif that transforms a monotonic stimulus representation to a non-monotonic one. The necessary ingredients are excitation, inhibition and as decisive factor, homeostatic plasticity and a straightforward connectivity pattern with one-to-one excitation and global inhibition. The result is a neuronal layer in which units only respond within a specific intensity range and are inactive for lower and higher intensities.

The necessary elements are present in the olfactory pathway of the fruit fly, which makes our model suitable to explain intensity specific learning. Indeed, by introducing a read-out neuron to the circuit, which sums the activity of the intensity specific units and incorporates the reinforcement signal through synaptic learning, we can reproduce the experimental results from Yarali et al. [10]. A similar model was qualitatively suggested by Mishra et al. [157]. It relies on ordered excitation and inhibition from one layer of neurons to the next. Additionally it requires almost twice as many neurons as our model, making it both more complicated to develop in a biological system and more resource intensive.

An anonymous reviewer provided an interesting alternative minimal solution. Could resonate-and-fire neurons also code for intensity? As discussed above, single neurons encode stimulus intensity as a rate code. A set of resonate-and-fire neurons with resonance frequencies covering the whole intensity range would respond then in an intensity specific way. A read-out neuron similar to the one proposed in our model could integrate over the activity of the intermediate resonate-and-fire neuron layer and provide a mean response. With the right tuning such a circuit should also be able to code for intensity and enable intensity specific learning. However fruit fly KCs do not show the properties of the suggested resonate-and-fire neuron layer suggested above. KC rates are variable during the response to one odor and across repeated responses of the same odor ([60, 62], also the case for locust KCs [158, 159]).

5.5 OUTLOOK

Theories and models should always be experimentally scrutinized. Only an experiment can eventually refute a theory or legitimate a further investigation and refinement. On the other hand a reduced model of a complex system can help to understand the underlying principles and in turn suggest well-defined and directed experiments to test a hypothesis.

This is also the very heart of the work in this thesis. The developed models shed a new light of understanding on principles underlying learning and memory, both in the fruit fly and in a broader conceptual framework. To continue the work experimentally we have suggested key experiments to test proposed the hypothesizes. In the case of event timing experiments interfering with the intra-cellular mechanisms underlying the timing-dependent model outcome would test the plausibility of the model.

For trace conditioning one can imagine experiments that manipulate the post-odor response of KCs. If data analysis of manipulated flies reveals problems in classifying odor responses and behavioral experiments show a decreased learning ability, it would justify a further investigation of KCs as a locus of the stimulus trace.

Also for the model concerned with intensity learning of fruit flies in chapter 3 we suggest key experiments that test the role of specific neurons. If flies show a decreased learning ability when these neurons are blocked specifically it will support the proposed model. When blocking has no effect on the learning ability the proposed scenario might be scrapped.

Also on a theoretical level the limits of the proposed models could be further investigated. How does the outcome of the models change for more complex stimuli, such as odor mixtures? Was happens in the case of the basic model for intensity learning if realistic neurons are modeled?

BIBLIOGRAPHY

[1] IP Pavlov. *Conditioned reflexes: an investigation of the physiological activity of the cerebral cortex.*, volume 4 of *10*. London: Oxford University Press, The address, 3 edition, 7 1927. ISBN 3257227892.

[2] Eric S. Murphy and Gwen J. Lupfer. *The Wiley Blackwell Handbook of Operant and Classical Conditioning*. John Wiley & Sons, Ltd, 2014. ISBN 9781118468135. doi: 10.1002/9781118468135.ch8.

[3] William G. Quinn, W A Harris, and S Benzer. Conditioned behavior in Drosophila melanogaster. *Proc. Natl. Acad. Sci. U. S. A.*, 71(3):708–712, 1974. ISSN 0027-8424. doi: VL-71.

[4] Tim Tully and William G. Quinn. Classical conditioning and retention in normal and mutant Drosophila melanogaster. *J. Comp. Physiol. A*, 157(2):263–277, September 1985. ISSN 03407594. doi: 10.1007/BF01350033.

[5] Hiromu Tanimoto, Martin Heisenberg, and Bertram Gerber. Experimental psychology: Event timing turns punishment to reward. *Nature*, 430(7003):983, August 2004. ISSN 0028-0836. doi: 10.1038/430983a.

[6] Dana Shani Galili, Alja Lüdke, C Giovanni Galizia, Paul Szyszka, and Hiromu Tanimoto. Olfactory trace conditioning in Drosophila. *J. Neurosci.*, 31(20):7240–7248, May 2011. ISSN 0270-6474. doi: 10.1523/JNEUROSCI.6667-10.2011.

[7] R L Solomon and J D Corbit. An opponent-process theory of motivation. I. Temporal dynamics of affect. *Psychol. Rev.*, 81(2):119–145, 1974. ISSN 0033-295X. doi: 10.1037/h0036128.

[8] R. L. Solomon. Recent experiments testing an opponent-process theory of acquired motivation. *Acta Neurobiol. Exp. (Wars).*, 40(8):271–289, 1980. ISSN 00651400. doi: 10.1037/0003-066X.35.8.691.

[9] Dana Shani Galili, Kristina V. Dylla, Alja Lüdke, Anja B. Friedrich, Nobuhiro Yamagata, Jin Yan Hilary Wong, Chien Hsien Ho, Paul Szyszka, and Hiromu Tanimoto. Converging circuits mediate temperature and shock aversive olfactory conditioning in Drosophila. *Curr. Biol.*, 24 (15):1712–1722, 2014. ISSN 09609822. doi: 10.1016/j.cub.2014.06.062.

[10] Ayse Yarali, Sabrina Ehser, Fatma Zehra Hapil, Ju Huang, and Bertram Gerber. Odour intensity learning in fruit flies. *Proc. Biol. Sci.*, 276(1672):3413–3420, October 2009. ISSN 0962-8452. doi: 10.1098/rspb.2009.0705.

[11] Hugo J Bellen, Chao Tong, and Hiroshi Tsuda. 100 years of Drosophila research and its impact on vertebrate neuroscience: a history lesson for the future. *Nat. Rev. Neurosci.*, 11(7):514–522, 2010. ISSN 1471-003X. doi: 10.1038/nrn2839.

[12] Martin Heisenberg. Mushroom body memoir: from maps to models. *Nat. Rev. Neurosci.*, 4(April):266–275, 2003. ISSN 1471003X. doi: 10.1038/nrn1074.

[13] Nicholas J. Strausfeld and John G. Hildebrand. Olfactory systems: Common design, uncommon origins? *Curr. Opin. Neurobiol.*, 9(5):634–639, 1999. ISSN 09594388. doi: 10.1016/S0959-4388(99)00019-7.

[14] Ronald L. Davis. Olfactory learning. *Neuron*, 44(1):31–48, 2004. ISSN 08966273. doi: 10.1016/j.neuron.2004.09.008.

[15] Barry W. Ache and Janet M. Young. Olfaction: Diverse species, conserved principles. *Neuron*, 48(3):417–430, 2005. ISSN 08966273. doi: 10.1016/j.neuron.2005.10.022.

[16] U Benjamin Kaupp. Olfactory signalling in vertebrates and insects: differences and commonalities. *Nat. Rev. Neurosci.*, 11(3):188–200, 2010. ISSN 1471-003X. doi: 10.1038/nrn2789.

[17] S.R Shanbhag, B. Müller, and R.A Steinbrecht. Atlas of olfactory organs of Drosophila melanogaster 2. Internal organization and cellular architecture of olfactory sensilla. *Int. J. Insect Morphol. Embryol.*, 29(3):211–229, 2000. ISSN 1467-8039. doi: 10.1016/S1467-8039(00)00028-1.

[18] Jean Pierre Rospars, Petr Lánský, Henry C. Tuckwell, and Arthur Vermeulen. Coding of odor intensity in a steady-state deterministic model of an olfactory receptor neuron. *J. Comput. Neurosci.*, 3(1):51–72, March 1996. ISSN 09295313. doi: 10.1007/BF00158337.

[19] Petr Lánský and Jean Pierre Rospars. Odorant concentration and receptor potential in olfactory sensory neurons. *BioSystems*, 48(1-3):131–138, 1998. ISSN 03032647. doi: 10.1016/S0303-2647(98)00058-6.

[20] Jean Pierre Rospars, Petr Lánský, Patricia Duchamp-Viret, and André Duchamp. Spiking frequency versus odorant concentration in olfactory receptor neurons. *BioSystems*, 58(1-3):133–141, 2000. ISSN 03032647. doi: 10.1016/S0303-2647(00)00116-7.

[21] J.P. Rospars, Philippe Lucas, and Mathieu Coppey. Modelling the early steps of transduction in insect olfactory receptor neurons. *Biosystems*, 89(1-3):101–109, 2007. doi: 10.1016/j.biosystems.2006.05.015.

[22] R. F. Stocker. The organization of the chemosensory system in Drosophila melanogaster: A review. *Cell Tissue Res.*, 275:3–26, 1994. ISSN 0302766X. doi: 10.1007/BF00305372.

[23] Marien De Bruyne, Kara Foster, and John R. Carlson. Odor coding in the Drosophila antenna. *Neuron*, 30 (2):537–552, May 2001. ISSN 08966273. doi: 10.1016/S0896-6273(01)00289-6.

[24] L B Vosshall, a M Wong, and R Axel. An olfactory sensory map in the fly brain. *Cell*, 102(2):147–159, July 2000. ISSN 00121606. doi: 10.1016/j.ydbio.2008.05.014.

[25] C Andrea Yao, Rickard Ignell, and John R Carlson. Chemosensory coding by neurons in the coeloconic sensilla of the Drosophila antenna. *J. Neurosci.*, 25(37):8359–8367, September 2005. ISSN 0270-6474. doi: 10.1523/JNEUROSCI.2432-05.2005.

[26] Africa Couto, Mattias Alenius, and Barry J. Dickson. Molecular, anatomical, and functional organization of the Drosophila olfactory system. *Curr. Biol.*, 15(17):1535–1547, September 2005. ISSN 09609822. doi: 10.1016/j.cub.2005.07.034.

[27] Richard Benton, Kirsten S. Vannice, Carolina Gomez-Diaz, and Leslie B. Vosshall. Variant Ionotropic Glutamate Receptors as Chemosensory Receptors in Drosophila. *Cell*, 136(1):149–162, 2009. ISSN 00928674. doi: 10.1016/j.cell.2008.12.001.

[28] P P Laissue, C Reiter, P R Hiesinger, S Halter, K F Fischbach, and R F Stocker. Three-dimensional reconstruction of the antennal lobe in Drosophila melanogaster. *J. Comp. Neurol.*, 405(4):543–552, March 1999. ISSN 0021-9967.

[29] Reinhard F. Stocker. Drosophila as a focus in olfactory research: Mapping of olfactory sensilla by fine structure, odor specificity, odorant receptor expression, and central connectivity. *Microsc. Res. Tech.*, 55(5):284–296, December 2001. ISSN 1059910X. doi: 10.1002/jemt.1178.

[30] Jing W. Wang, Allan M. Wong, Jorge Flores, Leslie B. Vosshall, and Richard Axel. Two-photon calcium imaging reveals an odor-evoked map of activity in the fly brain. *Cell*, 112(2):271–282, 2003. ISSN 00928674. doi: 10.1016/S0092-8674(03)00004-7.

[31] R F Stocker, M C Lienhard, A Borst, and K F Fischbach. Neuronal architecture of the antennal lobe in Drosophila melanogaster. *Cell Tissue Res.*, 262:9–34, 1990. ISSN 0302-766X. doi: 10.1007/BF00327741.

[32] Yoichi Seki, Jürgen Rybak, Dieter Wicher, Silke Sachse, and Bill S Hansson. Physiological and morphological

characterization of local interneurons in the Drosophila antennal lobe. *J. Neurophysiol.*, 104(2):1007–19, August 2010. ISSN 1522-1598. doi: 10.1152/jn.00249.2010.

[33] Ya-Hui Chou, Maria L Spletter, Emre Yaksi, Jonathan C S Leong, Rachel I Wilson, and Liqun Luo. Diversity and wiring variability of olfactory local interneurons in the Drosophila antennal lobe. *Nat. Neurosci.*, 13(4):439–49, April 2010. ISSN 1546-1726. doi: 10.1038/nn.2489.

[34] Nobuaki K. Tanaka, Keita Endo, and Kei Ito. Organization of antennal lobe-associated neurons in adult Drosophila melanogaster brain. *J. Comp. Neurol.*, 520(18):4067–4130, December 2012. ISSN 00219967. doi: 10.1002/cne.23142.

[35] G. S. Jefferis, E. C. Marin, R. F. Stocker, and L. Luo. Target neuron prespecification in the olfactory map of Drosophila. *Nature*, 414(6860):204–208, Nov 2001.

[36] Allan M. Wong, Jing W. Wang, and Richard Axel. Spatial representation of the glomerular map in the Drosophila protocerebrum. *Cell*, 109(2):229–241, 2002. ISSN 00928674. doi: 10.1016/S0092-8674(02)00707-9.

[37] Mehmet Fişek and Rachel I Wilson. Stereotyped connectivity and computations in higher-order olfactory neurons. *Nature neuroscience*, 17(December):280–8, December 2014. ISSN 1546-1726. doi: 10.1038/nn.3613.

[38] K. Wang, J. Gong, Q. Wang, H. Li, Q. Cheng, Y. Liu, S. Zeng, and Z. Wang. Parallel pathways convey olfactory information with opposite polarities in Drosophila. *Proc. Natl. Acad. Sci. U.S.A.*, 111(8):3164–3169, Feb 2014.

[39] Sophie J C Caron, Vanessa Ruta, L F Abbott, and Richard Axel. Random convergence of olfactory inputs in the Drosophila mushroom body. *Nature*, 497(7447):113–7, May 2013. ISSN 1476-4687. doi: 10.1038/nature12063.

[40] Antonia Strutz, Jan Soelter, Amelie Baschwitz, Abu Farhan, Veit Grabe, Jürgen Rybak, Markus Knaden,

Michael Schmuker, Bill S Hansson, and Silke Sachse. Decoding odor quality and intensity in the Drosophila brain. *Elife*, 3:1–21, 2014. ISSN 2050-084X. doi: 10.7554/eLife.04147.

[41] Yoshinori Aso, Daisuke Hattori, Yang Yu, Rebecca M Johnston, A Nirmala, Teri-tb Ngo, Heather Dionne, L F Abbott, Richard Axel, Hiromu Tanimoto, and Gerald M Rubin. The neuronal architecture of the mushroom body provides a logic for associative learning. *Elife*, pages 1–47, 2014. ISSN 2050-084X. doi: 10.7554/eLife.04577.

[42] David Owald, Johannes Felsenberg, Clifford B. Talbot, Gaurav Das, Emmanuel Perisse, Wolf Huetteroth, and Scott Waddell. Activity of Defined Mushroom Body Output Neurons Underlies Learned Olfactory Behavior in Drosophila. *Neuron*, 86(2):417–427, April 2015. ISSN 08966273. doi: 10.1016/j.neuron.2015.03.025.

[43] Elissa A. Hallem and John R. Carlson. Coding of Odors by a Receptor Repertoire. *Cell*, 125(1):143–160, April 2006. ISSN 00928674. doi: 10.1016/j.cell.2006.01.050.

[44] Katherine I Nagel and Rachel I Wilson. Biophysical mechanisms underlying olfactory receptor neuron dynamics. *Nat. Neurosci.*, 14(2):208–216, February 2011. ISSN 1097-6256. doi: 10.1038/nn.2725.

[45] a. F. Silbering, R. Rytz, Y. Grosjean, L. Abuin, P. Ramdya, G. S. X. E. Jefferis, and R. Benton. Complementary Function and Integrated Wiring of the Evolutionarily Distinct Drosophila Olfactory Subsystems, 2011. ISSN 0270-6474.

[46] M de Bruyne, Peter J Clyne, and John R Carlson. Odor coding in a model olfactory organ: the Drosophila maxillary palp. *J. Neurosci.*, 19(11):4520–4532, 1999. ISSN 1529-2401.

[47] Marcus C Stensmyr, Elena Giordano, Annalisa Balloi, Anna-Maria Angioy, and Bill S Hansson. Novel natural ligands for Drosophila olfactory receptor neurones. *J. Exp. Biol.*, 206(Pt 4):715–724, 2003. ISSN 00220949. doi: 10.1242/jeb.00143.

[48] Hokto Kazama and Rachel I Wilson. Origins of correlated activity in an olfactory circuit. *Nat. Neurosci.*, 12(9):1136–1144, September 2009. ISSN 1097-6256. doi: 10.1038/nn.2376.

[49] Kenta Asahina, Matthieu Louis, Silvia Piccinotti, and Leslie B Vosshall. A circuit supporting concentration-invariant odor perception in Drosophila. *J. Biol.*, 8(1):9, January 2009. ISSN 1475-4924. doi: 10.1186/jbiol108.

[50] Carlotta Martelli, John R. Carlson, and Thierry Emonet. Intensity invariant dynamics and odor-specific latencies in olfactory receptor neuron response. *J. Neurosci.*, 33 (15):6285–97, April 2013. ISSN 1529-2401. doi: 10.1523/JNEUROSCI.0426-12.2013.

[51] S.R Shanbhag, B. Müller, and R.A Steinbrecht. Atlas of olfactory organs of Drosophila melanogaster 1. Types, external organization, innervation and distribution of olfactory sensilla. *Int. J. Insect Morphol. Embryol.*, 28(4): 377–397, October 1999. ISSN 00207322. doi: 10.1016/S0020-7322(99)00039-2.

[52] Vikas Bhandawat, Shawn R Olsen, Nathan W Gouwens, Michelle L Schlief, and Rachel I Wilson. Sensory processing in the Drosophila antennal lobe increases reliability and separability of ensemble odor representations. *Nat. Neurosci.*, 10(11):1474–1482, November 2007. ISSN 1097-6256. doi: 10.1038/nn1976.

[53] Rachel I Wilson, Glenn C Turner, and Gilles Laurent. Transformation of olfactory representations in the Drosophila antennal lobe. *Science*, 303(5656):366–370, January 2004. ISSN 0036-8075. doi: 10.1126/science.1090782.

[54] Shawn R. Olsen, Vikas Bhandawat, and Rachel I. Wilson. Divisive normalization in olfactory population codes. *Neuron*, 66(2):287–299, April 2010. ISSN 08966273. doi: 10.1016/j.neuron.2010.04.009.

[55] Emre Yaksi and Rachel I. Wilson. Electrical Coupling between Olfactory Glomeruli. *Neuron*, 67(6):1034–1047,

September 2010. ISSN 08966273. doi: 10.1016/j.neuron.2010.08.041.

[56] Shawn R Olsen and Rachel I Wilson. Lateral presynaptic inhibition mediates gain control in an olfactory circuit. *Nature*, 452(7190):956–960, April 2008. ISSN 0028-0836. doi: 10.1038/nature06864.

[57] Cory M Root, Julia L Semmelhack, Allan M Wong, Jorge Flores, and Jing W Wang. Propagation of olfactory information in Drosophila. *Proc. Natl. Acad. Sci. U. S. A.*, 104(28):11826–11831, July 2007. ISSN 0027-8424. doi: 10.1073/pnas.0704523104.

[58] Sean X Luo, Richard Axel, and L F Abbott. Generating sparse and selective third-order responses in the olfactory system of the fly. *Proc. Natl. Acad. Sci.*, 107(23):10713–10718, June 2010. ISSN 0027-8424. doi: 10.1073/pnas.1005635107.

[59] Yalin Wang, Hui-Fu Guo, Thomas a Pologruto, Frances Hannan, Inessa Hakker, Karel Svoboda, and Yi Zhong. Stereotyped odor-evoked activity in the mushroom body of Drosophila revealed by green fluorescent protein-based Ca2+ imaging. *J. Neurosci.*, 24(29):6507–6514, 2004. ISSN 0270-6474. doi: 10.1523/JNEUROSCI.3727-03.2004.

[60] Glenn C Turner, Maxim Bazhenov, and Gilles Laurent. Olfactory representations by Drosophila mushroom body neurons. *J. Neurophysiol.*, 99(2):734–746, February 2008. ISSN 0022-3077. doi: 10.1152/jn.01283.2007.

[61] Kyle S. Honegger, Robert a. a. Campbell, and Glenn C. Turner. Cellular-resolution population imaging reveals robust sparse coding in the Drosophila mushroom body. *J. Neurosci.*, 31(33):11772–11785, August 2011. ISSN 0270-6474. doi: 10.1523/JNEUROSCI.1099-11.2011.

[62] Mala Murthy, Ila Fiete, and Gilles Laurent. Testing Odor Response Stereotypy in the Drosophila Mushroom Body. *Neuron*, 59(6):1009–1023, September 2008. ISSN 08966273. doi: 10.1016/j.neuron.2008.07.040.

[63] Silke Sachse, Erroll Rueckert, Andreas Keller, Ryuichi Okada, Nobuaki K Tanaka, Kei Ito, and Leslie B Vosshall. Activity-Dependent Plasticity in an Olfactory Circuit. *Neuron*, 56(5):838–850, 2007. ISSN 08966273. doi: 10.1016/j.neuron.2007.10.035.

[64] Greg S B Suh, Allan M Wong, Anne C Hergarden, Jing W Wang, Anne F Simon, Seymour Benzer, Richard Axel, and David J Anderson. A single population of olfactory sensory neurons mediates an innate avoidance behaviour in Drosophila. *Nature*, 431(7010):854–859, 2004. ISSN 0028-0836. doi: 10.1038/nature02980.

[65] Sandeep Robert Datta, Maria Luisa Vasconcelos, Vanessa Ruta, Sean Luo, Allan Wong, Ebru Demir, Jorge Flores, Karen Balonze, Barry J Dickson, and Richard Axel. The Drosophila pheromone cVA activates a sexually dimorphic neural circuit. *Nature*, 452(7186):473–477, 2008. ISSN 0028-0836. doi: 10.1038/nature06808.

[66] Cory M. Root, Kaoru Masuyama, David S. Green, Lina E. Enell, Dick R. Nässel, Chi Hon Lee, and Jing W. Wang. A Presynaptic Gain Control Mechanism Fine-Tunes Olfactory Behavior. *Neuron*, 59(2):311–321, 2008. ISSN 08966273. doi: 10.1016/j.neuron.2008.07.003.

[67] Vanessa Ruta, Sandeep Robert Datta, Maria Luisa Vasconcelos, Jessica Freeland, Loren L Looger, and Richard Axel. A dimorphic pheromone circuit in Drosophila from sensory input to descending output. *Nature*, 468(7324):686–690, 2010. ISSN 0028-0836. doi: 10.1038/nature09554.

[68] Mathias Ditzen, Jan Felix Evers, and C. Giovanni Galizia. Odor similarity does not influence the time needed for odor processing. *Chem. Senses*, 28(9):781–789, 2003. ISSN 0379864X. doi: 10.1093/chemse/bjg070.

[69] Geraldine a Wright, Mitchell G a Thomson, and Brian H Smith. Odour concentration affects odour identity in honeybees. *Proc. Biol. Sci.*, 272(1579):2417–2422, November 2005. ISSN 0962-8452. doi: 10.1098/rspb.2005.3252.

[70] Thomas a. Cleland, Szu-Yu T. Chen, Katarzyna W. Hozer, Hope N. Ukatu, Kevin J. Wong, and Fangfei Zheng. Sequential mechanisms underlying concentration invariance in biological olfaction, 2012. ISSN 1662-6443.

[71] C. Giovanni Galizia and Paul Szyszka. Olfactory coding in the insect brain: Molecular receptive ranges, spatial and temporal coding. *Entomol. Exp. Appl.*, 128(1):81–92, July 2008. ISSN 00138703. doi: 10.1111/j.1570-7458.2007.00661.x.

[72] Roberto Fdez Galán, Silke Sachse, C Giovanni Galizia, and Andreas V M Herz. Odor-driven attractor dynamics in the antennal lobe allow for simple and rapid olfactory pattern classification. *Neural Comput.*, 16(5):999–1012, May 2004. ISSN 0899-7667. doi: 10.1162/089976604773135078.

[73] Karl Pearson. LIII. On lines and planes of closest fit to systems of points in space. *London, Edinburgh, Dublin Philos. Mag. J. Sci.*, 2:559–572, 1901. ISSN 1941-5982. doi: 10.1080/14786440109462720.

[74] I. T. Jolliffe. *Principal Component Analysis*. Springer-Verlag, Berlin; New York, 1986.

[75] R. A. FISHER. THE USE OF MULTIPLE MEASUREMENTS IN TAXONOMIC PROBLEMS. *Ann. Eugen.*, 7(2):179–188, September 1936. ISSN 20501420. doi: 10.1111/j.1469-1809.1936.tb02137.x.

[76] V Vapnik and a Lerner. Pattern recognition using generalized portrait method. *Autom. Remote Control*, 24:774–780, 1963. ISSN 0005-1179. doi: citeulike-article-id:619639.

[77] Bernhard E. Boser, IM Isabelle M. Guyon, and VN Vladimir N. Vapnik. A training algorithm for optimal margin classifiers. In *Proc. 5th Annu. ACM Work. Comput. Learn. Theory*, pages 144 – 152. ACM Press, 1992. ISBN 089791497X. doi: 10.1.1.21.3818.

[78] Corinna Cortes and Vladimir Vapnik. Support-vector networks. *Mach. Learn.*, 20(3):273–297, September 1995. ISSN 08856125. doi: 10.1007/BF00994018.

[79] Vladimir N. Vapnik. *The Nature of Statistical Learning Theory*. Springer-Verlag New York, Inc., New York, NY, USA, 1995. ISBN 0-387-94559-8.

[80] B Schölkopf and RC Williamson. Support Vector Method for Novelty Detection. *NIPS*, pages 582–588, 1999.

[81] Patrick J Drew and L F Abbott. Extending the effects of spike-timing-dependent plasticity to behavioral timescales. *Proc. Natl. Acad. Sci. U. S. A.*, 103(23): 8876–8881, 2006. ISSN 0027-8424. doi: 10.1073/pnas.0600676103.

[82] Henry Markram, J Lübke, Michael Frotscher, A Roth, and B. Sakmann. Regulation of Synaptic Efficacy by Coincidence of Postsynaptic APs and EPSPs. *J. Physiol.*, 500 (Pt 2(5297):409–440, 1997. ISSN 0022-3751. doi: 10.1126/science.275.5297.213.

[83] J C Magee and D Johnston. A synaptically controlled, associative signal for Hebbian plasticity in hippocampal neurons. *Science*, 275(5297):209–213, 1997. ISSN 00368075. doi: 10.1126/science.275.5297.209.

[84] Donald O Hebb. The Organization of Behavior. *Organ. Behav.*, (4):60–78, 1949.

[85] G.Q. Bi and Jonathan Rubin. Timing in synaptic plasticity: from detection to integration. *TRENDS Neurosci.*, 28(5): 222–228, 2005. doi: 10.1016/j.tins.2005.02.002.

[86] Michael Graupner and Nicolas Brunel. STDP in a bistable synapse model based on CaMKII and associated signaling pathways. *PLoS Comput. Biol.*, 3(11):2299–2323, November 2007. ISSN 1553734X. doi: 10.1371/journal.pcbi.0030221.

[87] Natalia Caporale and Yang Dan. Spike timing-dependent plasticity: a Hebbian learning rule. *Annu. Rev. Neurosci.*, 31:25–46, 2008. ISSN 0147-006X. doi: 10.1146/annurev.neuro.31.060407.125639.

[88] Michael Graupner and Nicolas Brunel. Mechanisms of induction and maintenance of spike-timing dependent plasticity in biophysical synapse models. *Front. Comput. Neurosci.*, 4(September):1–19, January 2010. ISSN 1662-5188. doi: 10.3389/fncom.2010.00136.

[89] Yang Dan and Mu-ming Poo. Spike timing-dependent plasticity of neural circuits. *Neuron*, 44(1):23–30, 2004.

[90] Yang Dan and Mu-Ming Poo. Spike timing-dependent plasticity: from synapse to perception. *Physiol. Rev.*, 86(3): 1033–1048, 2006. ISSN 0031-9333. doi: 10.1152/physrev.00030.2005.

[91] Jiang Hao and Thomas G Oertner. Depolarization gates spine calcium transients and spike-timing-dependent potentiation. *Curr. Opin. Neurobiol.*, 22:509–515, November 2012. ISSN 09594388. doi: 10.1016/j.conb.2011.10.004.

[92] M. Graupner and N. Brunel. Calcium-based plasticity model explains sensitivity of synaptic changes to spike pattern, rate, and dendritic location. *Proc. Natl. Acad. Sci.*, 109:3991–3996, February 2012. ISSN 0027-8424. doi: 10.1073/pnas.1109359109.

[93] P Jesper Sjöström, Ede A Rancz, Arnd Roth, and Michael Häusser. Dendritic excitability and synaptic plasticity. *Physiol. Rev.*, 88(2):769–840, 2008. ISSN 0031-9333. doi: 10.1152/physrev.00016.2007.

[94] G Bi and M Poo. Synaptic modification by correlated activity: Hebb's postulate revisited. *Annu. Rev. Neurosci.*, 24:139–166, 2001. ISSN 0147-006X. doi: 10.1146/annurev.neuro.24.1.139.

[95] John E. Lisman and Charmian C. McIntyre. Synaptic plasticity: A molecular memory switch. *Curr. Biol.*, 11(19): R788–91, October 2001. ISSN 09609822. doi: 10.1016/S0960-9822(01)00472-9.

[96] J E Lisman. A mechanism for memory storage insensitive to molecular turnover: a bistable autophosphorylating kinase. *Proc. Natl. Acad. Sci. U. S. A.*, 82(9):3055–3057, 1985. ISSN 0027-8424. doi: 10.1073/pnas.82.9.3055.

[97] L F Abbott and S B Nelson. Synaptic plasticity: taming the beast. *Nat. Neurosci.*, 3 Suppl(november):1178–1183, November 2000. ISSN 1097-6256. doi: 10.1038/81453.

[98] Stijn Cassenaer and Gilles Laurent. Hebbian STDP in mushroom bodies facilitates the synchronous flow of olfactory information in locusts. *Nature*, 448(7154):709–13, August 2007. ISSN 1476-4687. doi: 10.1038/nature05973.

[99] Nicolas Gervasi, Paul Tchénio, and Thomas Preat. PKA Dynamics in a Drosophila Learning Center: Coincidence Detection by Rutabaga Adenylyl Cyclase and Spatial Regulation by Dunce Phosphodiesterase. *Neuron*, 65(4):516–529, February 2010. ISSN 08966273. doi: 10.1016/j.neuron.2010.01.014.

[100] Iori Ito, Rose Chik-ying Ong, Baranidharan Raman, and Mark Stopfer. Olfactory learning and spike timing dependent plasticity. *Commun. Integr. Biol.*, 1(2):170–171, 2008. ISSN 1942-0889. doi: 10.4161/cib.1.2.7140.

[101] Katrin Vogt, Christopher Schnaitmann, K.V. Dylla, S Knapek, Y Aso, G.M. Rubin, and H Tanimoto. Shared mushroom body circuits operate visual and olfactory memories in Drosophila. *Elife*, pages 1–22, 2014. ISSN 2050-084X. doi: 10.7554/eLife.02395.

[102] M Heisenberg, A Borst, S Wagner, and D Byers. Drosophila mushroom body mutants are deficient in olfactory learning. *J. Neurogenet.*, 2(1):1–30, 1985. ISSN 0167-7063. doi: 10.3109/01677068509100140.

[103] J S de Belle and M Heisenberg. Associative odor learning in Drosophila abolished by chemical ablation of mushroom bodies. *Science*, 263(5147):692–695, 1994. ISSN 0036-8075. doi: 10.1126/science.8303280.

[104] John B Connolly, I J Roberts, J Douglas Armstrong, Kim Kaiser, Michael Forte, Tim Tully, and Cahir J O'Kane. Associative learning disrupted by impaired Gs signaling in Drosophila mushroom bodies. *Science*, 274(5295):2104–2107, 1996. ISSN 0036-8075. doi: 10.1126/science.274.5295.2104.

[105] T Zars, M Fischer, R Schulz, and M Heisenberg. Localization of a short-term memory in Drosophila. *Science*, 288 (5466):672–675, 2000. ISSN 00368075. doi: 10.1126/science.288.5466.672.

[106] Sean E McGuire, Phuong T Le, Alexander J Osborn, Kunihiro Matsumoto, and Ronald L Davis. Spatiotemporal rescue of memory dysfunction in Drosophila. *Science*, 302(5651):1765–1768, 2003. ISSN 0036-8075. doi: 10.1126/science.1089035.

[107] Zhengmei Mao, Gregg Roman, Lin Zong, and Ronald L Davis. Pharmacogenetic rescue in time and space of the rutabaga memory impairment by using Gene-Switch. *Proc. Natl. Acad. Sci. U. S. A.*, 101(1):198–203, 2004. ISSN 0027-8424. doi: 10.1073/pnas.0306128101.

[108] Michael J. Krashes, Alex C. Keene, Benjamin Leung, J. Douglas Armstrong, and Scott Waddell. Sequential Use of Mushroom Body Neuron Subsets during Drosophila Odor Memory Processing. *Neuron*, 53(1):103–115, 2007. ISSN 08966273. doi: 10.1016/j.neuron.2006.11.021.

[109] J Dubnau, L Grady, T Kitamoto, and T Tully. Disruption of neurotransmission in Drosophila mushroom body blocks retrieval but not acquisition of memory. *Nature*, 411(6836):476–80, May 2001. ISSN 0028-0836. doi: 10.1038/35078077.

[110] S E McGuire, P T Le, and R L Davis. The role of Drosophila mushroom body signaling in olfactory memory. *Science*, 293(5533):1330–1333, 2001. ISSN 00368075. doi: 10.1126/science.1062622.

[111] Martin Schwaerzel, Martin Heisenberg, and Troy Zars. Extinction antagonizes olfactory memory at the subcellular level, 2002. ISSN 08966273.

[112] Martin Schwaerzel, Maria Monastirioti, Henrike Scholz, Florence Friggi-Grelin, Serge Birman, and Martin Heisenberg. Dopamine and octopamine differentiate between aversive and appetitive olfactory memories in Drosophila.

J. Neurosci., 23(33):10495–502, November 2003. ISSN 1529-2401.

[113] Thomas Riemensperger, Thomas Völler, Patrick Stock, Erich Buchner, and André Fiala. Punishment prediction by dopaminergic neurons in Drosophila. *Curr. Biol.*, 15 (21):1953–1960, 2005. ISSN 09609822. doi: 10.1016/j.cub.2005.09.042.

[114] Young-Cho Kim, Hyun-Gwan Lee, and Kyung-An Han. D1 dopamine receptor dDA1 is required in the mushroom body neurons for aversive and appetitive learning in Drosophila. *J. Neurosci.*, 27(29):7640–7647, 2007. ISSN 0270-6474. doi: 10.1523/JNEUROSCI.1167-07.2007.

[115] Adam Claridge-Chang, Robert D. Roorda, Eleftheria Vrontou, Lucas Sjulson, Haiyan Li, Jay Hirsh, and Gero Miesenböck. Writing Memories with Light-Addressable Reinforcement Circuitry. *Cell*, 139(2):405–415, 2009. ISSN 00928674. doi: 10.1016/j.cell.2009.08.034.

[116] Yoshinori Aso, Igor Siwanowicz, Lasse Bräcker, Kei Ito, Toshihiro Kitamoto, and Hiromu Tanimoto. Specific dopaminergic neurons for the formation of labile aversive memory. *Curr. Biol.*, 20(16):1445–1451, 2010. ISSN 09609822. doi: 10.1016/j.cub.2010.06.048.

[117] Dinghui Yu, David Benjamin G Akalal, and Ronald L. Davis. Drosophila α/β Mushroom Body Neurons Form a Branch-Specific, Long-Term Cellular Memory Trace after Spaced Olfactory Conditioning. *Neuron*, 52(5):845–855, 2006. ISSN 08966273. doi: 10.1016/j.neuron.2006.10.030.

[118] Yalin Wang, Akira Mamiya, Ann-shyn Chiang, and Yi Zhong. Imaging of an early memory trace in the Drosophila mushroom body. *J. Neurosci.*, 28(17):4368–4376, 2008. ISSN 0270-6474. doi: 10.1523/JNEUROSCI.2958-07.2008.

[119] Seth M Tomchik and Ronald L Davis. Dynamics of learning-related cAMP signaling and stimulus integration in the Drosophila olfactory pathway. *Neuron*, 64(4): 510–21, November 2009. ISSN 1097-4199. doi: 10.1016/j.neuron.2009.09.029.

[120] Julien Séjourné, Pierre-Yves Plaçais, Yoshinori Aso, Igor Siwanowicz, Séverine Trannoy, Vladimiros Thoma, Stevanus R Tedjakumala, Gerald M Rubin, Paul Tchénio, Kei Ito, Guillaume Isabel, Hiromu Tanimoto, and Thomas Preat. Mushroom body efferent neurons responsible for aversive olfactory memory retrieval in Drosophila. *Nat. Neurosci.*, 14(7):903–10, July 2011. ISSN 1546-1726. doi: 10.1038/nn.2846.

[121] Gregg Roman, Gregg Roman, Ronald L Davis, and Ronald L Davis. Molecular biology and anatomy of. *BioEssays*, pages 571–581, 2001.

[122] I P Pavlov. An Investigation of the Physiological Activity of the Cerebral Cortex. *Oxford Univ. Press*, 1927. ISSN 08854173. doi: 10.2307/1134737.

[123] Edwin B. Twitmyer. Knee jerks without stimulation of the patellar tendon. *Psychological Bulletin*, 2:43–44, 1905.

[124] I Gormezano, N Schneiderman, E Deaux, and I Fuentes. Nictitating membrane: classical conditioning and extinction in the albino rabbit. *Science*, 138:33–34, 1962. ISSN 0036-8075. doi: 10.1126/science.138.3536.33.

[125] N SCHNEIDERMAN, I FUENTES, and I GORMEZANO. Acquisition and extinction of the classically conditioned eyelid response in the albino rabbit. *Science*, 136(1):650–652, 1962. ISSN 0036-8075. doi: 10.1126/science.136.3516.650.

[126] David a. Mccormick, David G. Lavond, Gregory a. Clark, Ronald E. Kettner, Christina E. Rising, and Richard F. Thompson. The engram found? Role of the cerebellum in classical conditioning of nictitating membrane and eyelid responses. *Bull. Psychon. Soc.*, 18(3):103–105, September 1981. ISSN 0090-5054. doi: 10.3758/BF03333573.

[127] D a McCormick and R F Thompson. Neuronal responses of the rabbit cerebellum during acquisition and performance of a classically conditioned nictitating membrane-eyelid response. *J. Neurosci.*, 4(11):2811–2822, 1984. ISSN 0270-6474.

[128] D a McCormick and R F Thompson. Cerebellum: essential involvement in the classically conditioned eyelid response. *Science*, 223(4633):296–299, 1984. ISSN 0036-8075. doi: 10.1126/science.6701513.

[129] Andrew M Poulos and Richard F Thompson. Localization and characterization of an essential associative memory trace in the mammalian brain. *Brain Res.*, pages 1–8, November 2014. ISSN 00068993. doi: 10.1016/j.brainres.2014.10.068.

[130] J. L. Kwapis, T. J. Jarome, J. C. Schiff, and F. J. Helmstetter. Memory consolidation in both trace and delay fear conditioning is disrupted by intra-amygdala infusion of the protein synthesis inhibitor anisomycin, 2011. ISSN 1072-0502.

[131] Daniel E. Kochli, Elaine C. Thompson, Elizabeth A. Fricke, Abagail F. Postle, and Jennifer J. Quinn. The amygdala is critical for trace, delay, and contextual fear conditioning. *Learn. Mem.*, 22(2):92–100, February 2015. ISSN 1549-5485. doi: 10.1101/lm.034918.114.

[132] Gene V. Wallenstein, Howard Eichenbaum, and Michael E. Hasselmo. The hippocampus as an associator of discontiguous events. *Trends Neurosci.*, 21(8):317–323, 1998. ISSN 01662236. doi: 10.1016/S0166-2236(97)01220-4.

[133] C J Han, Colm M O'Tuathaigh, Laurent van Trigt, Jennifer J Quinn, Michael S Fanselow, Raymond Mongeau, Christof Koch, and David J Anderson. Trace but not delay fear conditioning requires attention and the anterior cingulate cortex. *Proc. Natl. Acad. Sci. U. S. A.*, 100(22):13087–13092, 2003. ISSN 0027-8424. doi: 10.1073/pnas.2132313100.

[134] Kaori Takehara, Shigenori Kawahara, and Yutaka Kirino. Time-dependent reorganization of the brain components underlying memory retention in trace eyeblink conditioning. *J. Neurosci.*, 23(30):9897–9905, 2003. ISSN 1529-2401. doi: 23/30/9897[pii].

[135] Larry R Squire, Craig E L Stark, and Robert E Clark. The medial temporal lobe. *Annu. Rev. Neurosci.*, 27:279–306, 2004. ISSN 0147-006X. doi: 10.1146/annurev.neuro.27.070203.144130.

[136] Yi Yang, Chen Lei, Hua Feng, and Jian-feng Sui. The neural circuitry and molecular mechanisms underlying delay and trace eyeblink conditioning in mice. *Behav. Brain Res.*, 278:307–314, 2015. ISSN 01664328. doi: 10.1016/j.bbr.2014.10.006.

[137] T J Carew, E T Walters, and E R Kandel. Classical conditioning in a simple withdrawal reflex in Aplysia californica. *J. Neurosci.*, 1(12):1426–1437, March 1981. ISSN 1529-2401. doi: 10.1177/0269881107067097.

[138] Masutaro Kuwabara. Bildung des bedingten Reflexes von Pavlovs Typus bei der Honigbiene, Apis mellifica. *J Fac Sci Hokkaido Univ Ser VI Zool*, 13(08):458–464, 1957. ISSN 0368-2188.

[139] M E Bitterman, R Menzel, A Fietz, and S Schäfer. Classical conditioning of proboscis extension in honeybees (Apis mellifera). *J. Comp. Psychol.*, 97(2):107–119, 1983. ISSN 0735-7036. doi: 10.1037/0735-7036.97.2.107.

[140] Julie H Simpson. Mapping and manipulating neural circuits in the fly brain. *Adv. Genet.*, 65:79–143, January 2009. ISSN 0065-2660. doi: 10.1016/S0065-2660(09)65003-3.

[141] Marla B Sokolowski. Drosophila: genetics meets behaviour. *Nat. Rev. Genet.*, 2(11):879–890, 2001. ISSN 1471-0056. doi: 10.1038/35098592.

[142] Heiko Dankert, Liming Wang, Eric D Hoopfer, David J Anderson, and Pietro Perona. Automated monitoring and analysis of social behavior in Drosophila. *Nat. Methods*, 6(4):297–303, 2009. ISSN 1548-7091. doi: 10.1038/nmeth.1310.

[143] E. D. Adrian. The impulses produced by sensory nerve-endings. *J. Physiol.*, 62(1):33–51, 1926. ISSN 0022-3751. doi: 16993776.

[144] Tim Gollisch and Markus Meister. Rapid neural coding in the retina with relative spike latencies. *Science*, 319(5866): 1108–1111, 2008. ISSN 0036-8075. doi: 10.1126/science.1149639.

[145] Marcelo a. Montemurro, Malte J. Rasch, Yusuke Murayama, Nikos K. Logothetis, and Stefano Panzeri. Phase-of-Firing Coding of Natural Visual Stimuli in Primary Visual Cortex. *Curr. Biol.*, 18(5):375–380, 2008. ISSN 09609822. doi: 10.1016/j.cub.2008.02.023.

[146] Eric T Reifenstein, Richard Kempter, Susanne Schreiber, Martin B Stemmler, and Andreas V M Herz. Grid cells in rat entorhinal cortex encode physical space with independent firing fields and phase precession at the single-trial level. *Proc. Natl. Acad. Sci. U. S. A.*, 109(16):6301–6, April 2012. ISSN 1091-6490. doi: 10.1073/pnas.1109599109.

[147] J O'Keefe and J Dostrovsky. The hippocampus as a spatial map. Preliminary evidence from unit activity in the freely-moving rat. *Brain Res.*, 34(1):171–175, 1971. ISSN 00068993. doi: 10.1016/0006-8993(71)90358-1.

[148] Marianne Fyhn, Sturla Molden, Menno P Witter, Edvard I Moser, and May-Britt Moser. Spatial representation in the entorhinal cortex. *Science*, 305(5688):1258–1264, 2004. ISSN 1095-9203. doi: 10.1126/science.1099901.

[149] Alexander Mathis, Andreas V. M. Herz, and Martin Stemmler. Optimal Population Codes for Space: Grid Cells Outperform Place Cells, 2012. ISSN 0899-7667.

[150] Robert a a Campbell, Kyle S Honegger, Hongtao Qin, Wanhe Li, Ebru Demir, and Glenn C Turner. Imaging a population code for odor identity in the Drosophila mushroom body. *J. Neurosci.*, 33(25):10568–81, June 2013. ISSN 1529-2401. doi: 10.1523/JNEUROSCI.0682-12.2013.

[151] Paul Szyszka, Christiane Demmler, Mariann Oemisch, Ludwig Sommer, Stephanie Biergans, Benjamin Birnbach, Ana F Silbering, and C Giovanni Galizia. Mind the

gap: olfactory trace conditioning in honeybees. *J. Neurosci.*, 31(20):7229–7239, May 2011. ISSN 0270-6474. doi: 10.1523/JNEUROSCI.6668-10.2011.

[152] Ayse Yarali, Thomas Niewalda, Yi Chun Chen, Hiromu Tanimoto, Stefan Duerrnagel, and Bertram Gerber. 'Pain relief' learning in fruit flies. *Anim. Behav.*, 76:1173–1185, 2008. ISSN 00033472. doi: 10.1016/j.anbehav.2008.05.025.

[153] A J Hudspeth. How the ear's works work. *Nature*, 341(6241):397–404, 1989. ISSN 0028-0836. doi: 10.1038/341397a0.

[154] Brian C J Moore. Coding of sounds in the auditory system and its relevance to signal processing and coding in cochlear implants. *Otol. Neurotol.*, 24(2):243–254, 2003. ISSN 1531-7129. doi: 10.1097/00129492-200303000-00019.

[155] M. Zhou, H. W. Tao, and L. I. Zhang. Generation of Intensity Selectivity by Differential Synaptic Tuning: Fast-Saturating Excitation But Slow-Saturating Inhibition. *J. Neurosci.*, 32(50):18068–18078, December 2012. ISSN 0270-6474. doi: 10.1523/JNEUROSCI.3647-12.2012.

[156] Yali V Zhang, Jinfei Ni, and Craig Montell. The molecular basis for attractive salt-taste coding in Drosophila. *Science*, 340(6138):1334–8, June 2013. ISSN 1095-9203. doi: 10.1126/science.1234133.

[157] Dushyant Mishra, Yi-Chun Chen, Ayse Yarali, Tuba Oguz, and Bertram Gerber. Olfactory memories are intensity specific in larval Drosophila. *J. Exp. Biol.*, 216(Pt 9):1552–60, 2013. ISSN 1477-9145. doi: 10.1242/jeb.082222.

[158] Mark Stopfer, Vivek Jayaraman, and Gilles Laurent. Intensity versus identity coding in an olfactory system. *Neuron*, 39(6):991–1004, September 2003. ISSN 08966273. doi: 10.1016/j.neuron.2003.08.011.

[159] Kai Shen, Sina Tootoonian, and Gilles Laurent. Encoding of mixtures in a simple olfactory system. *Neuron*, 80(5):1246–1262, 2013. ISSN 08966273. doi: 10.1016/j.neuron.2013.08.026.

ACKNOWLEDGMENTS

I want to thank everyone who supported me to finish this thesis.

Andreas Herz gave me the opportunity, support and freedom to work on the subject. Ayse Yarali was an immense help with everything regarding biology. The computational neuroscience department and the Bernstein Center for computational neuroscience Munich were an inspiration in both scientific an non-scientific ways. The Graduate School of Systemic Neurosciences gave the framework for the dissertation and the opportunity to look beyond the own field of research. My thesis advisory committee with Hiromu Tanimoto and Alexander Borst for fruitful discussions. And Alja Lüdke, Paul Szyszka and Giovanni Galizia for generously sharing their data and discussing it. Thanks go also to André Miede (`http://www.miede.de`) for sharing the classicthesis style.

The biggest thanks goes to my family for their continued patience and support. It would not have been possible without them.

PUBLICATIONS

Ayse Yarali, Johannes Nehrkorn, Hiromu Tanimoto, Andreas V. M. Herz (2012). "Event Timing in Associative Learning: From Biochemical Reaction Dynamics to Behavioural Observations". *PLoS ONE*, 7(3): e32885.

Johannes Nehrkorn, Hiromu Tanimoto, Andreas V. M. Herz, Ayse Yarali (2015). "A model for non-monotonic intensity coding".
R. Soc. open sci. 2015 2 150120.

SELECTED CONFERENCE CONTRIBUTIONS

A. Yarali, J. Nehrkorn, H. Tanimoto, A. V. M. Herz (2012). "Event timing in associative learning: From biochemical reaction dynamics to behavioral observations". *Cosyne Abstracts*, Salt Lake City.

J. Nehrkorn, A. Yarali, T. Oguz, H. Tanimoto, A. V. M. Herz (2012). "Modeling fruit fly olfactory receptor neuron-responses". *Society for Neuroscience Conference*, New Orleans.

J. Nehrkorn, H. Tanimoto, A. V. M. Herz, A. Yarali (2013). "Learning about absolute odor intensities: A model for Drosophila melanogaster". *Bernstein Conference*, Tübingen.

EIDESSTATTLICHE VERSICHERUNG / AFFIDAVIT

Hiermit versichere ich an Eides statt, dass ich die vorliegende Dissertation *Olfactory Learning in* Drosophila*: Learning from Models* selbstständig angefertigt habe, mich außer der angegebenen keiner weiteren Hilfsmittel bedient und alle Erkenntnisse, die aus dem Schrifttum ganz oder annähernd übernommen sind, als solche kenntlich gemacht und nach ihrer Herkunft unter Bezeichnung der Fundstelle einzeln nachgewiesen habe.

I hereby confirm that the dissertation *Olfactory Learning in* Drosophila*: Learning from Models* is the result of my own work and that I have only used sources or materials listed and specified in the dissertation.

Date, place

Johannes Nehrkorn

AUTHOR CONTRIBUTIONS

Event Timing in Associative Learning: From Biochemical Reaction Dynamics to Behavioural Observations

Ayse Yarali, Johannes Nehrkorn, Hiromu Tanimoto, Andreas V. M. Herz (2012). PLoS ONE 7(3): e32885. Conceived and designed the experiments: AY, JN, HT, AVMH. Performed the experiments: AY, JN. Analyzed the data: AY, JN. Wrote the paper: AY, JN, HT, AVMH.

A model for non-monotonic intensity coding

Johannes Nehrkorn, Hiromu Tanimoto, Andreas V. M. Herz, Ayse Yarali (2015). R. Soc. open sci. 2015 2 150120. JN carried out the implementation of the model. JN, HT, AVMH. and AY conceived the model and drafted the manuscript. All authors gave final approval for publication.

Olfactory trace conditioning in Drosophila *as revealed by machine learning techniques at the single-fly level*

Johannes Nehrkorn, Alja Lüdke, Paul Szyszka, Giovanni Galizia, Andreas V. M. Herz. JN and AVMH conceived and designed research. JN carried out research. AL performed experiments. JN, AL, PS, GG, AVMH discussed the results. JN, AVMH drafted the current state of the manuscript.

Date, place	Johannes Nehrkorn
Date, place	Prof. Andreas V. M. Herz